NASA/CR-1998-207667

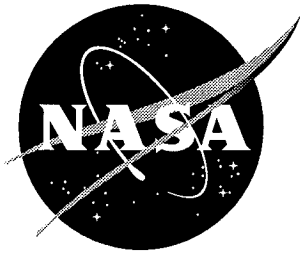

Analysis and Testing of Plates With Piezoelectric Sensors and Actuators

Jeffrey S. Bevan
Old Dominion University, Norfolk, Virginia

National Aeronautics and
Space Administration

Langley Research Center
Hampton, Virginia 23681-2199

Prepared for Langley Research Center
under Grant NAG1-1684

April 1998

Available from the following:

NASA Center for AeroSpace Information (CASI)
7121 Standard Drive
Hanover, MD 21076-1320
(301) 621-0390

National Technical Information Service (NTIS)
5285 Port Royal Road
Springfield, VA 22161-2171
(703) 487-4650

ABSTRACT

ANALYSIS AND TESTING OF PLATES WITH PIEZOELECTRIC SENSORS AND ACTUATORS

Jeffrey S. Bevan

Old Dominion University, 1997

Director: Dr. Chuh Mei

Piezoelectric material inherently possesses coupling between electrostatics and structural dynamics. Utilizing linear piezoelectric theory results in an intrinsically coupled pair of piezoelectric constitutive equations. One set describes the direct piezoelectric effect, where strains produce an electric field, and the other set describes the converse effect, where an applied electrical field produces strain. The purpose of this study is to compare the finite element analysis and experiments of a thin plate with bonded piezoelectric material.

Since an isotropic plate in combination with a thin piezoelectric layer constitutes a laminated composite, the classical laminate plate theory is used in the formulation to accommodate generic laminated composite panels with multiple bonded and embedded piezoelectric layers. Additionally, the von Karman large deflection plate theory is incorporated in the stress-strain relations of the laminate. The formulation results in laminate constitutive equations that are amenable to the inclusion of the piezoelectric constitutive equations, yielding a fully coupled electrical-structural composite laminate.

Using the finite element formulation, the governing differential equations of motion of a composite laminate with embedded piezoelectric layers are determined. The finite element model (FEM) not only considers structural nodal degrees of freedom (d.o.f.) but an additional electrical d.o.f. for each piezoelectric layer.

Comparison is performed by treating the piezoelectric first as a sensor, and then again as an actuator. To assess the piezoelectric layer as a sensor, uniformly distributed pressure loads were applied and the corresponding generated voltages were determined using both linear and nonlinear finite element analyses. Experiments were carried out by applying the same uniform distributed loads and measuring the resulting generated voltages and corresponding maximum plate deflections. It is found that a highly nonlinear relation exists between maximum deflection and voltage versus pressure loading.

The dynamic sensor was evaluated by comparing the predicted sensor voltage with the experimental voltage due to a sinusoidal point excitation. In order to assess piezoelectric actuation, a sinusoidal excitation voltage was applied and the center plate deflection was measured experimentally and compared to the predicted displacement. The plate deflection, as a function of time, was determined using the linear finite element analysis.

FOREWORD

The research results contained herein partially fulfill the requirements of NASA research grant NAG1-1684, entitled "Experimental and Numerical Analysis of Structural Acoustic Control for Interior Noise Reduction." This Masters of Science thesis prepared by Jeffrey S. Bevan under the guidance of Professor Chuh Mei of Old Dominion University, Aerospace Engineering Department, constitutes the research results contained herein. The report presents a coupled electrical-structural finite element formulation, finite element analysis, and experimental results of a panel with a bonded piezoelectric sensor and actuator. The Aerospace Engineering Department, Old Dominion University and Langley Research Center Structural Acoustic Branch both provided computational and experimental facilities required to complete the research study. Mr. Travis L. Turner of Langley Research Center Structural Acoustic Branch was the technical monitor.

ACKNOWLEDGMENTS

I would like to express my immense gratitude and appreciation to my advisor Professor Chuh Mei for his never ending encouragement, motivation, and patience throughout this investigation. I am grateful for his uncanny ability to abate seemingly insurmountable tasks into uncomplicated and realizable challenges. This particular ability and his direction afforded me the perseverance and dedication to complete this work.

Additionally I would like to extend my sincere gratitude and appreciation toward my thesis committee members, Dr. Stephen A. Rizzi and Dr. Thomas E. Alberts for providing invaluable assistance and guidance. Also I would like to compliment the Old Dominion University's Aerospace Engineering department and faculty for their dedication, commitment, and invaluable lectures. Special thanks is extended to PCB Piezotronics, Inc. for providing technical assistance, and in particular Lou Zagst for arranging PCB to donate the specialized instrumentation required to complete the experiments.

Appreciation and gratitude must also be extended to the NASA Langley Research Center Structural Acoustics Branch for providing the opportunity to work on this exciting and challenging task. In particular I would like to thank Dr. Richard J. Silcox, Travis L. Turner, and Dr. Gary P. Gibbs of the Structural Acoustics Branch for their efforts and opportunity to complete this work pursuant to Research Grant NAG1-1684.

Most importantly deepest appreciation is extended to my family for their never ending encouragement and personal sacrifices. I am forever grateful for their continued guidance and support toward all my endeavors. My gratitude is expressed not only to my immediate family but also to my extended family, especially Joseph Marklewicz for the expert consultation he provided on the test fixture.

TABLE OF CONTENTS

Page

FOREWORD v

ACKNOWLEDGMENTS vi

LIST OF TABLES x

LIST OF FIGURES xi

LIST OF SYMBOLS xiii

Chapter

I. INTRODUCTION 1

1.1 Historical Perspective 1

1.2 Objective and Outline 5

II. PIEZOELECTRICITY 6

2.1 Introduction 6

2.2 Electrically Equivalent Piezoelectric Model 7

2.3 Piezoelectric Constitutive Equations 9

III. FINITE ELEMENT FORMULATION 15

3.1 Introduction 15

3.2 Displacement Functions 15

3.2.1 Linear Analysis 17

3.2.2 Large Deflection Analysis 19

3.3 Electric Field and Electric Displacement Density 21

3.4 Constitutive Equations 23

3.5 Equations of Motion 24

3.5.1 Generalized Hamilton's Principle 24

3.5.2 Resultant Forces and Moments 26

3.5.3 Stress Resultants for Small Deflections 27

3.5.4 Stress Resultants for Large Deflections 28
3.5.5 Piezoelectric Resultant Forces and Moments 29
3.6 Element Matrices 30
3.6.1 Introduction 30
3.6.2 Linear Stiffness Matrices 30
3.6.3 Large Deflection Equations 34
3.6.4 Mass Matrices 40
3.6.5 External Force Vector 41
3.6.6 Element Equations of Motion 42
3.7 System Matrices 42
3.8 Solution of Static Sensor Equation 44
3.8.1 Newton-Raphson Iteration Method 45
IV. EXPERIMENTAL SETUP 58
4.1 Introduction 58
4.2 Establishment of Clamped Boundary Conditions 58
4.3 Piezoelectric Wafer Preparation 59
4.4 Piezoelectric Lead Attachment 59
4.5 Piezoelectric Wafer Bonding 60
4.6 Uniform Distributed Loading 61
4.7 Material Properties 62
V. NUMERICAL AND EXPERIMENTAL RESULTS 70
5.1 Introduction 70
5.1.1 Static Small Deflection 70
5.1.2 Static Large Deflection 71
5.1.3 Static Sensor 71
5.2 Experimental and Analytical Comparison 73
5.2.1 Static Sensor 74

5.2.2 Dynamic Sensor 75
5.2.3 Dynamic Actuator 77
VI CONCLUSIONS 92
REFERENCES 94
APPENDICES 96
A TRANSFORMATION MATRICES 96
B COORDINATE TRANSFORMATION 101
B.1 Transformed Reduced Stiffness Matrix 101
B.2 Transformation of Piezoelectric *"d"* Constants 102
C ELECTROSTATICS 105
C.1 Introduction 105
C.2 Electrostatic Fields 105
C.3 Electric Displacement and Displacement Density 107
C.4 Potential Function 108
C.5 Capacitance 109
C.6 Electrostatic Energy 110
D Piezoceramic Adhesive 113
E Charge Amplifier Data 114

LIST OF TABLES

Table **Page**

4.1 Piezoceramic Properties 63

4.2 Aluminum Panel Properties 63

5.1 Natural Frequencies and Damping Values 74

LIST OF FIGURES

Figure		Page
2.1	Elastic, thermal, and electrical properties of piezoelectrics	12
2.2	Physical description of the piezoelectric element	13
2.3	Piezoelectric electrical equivalent actuator circuit	14
3.1	Nodal degrees of freedom of a piezoelectric element	54
3.2	Geometry of a laminate with embedded piezoceramics	55
3.3	Isotropic panel with surface mounted piezoceramics	56
3.4	Piezoceramic element for two patches	57
4.1	Plate clamping fixture	64
4.2	Bolt tightening sequence	65
4.3	Piezoceramic location	66
4.4	Piezoceramic mounting preparation	67
4.5	Piezoceramic adhesive preparation	68
4.6	Vacuum plate	69
5.1	Navier solution vs. finite element analysis non-dimensional displacement	79
5.2	Single mode solution vs. finite element analysis non-dimensional displacement	80
5.3	Effective electrode area	81
5.4	Navier solution vs. finite element analysis sensor voltage	82
5.5	Finite element mesh used for comparison with experiment	83
5.6	Comparison of static sensor voltage from linear finite element analysis and experiment	84
5.7	Comparison of non-dimensional displacement from nonlinear finite element analysis and experiment	85
5.8	Comparison of large deflection static sensor voltage from nonlinear finite element and experiment	86
5.9	Shaker location	87

5.10 Comparison of dynamic sensor voltage output from finite element analysis and experiment 88

5.11 Comparison of dynamic plate displacement from finite element analysis and experiment 89

5.12 Time history of electrical actuator signal used in finite element analysis 90

5.13 Comparison of actuator plate displacement from finite element and experiment 91

B1 Principle material coordinates 104

LIST OF SYMBOLS

$[A],[B],[D]$	extension, coupling, and bending panel stiffness matrices
a, b	panel length and width
$\{a\},\{b\}$	generalized coordinates
C	electric capacity
D	plate bending rigidity
D_3	electric displacement density
d_{31}, d_{32}	stress/charge constants
$[e]$	strain/charge constants
E_1, E_2	Young's moduli in principal material directions
E_3	electric field
F	force, surface traction
G_{12}	inplane shear modulus
h	thickness
H	enthalpy
J	current density
$[K],[k]$	system and element stiffness matrices
$[M],[m]$	system and element mass matrices
$\{M\}$	moment vector
$\{N\}$	membrane force vector
$[N1],[n1]$	first-order nonlinear stiffness matrices
$[N2],[n2]$	second-order nonlinear stiffness matrices
$\{P\},\{p\}$	load vectors
Q, q	charge
T	kinetic energy
$[T$	transformation matrix
U	strain energy

V	voltage
u, v	membrane displacements
w	transverse plate displacement
W	work
x, y, z	Cartesian coordinates

Greek Symbols

$\{\varepsilon\}$	total strain vector
β	dielectric impermeability
ϵ	dielectric permittivity
ϵ_o	dielectric permittivity of free space
ϵ_r	relative dielectric permittivity
$[\theta], \{\theta\}$	slope matrix and vector
$\{\kappa\}$	curvature vector
$[\gamma]$	piezoelectric force/volt matrix
υ	Poisson's ratio
ρ	equivalent mass density
ρ_{cs}	surface charge density
$\{\sigma\}$	stress vector
Ψ	electric displacement density

Subscripts

b	bending
cs	surface charge
k	layer number
m	membrane
M	bending moment
np	number of piezoelectric layers
N	membrane force
p	piezoelectric
ϕ	electric degree of freedom

Superscripts

b	body domain
e	electrical
E	constant electric field
o	membrane
σ	constant stress
ε	constant strain
S	surface area
T	transpose

CHAPTER I

INTRODUCTION

1.1 Historical Perspective

The piezoelectric effect was first identified in 1880 by Pierre and Jaques Curie [1] and has remained an active research topic ever since. The Curie's discovered the direct piezoelectric effect by placing a weight upon a crystal and observing that a charge proportional to the weight was generated. Shortly thereafter they confirmed the converse piezoelectric effect by observing an induced strain resulted when a voltage was applied to the crystal. Hence the term piezoelectricity, meaning pressure electricity, was coined to describe this phenomenon. Piezoelectricity remained somewhat of a scientific curiosity since the complexity of the coupled electrical and mechanical properties were unknown. Thus one of the objectives of the earliest research efforts was to better understand the coupled electrical-structural properties of piezoelectric material and to develop accurate analytical models to support and direct engineering design applications.

A portion of the mysterious veil was lifted from piezoelectricity during World War 1 when Professor Langevin, under the auspices of the French government, set out to determine a method to detect submarines [1]. Professor Langevin used piezoelectric crystals in a device that, when submerged underwater, generated a voltage when a disturbing wave front would impinge upon it. Conversely when the device was electrically excited it would vibrate and emit a longitudinal underwater wave. Professor Langevin was unable to conclude his research until after the war, however his device was the predecessor of today's modern sonar transducer.

Another early application of piezoelectricity was discrete crystal circuit devices such as oscillators and filters. The crystal oscillators were extremely stable and were used extensively in military communication equipment. At one point there were in excess of 30 million crystals in military equipment in one year [1]. The crystal controlled oscillators resulted from the research efforts of Cady at Weslyan University [1]. Not only

do piezoelectric crystals possess a characteristic stable resonance, they also are extremely selective, which is indicated by their high mechanical Q values. This sharpness provided the ability to design extremely discriminate filters, resulting in precision circuitry capable of separating simultaneous multiplexed conversations over a single pair of wires. It is not difficult to realize the important role that piezoelectric crystals had in the development of today's modern telecommunications industry.

Another milestone in understanding piezoelectric phenomena was contributed by Professor Mindlin. Mindlin began ground breaking analysis on waves and vibrations in isotropic elastic plates concurrently with high frequency vibration of crystal plates [2]. Subsequent work on isotropic bars and plates lead to unprecedented design and development of electromechanical filters and discrete time delaying devices. Mindlin's pioneering papers on crystal plates may be considered the most significant in modern piezoelectric research, since it clarified the complicated coupled piezoelectric phenomena, leading the way to improved piezoelectric designs for quartz crystal filters. Mindlin's research lead to a sole-supplier contract in 1955 from the U.S. Army Signal Corps, a long time sponsor of the research on crystal plate vibrations, resulting in a monograph entitled "An Introduction to the Mathematical Theory of Elastic Plates". Since the application of quartz filters and other circuit devices such as surface acoustic wave devices, piezoelectric materials have found uses in numerous applications such as dot-matrix printers, computer keyboards, high-frequency stereo speakers, igniters, microphones, accelerometers, and various transducers (force, strain, and pressure), however a new and active research area commonly referred to as smart structures has become a very popular research topic.

The concept of smart structures is a relatively new and diverse field. The fundamental core of smart structures integrates sensors and actuators to structural elements to obtain a state of desirable static and, or dynamic control [3]. The development of smart structures has resulted from three recent significant trends [4]. The

first is the increased utilization of traditional laminated composite structures. The composite material theory incorporates smaller constitutive elements thus permitting the inclusion of piezoelectric constitutive relations with relative ease. It is not unreasonable to visualize a structural member consisting of multiple sensors, actuators, and signal processors.

The second trend is the consideration of coupling the structural and electrical properties by utilizing the off-diagonal terms of the constitutive relations. This practice has been utilized by the large deflection laminated composite theory by including the coupled bending-extensional laminate stiffness. The third trend is the advanced rate of growth within the computer science and electrical engineering disciplines. Hardware improvements such as miniaturization and increased computational power permit faster and more complex algorithms resulting in greater adaptability of the smart structure.

Even though Mindlin's work transformed piezoelectricity from a state of scientific curiosity to an applied science, his higher-order theory of wave propagation is not directly applicable to low frequency structural vibrations of laminated structures. Considering that the physical geometry dictates that the structural resonances occur several orders of magnitude below the piezoelectric crystal's natural frequency, linear piezoelectric theory is exploited where the only electrical and structural interaction arises from the linear piezoelectric constitutive relations [5].

The governing equations for distributed piezoelectric using linear piezoelectric theory combined with the classical laminate plate theory was presented by Lee [6]. Subsequent research has exploited linear piezoelectric theory for numerous smart structure applications such as self-sensing piezoelectric actuators [7] and modal analysis using piezoelectric sensors [8]. The self-sensing piezoelectric actuator results in a truly collocated sensoriactuator capable of simultaneously measuring a structure's dynamic response while providing a controlling input. The collocation characteristic provides a cost benefit by reducing the number of transducers [9]. Furthermore a classical coupled

electrical-structural analysis approach was demonstrated by Lai [10] to control panel flutter.

The classical analytical solution method of piezoelectric structural analysis has been extremely useful, however their solutions are restricted to relatively simple geometries and boundary conditions. Since the finite element method has proved to be a powerful and popular technique for the analysis of complicated structures and multi-field problems it may be applied to the coupled electrical-structural piezoelectric system.

Piezoelectric solid finite elements were formulated and applied to transducers and oscillators by Allik and Hughes [11]. However since smart structures typically consist of thin piezoelectric layers attached to structures that are several orders of magnitude greater in thickness, the solid finite element formulation leads to an inherently inefficient process in which to model the complete physical structure. Thus Tzou and Tseng formulated a new thin piezoelectric solid finite element coupled to shell and plate finite elements [12]. The intrinsic parasitic shear effects associated with such finite elements were eliminated by the introduction of internal d.o.f.'s within the piezoelectric plate element.

One such application of the finite element method incorporating piezoelectric sensors and actuator was presented by Zhou in analyzing and suppressing panel flutter [13]. The flexibility of the finite element method was demonstrated by Zhou by formulating a structural, electrical, and thermal coupled analysis resulting in the control and suppression of panel flutter of composite laminated panels at elevated temperatures. Zhou provided simulation results for aerodynamically induced large deflections with multiple embedded piezoceramic actuators for various ply orientations. In addition Zhou introduced a novel time domain nonlinear solution method by developing a set of forced Duffing equations in reduced modal coordinates. By introducing the modal transformation, the number of equations to be solved is greatly reduced thus affording great computational savings.

1.2 Objective and Outline

Much research has been conducted using linear piezoelectric theory for control in a variety of structural vibration applications. Both classical analysis and the finite element method has been utilized. The objective of this research is to compare the fully coupled electrical-structural finite element analysis of an isotropic panel with a surface mounted piezoelectric patch to experimental test results.

This thesis is organized as follows. In Chapter I, a historical background and the objective of this study is presented. Chapter II introduces the piezoelectric phenomena. In addition, an electrical equivalent model and the coupled linear piezoelectric constitutive relations are introduced. Chapter III presents the finite element formulation, including the fully coupled electrical-structural constitutive relations. An effort has been made to develop the most general formulation applicable to laminated composite plates. To this end, the von Karman large deflection theory was incorporated, based on the results obtained from the experiments conducted. The finite element formulation is then modified to accommodate the inclusion of the electrical degree of freedom to satisfy the electrical-structural coupled linear piezoelectric constitutive relations. Next, the finite element matrices are derived using Hamilton's principle and the subsequent equations of motion assembled. Lastly, solution procedures for the static and dynamic sensor and dynamic actuator are presented. Chapter IV presents the experimental aspects and the test plate clamping fixture design. The fixture design specifications and boundary conditions are discussed along with the applied loading procedures. In addition a discussion of piezoelectric wafer preparation and mounting is presented. Chapter V presents and compares the predicted and experimental results. Comparison of the results obtained from test and analysis of a quasi-static sensor subjected to uniformly distributed loading is presented, along with results for a dynamic sensor due to mechanical point loading and dynamic piezoelectric actuation. Chapter VI provides a discussion of the results and conclusions.

CHAPTER II

PIEZOELECTRICITY

2.1 Introduction

When a piezoelectric material is subjected to mechanical strains or stresses it gives rise to an electric polarization, or it simply generates an electric charge. This phenomenon is referred to as the *direct piezoelectric* effect. Conversely, a piezoelectric material will undergo strain when it is electrically polarized, or subjected to an electric field. This action is referred to as the *converse* or *reciprocal piezoelectric* effect. It is important to note that piezoelectric materials are polarized such that elastic deformation depends on the sign and magnitude of the applied electric field. That is to say, piezoelectric material may undergo either elongation or contraction, simply by reversing the polarity of the applied electric field. It is this polarization that differentiates piezoelectricity from electrostriction. Electrostriction is a function of the square of the electric field, thus sign independent [14]. Since piezoelectric materials exhibit both direct and reciprocal effects the same specimen may be implemented as an actuator or sensor, or both simultaneously [7,15]. The reciprocal effect facilitates actuation and the direct effect favors sensing of structural vibrations. The piezoelectric effect maintains a linear relationship between the electrical and mechanical quantities [5]. Thus linear piezoelectric theory couples quasi-electrostatic field equations with a dynamic structural system. This quasi-electrostatic approximation is valid since the phase velocities of the structural vibrations are several orders of magnitude less than the phase velocities of the electromagnetic waves [5]. The direct and reciprocal piezoelectric property constitutes an inherent electromechanical coupling that is included in the constitutive relations of the structural analysis problem considered herein.

As stated in Section 1.1 piezoelectricity was first discovered in the 1800's. The initial piezoelectric observations utilized naturally occurring crystals such as quartz, tourmaline, and Rochelle salt. Piezoceramics, a manufactured polarized ferroelectric material, are

commonly used in commercial transducer applications and will be analyzed and tested in this study.

Even though piezoelectricity is a linear effect, a complex relationship exists between elastic, mechanical, thermal, and electrical properties. The relationships are shown schematically in Figure 2.1 [14]. The corners of each of the triangles are functions representing the **E** electric field, **D** electric displacement, σ stress, ε strain, T temperature, and S entropy. The piezoelectric effect is shown by the left-hand side of Figure 2.1 indicated by the independent variables *d, g, e,* and *h,* which are the piezoelectric coefficients, the dielectric permittivity ϵ and impermeability β, the stiffness *c* and compliance *s*. Linear piezoelectric theory assumes constant entropy therefore it is an adiabatic process, thus mechanical strains do not contribute to the thermodynamic state of the piezoelectric.

2.2 Electrically Equivalent Piezoelectric Model

The piezoceramic used for this work is in the shape of a thin plate with electroplated electrodes on the top and bottom surfaces as depicted in Figure 2.2. Physically the piezoceramic consists of two conductors separated by a dielectric material. Electric circuit theory calls such a device a capacitor. In circuit theory a capacitor is a passive device, however the piezoceramic is a polarized ferroelectric material that generates a charge proportional to strain as dictated by the direct piezoelectric effect. Thus an electrically equivalent model of the piezoelectric material consists of two charge generators, a capacitor and a resistor as shown in Figure 2.3 [7]. The charge generators q_a, q_p shown in Figure 2.3 represent the applied charge and self-induced charge, respectively. The resistance R_p is the intrinsic electrical resistance of the dielectric which in most cases is very large and represents an electrical open circuit condition which impedes the flow of electric current.

In reference to piezoceramic materials, the applied charge results from an externally applied voltage, and since the piezoceramic is capacitive, the charge accumulates on the

electrodes. By definition electric current is charge in motion, hence the total current flowing out of an enclosed volume must equal the loss of charge within the volume. This is a statement of conservation of charge and leads to the explanation of why current flows in the leads of a capacitor being charged (or discharged) when no current flows between the capacitor plates. Since the piezoelectric specimen behaves as a capacitor the current flow through a piezoelectric by an applied constant voltage is analogous to the charging or discharging of a capacitor [16]. Current flows across the open circuit plates of a capacitor since there is an accumulation of charge on the plates. This can be shown by examination of statement of conservation of charge

$$\oint \mathrm{J} \cdot d\mathrm{a} = -\frac{d}{dt} \int_V \rho_c dV \tag{2.1}$$

where **J** is defined as current density, that is current per meter width, ρ_c is the charge density, and $d\mathbf{a}$ is the differential area with a unit normal vector.

If the volume enclosing the charge remains constant with respect to time then the time derivative may be moved into the volume integral thus

$$\oint \mathrm{J} \cdot d\mathrm{a} = -\int_V \frac{\partial \rho_c}{\partial t} dV \tag{2.2}$$

By applying the divergence theorem, the surface integral is converted into a volume integral so that Eq. (2.2) becomes the time-varying equation of continuity and can be written as

$$\nabla \cdot \mathrm{J} = -\frac{\partial \rho_c}{\partial t} \tag{2.3}$$

If Gauss's law, $\nabla \cdot \mathrm{D} = \rho_c$ is substituted into Eq. (2.3) it becomes

$$\nabla \cdot \mathrm{J} = -\frac{\partial}{\partial t} \nabla \cdot \mathrm{D} \tag{2.4}$$

The electric displacement density **D** is frequently called flux density, and a more complete description may be found in Appendix C. Interchanging differentiation with respect to space and time in Eq. (2.4) yields

$$\nabla \cdot \left(\frac{\partial \mathrm{D}}{\partial t} + \mathrm{J} \right) = 0 \tag{2.5}$$

Casting Eq. (2.5) in integral form and applying the divergence theorem results in

$$\oint \left(\frac{\partial \mathrm{D}}{\partial t} + \mathrm{J} \right) \cdot d\mathrm{a} = 0 \tag{2.6}$$

Hence Eq. (2.6) indicates that the total current of time-varying fields is $\left(\frac{\partial \mathrm{D}}{\partial t} + \mathrm{J} \right)$, where $\frac{\partial \mathrm{D}}{\partial t}$ is a displacement current density due to the time rate of change of the electric displacement density and **J** is the current density resulting from the flow of charge. Thus when considering a capacitor being charged with a direct current, the time varying current density **J** is zero due to the open circuit condition, but Eq. (2.6) indicates the existence of a displacement current density $\frac{\partial \mathrm{D}}{\partial t}$ flowing through the leads of the capacitor being charged, or the piezoceramic.

2.3 Piezoelectric Constitutive Equations

Electric enthalpy density H describes the amount of energy stored within the piezoelectric material. Given the electrical-structural coupling of the piezoelectric material, the electric enthalpy density is the internal coupled strain energy less the stored electrostatic energy density [17]. The stored electrostatic energy density is analogous to the structural elastic strain energy. A detailed derivation of the electrostatic energy may be found in Appendix C. The electric enthalpy density is defined as

$$H = U - \mathbf{D} \cdot \mathbf{E} \tag{2.7}$$

where U is the strain energy, **D** and **E** are the electric displacement density and electric field, respectively whose product represents the electrostatic energy density. The enthalpy may be expanded to yield the following relationship

$$\mathrm{H} = \frac{1}{2}\{\varepsilon\}[Q]^{E}\{\varepsilon\} - \{E\}^{T}[e]\{\varepsilon\} - \frac{1}{2}\{E\}^{T}[\epsilon]^{\varepsilon}\{E\} \tag{2.8}$$

so that

$$\sigma_{ij} = \frac{\partial H}{\partial \varepsilon_{ij}} \tag{2.9}$$

$$D_i = -\frac{\partial H}{\partial E_i} \tag{2.10}$$

where σ_{ij}, ε_{ij} are the stress and strain respectively, D_i and E_i are the electric displacement and electric field respectively, $[Q]^{E}$ is the stiffness matrix measured at constant electric field (short circuit), $[\epsilon]^{\varepsilon}$ is the dielectric permittivity matrix measured at constant strain (clamped), $[e]$ is a matrix of piezoelectric strain constants, and superscript T represents matrix transpose.

Application of Eqs. (2.9) and (2.10) to Eq. (2.8) produces the following coupled electrical-structural piezoelectric constitutive equations

$$\{\sigma\} = [Q]^{E}\{\varepsilon\} - [e]^{T}\{E\} \tag{2.11}$$

$$\{D\} = [e]\{\varepsilon\} + [\epsilon]^{\varepsilon}\{E\} \tag{2.12}$$

Due to practical engineering considerations the piezoelectric strain constants $[e]$ and clamped permittivity matrix $[\epsilon]^{\varepsilon}$ are not typically available. However, the stress constants $[d]$ and the free permittivity matrix $[\epsilon]^{\sigma}$ are readily available and are related to $[e]$ and $[\epsilon]^{\varepsilon}$ by the following relations [12]

$$[e] = [d][Q]^{E} \tag{2.13}$$

$$[\epsilon]^{\varepsilon} = [\epsilon]^{\sigma} - [d][Q]^{E}[d]^{T} \tag{2.14}$$

Thus the piezoelectric constitutive equations can be expressed as

$$\{\sigma\} = [Q]^{E}\left(\{\varepsilon\} - [d]^{T}\{E\}\right) \tag{2.15}$$

$$\{D\} = [d]\{\sigma\} + [\epsilon]^{\sigma}\{E\} \tag{2.16}$$

Furthermore Eq. (2.15) may be substituted into Eq. (2.16) yielding

$$\{D\} = [d][Q]^{E}\left(\{\varepsilon\} - [d]^{T}\{E\}\right) + [\epsilon]^{\sigma}\{E\} \tag{2.17}$$

The following electromagnetic constitutive relation between the electric displacement density and the electric field may be used to clarify the physical meaning of Eq. (2.17)

$$\{D\} = [\epsilon]\left\{\hat{E}\right\} \tag{2.18}$$

Thus Eq. (2.17) can be written as

$$\left\{\hat{E}\right\} = [\beta]^{\sigma}[d]\{\sigma\} + \{E\} \tag{2.19}$$

where $[\beta]^{\sigma}$ is the free dielectric impermeability defined by $[\beta]^{\sigma} = [\epsilon]^{-\sigma}$, and $\{E\}$ is an externally applied electrical field. Thus the direct piezoelectric effect results in an electric field comprised of two components or sources; one self-generated as shown in the first term on the right hand side of Eq. (2.19), and the other due to an externally applied voltage as shown in the second term of the right hand side of Eq. (2.19).

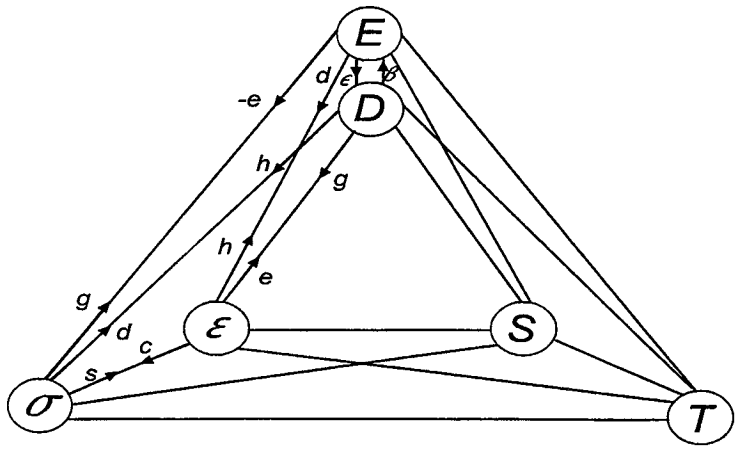

Fig. 2.1 Elastic, thermal, and electrical properties of piezoelectrics

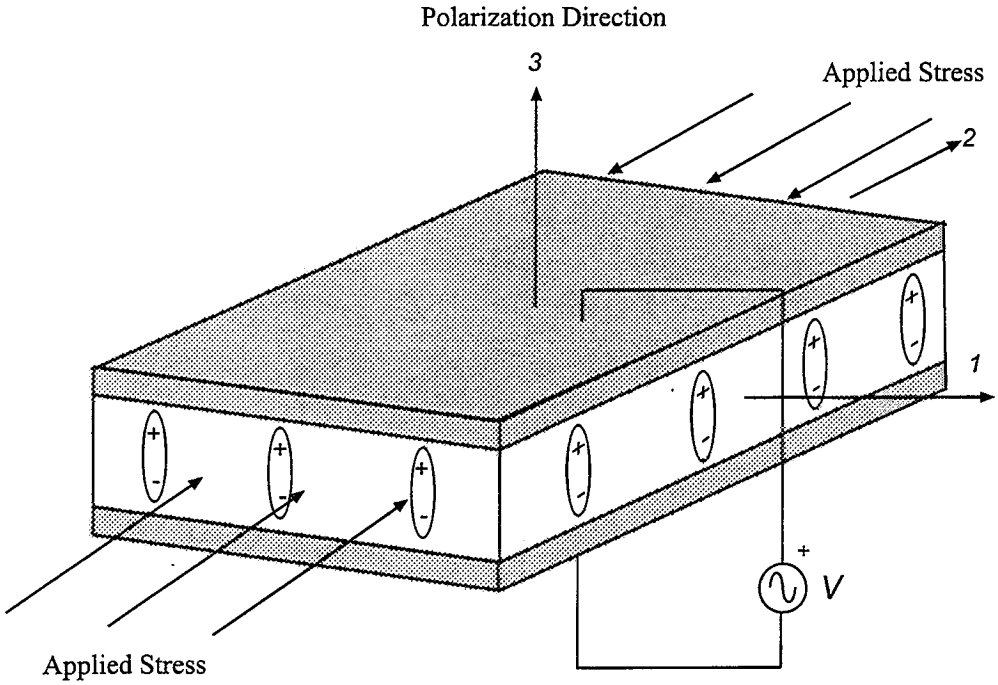

Fig. 2.2 Physical description of the piezoelectric element

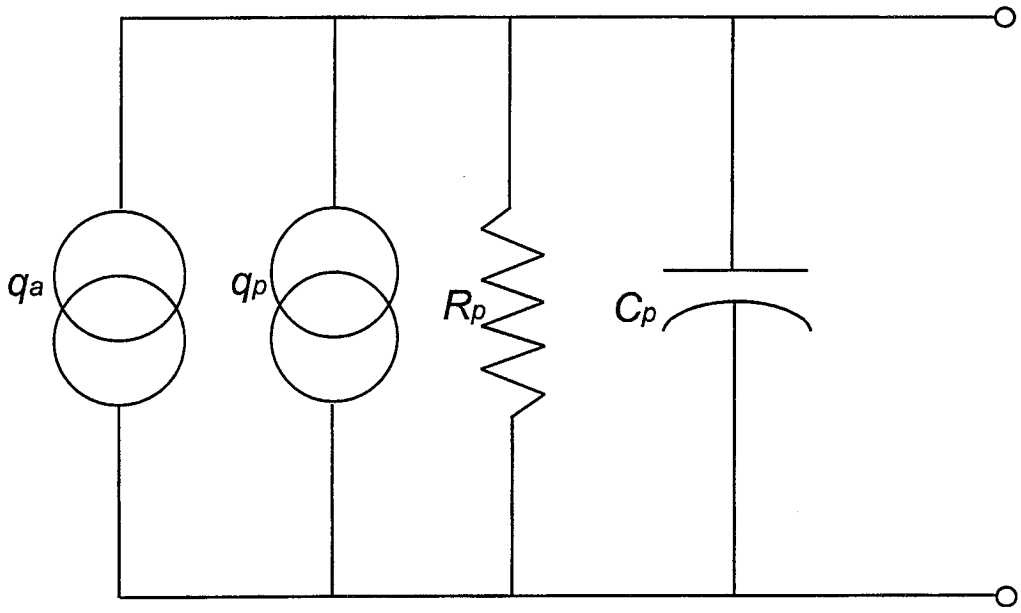

Fig. 2.3 Physical description of the piezoelectric element

CHAPTER III

FINITE ELEMENT FORMULATION

3.1 Introduction

The derivation of the governing differential equations of motion for a panel with embedded piezoelectric layers is introduced in this chapter. The formulation is based on the classic laminate plate theory, including the plane stress assumption and the von Karman large deflection theory. The variational energy method facilitates the formulation of the linear and nonlinear finite element equations of motion in terms of the nodal degrees of freedom (d.o.f.) and the fully coupled structural-electrical properties.

3.2 Displacement Functions

The panel with piezoelectric layers shown in Figure 3.1 is modeled using the four-node modified C^1 conforming straight-sided rectangular plate element. Each element consists of twenty-four structural degrees of freedom. Each node of the element contains four bending d.o.f.'s and two membrane d.o.f.'s to represent the transverse, or out of plane and membrane displacements, respectively. A piezoelectric element maintains consistent structural d.o.f.'s, however an additional electrical d.o.f. is required to satisfy the electrical coupling. Thus the nodal displacement vector is augmented by adding an electrical (voltage) d.o.f for each piezoelectric layer present within the element. The voltage may either be applied to, or generated by the piezoceramic layer or layers. In essence, the electrical d.o.f.'s can be treated as structural displacements.

The element nodal displacement vector consists of the bending and membrane displacements and the voltages which can be written as

$$\{w\} = \{w_b \quad w_m \quad w_\phi\}^T \tag{3.1}$$

The bending and membrane displacements of Eq. (3.1) represent the nodal displacements and are respectively shown as

$$\{w_b\}^T = \{w_1 \quad w_2 \quad w_3 \quad w_4 \quad w_{,x1} \quad w_{,x2} \quad w_{,x3} \quad w_{,x4}$$
$$w_{,y1} \quad w_{,y2} \quad w_{,y3} \quad w_{,y4} \quad w_{,xy1} \quad w_{,xy2} \quad w_{,xy3} \quad w_{,xy4}\} \tag{3.2}$$

$$\{w_m\}^T = \{u_1 \quad u_2 \quad u_3 \quad u_4 \quad v_1 \quad v_2 \quad v_3 \quad v_4\} \tag{3.3}$$

where w represents the transverse deflection, $w_{,x}, w_{,y}$ are the slopes in the x and y directions respectively, $w_{,xy}$ is the second order twist derivative, u and v are the x and y membrane displacements, and the numerical subscript denotes the node number. The electrical d.o.f.'s represented by $\{w_\phi\}$ has voltage components corresponding to each piezoelectric layer and will be subsequently described in greater detail in Section 3.3.

The continuous bending or transverse displacement is approximated using a cubic polynomial given as

$$w = a_1 + a_2 x + a_3 y + a_4 x^2 + a_5 xy + a_6 y^2 + a_7 x^3$$
$$+ a_8 x^2 y + a_9 xy^2 + a_{10} y^3 + a_{11} x^3 y + a_{12} x^2 y^2$$
$$+ a_{13} xy^3 + a_{14} x^3 y^2 + a_{15} x^2 y^3 + a_{16} x^3 y^3 \tag{3.4}$$

which can be written in compact matrix form as

$$w = \lfloor H_w \rfloor \{a\} \tag{3.5}$$

Similarly the continuous in-plane displacements u and v are approximated using bilinear polynomials such as

$$u = b_1 + b_2 x + b_3 y + b_4 xy$$
$$v = b_5 + b_6 x + b_7 y + b_8 xy \tag{3.6}$$

which can also be written in compact vector notation as

$$u = \lfloor H_u \rfloor \{b\} \tag{3.7}$$

$$v = \lfloor H_v \rfloor \{b\} \tag{3.8}$$

The generalized coordinates $\{a\}$ and $\{b\}$ maintain a spatial relationship to the nodal displacements through coordinate transformations and are functions of time only. The transformation relationship is given by

$$\{a\} = [T_b]\{w_b\} \tag{3.9}$$

$$\{b\} = [T_m]\{w_m\} \tag{3.10}$$

Appendix A provides a comprehensive derivation of the bending and membrane transformation matrices $[T_b]$, $[T_m]$. Since the electrical degrees-of-freedom $\{w_\phi\}$ vector represents the voltage per piezoelectric layer and does not possess any preferred geometrical orientation, coordinate transformation is not required.

The displacement field may be expressed in terms of the nodal d.o.f.'s by substituting the respective coordinate transformations into the displacement field approximations, thus substituting Eq. (3.9) into Eq. (3.5) and Eq. (3.10) into Eqs. (3.7) and (3.8) yields

$$\{w\} = \lfloor H_w \rfloor [T_b]\{w_b\} = [B_w]\{w_b\} \tag{3.11}$$

$$\{u\} = \lfloor H_u \rfloor [T_m]\{w_m\} = [B_u]\{w_m\} \tag{3.12}$$

$$\{v\} = \lfloor H_v \rfloor [T_m]\{w_m\} = [B_v]\{w_m\} \tag{3.13}$$

where the $[B_w]$, $[B_u]$, and $[B_v]$ matrices are the shape or interpolation function matrices.

3.2.1 Linear Analysis

The majority of the work considered herein is based on the assumption of small displacements. The strains are therefore comprised of inplane or membrane strains and bending curvatures as

$$\{\varepsilon\} = \{\varepsilon^0\} + z\{\kappa\} \tag{3.14}$$

which can be expanded as

$$\begin{Bmatrix} \varepsilon_x \\ \varepsilon_y \\ \gamma_{xy} \end{Bmatrix} = \begin{Bmatrix} \varepsilon_x^0 \\ \varepsilon_y^0 \\ \gamma_{xy}^0 \end{Bmatrix} + z \begin{Bmatrix} \kappa_x \\ \kappa_y \\ \kappa_{xy} \end{Bmatrix} \tag{3.15}$$

where $\{\varepsilon^0\}$ is the membrane strain vector and $\{\kappa\}$ is the bending curvature vector. The membrane strains and curvatures are functions of the inplane and bending displacement respectively and are defined as

$$\begin{Bmatrix} \varepsilon_x^0 \\ \varepsilon_y^0 \\ \gamma_{xy}^0 \end{Bmatrix} = \begin{Bmatrix} u_{,x} \\ v_{,y} \\ u_{,y}+v_{,x} \end{Bmatrix} \tag{3.16}$$

and

$$\begin{Bmatrix} \kappa_x \\ \kappa_y \\ \kappa_{xy} \end{Bmatrix} = \begin{Bmatrix} -w_{,xx} \\ -w_{,yy} \\ -2w_{,xy} \end{Bmatrix} \tag{3.17}$$

By introducing the approximations for the displacement field as previously defined and recalling the generalized coordinate relationship, the strain vector can be expressed as

$$\{\varepsilon^0\} = \begin{bmatrix} \lfloor H_u \rfloor_{,x} \\ \lfloor H_v \rfloor_{,y} \\ \lfloor H_u \rfloor_{,y} + \lfloor H_v \rfloor_{,x} \end{bmatrix} \{b\} = [C_m]\{b\} \tag{3.18}$$

Similarly the curvature may be expressed in terms of the generalized coordinates as

$$\{\kappa\} = \begin{Bmatrix} -\lfloor H_w \rfloor_{,xx} \\ -\lfloor H_w \rfloor_{,yy} \\ -2\lfloor H_w \rfloor_{,xy} \end{Bmatrix} \{a\} = [C_b]\{a\} \tag{3.19}$$

where the matrices $[C_m]$ and $[C_b]$ result from the differentiation of the shape functions with respect to the dependent variables x and y. Thus $[C_m]$ and $[C_b]$ are defined as

$$[C_m]=\begin{bmatrix}0 & 1 & 0 & y & 0 & 0 & 0 & 0\\ 0 & 0 & 0 & 0 & 0 & 0 & 1 & x\\ 0 & 0 & 1 & x & 0 & 1 & 0 & y\end{bmatrix} \tag{3.20}$$

$$[C_b]=-\begin{bmatrix}0 & 0 & 0 & 2 & 0 & 0 & 6x & 2y & 0 & 0 & 6xy & 2y^2 & 0 & 6xy^2 & 2y^3 & 6xy^3\\ 0 & 0 & 0 & 0 & 0 & 2 & 0 & 0 & 2x & 6y & 0 & 2x^2 & 6xy & 2x^3 & 6x^2y & 6x^3y\\ 0 & 0 & 0 & 0 & 2 & 0 & 0 & 4x & 4y & 0 & 6x^2 & 8xy & 6y^2 & 12x^2y & 12xy^2 & 18x^2y^2\end{bmatrix} \tag{3.21}$$

Expressing the generalized coordinates in terms of the nodal d.o.f.'s the strain and curvature vectors may be written as

$$\{\varepsilon^0\}=[C_m][T_m]\{w_m\}=[B_m]\{w_m\} \tag{3.22}$$

$$\{\kappa\}=[C_b][T_b]\{w_b\}=[B_b]\{w_b\} \tag{3.23}$$

where $[B_m]$ and $[B_b$ are the strain interpolation matrices. Thus the strains in Eq. (3.14) can be written in terms of nodal d.o.f.'s as

$$\{\varepsilon\}=[B_m]\{w_m\}+z[B_b]\{w_b\} \tag{3.24}$$

3.2.2 Large Deflection Analysis

The von Karman plate theory is a geometrical nonlinear theory that accounts for moderately large deflections and small rotations of the mid-surface of the plate. Thus the von Karman large deflection strain-displacement relations are defined as

$$\{\varepsilon\}=\{\varepsilon^0\}+z\{\kappa\} \tag{3.25}$$

where

$$\{\varepsilon^0\}=\{\varepsilon_m^0\}+\{\varepsilon_\theta^0\} \tag{3.26}$$

Hence $\{\varepsilon_m^0\}$ is identical to the previously defined membrane strains $\{\varepsilon^0\}$, and $\{\varepsilon_\theta^0\}$ is the membrane strains induced by the large transverse deflection. The strain-displacement relations for moderately large displacements is defined as

$$\begin{Bmatrix}\varepsilon_x\\ \varepsilon_y\\ \gamma_{xy}\end{Bmatrix}=\begin{Bmatrix}u_{,x}\\ v_{,y}\\ u_{,y}+v_{,x}\end{Bmatrix}+\frac{1}{2}\begin{Bmatrix}w_{,x}^2\\ w_{,y}^2\\ 2w_{,x}\,w_{,y}\end{Bmatrix}+z\begin{Bmatrix}-w_{,xx}\\ -w_{,yy}\\ -2w_{,xy}\end{Bmatrix} \tag{3.27}$$

In future derivations it will become apparent that it is convenient to express the large deflection strain in terms of the slope matrix and slope vector as

$$\{\varepsilon_\theta^0\}=\frac{1}{2}[\theta]\{\theta\} \tag{3.28}$$

where the slope matrix and vector elements are the derivatives of the transverse displacement function. Thus the slope matrix and vector are defined respectively as

$$[\theta]=\begin{bmatrix}w_{,x} & 0\\ 0 & w_{,y}\\ w_{,y} & w_{,x}\end{bmatrix} \tag{3.29}$$

$$\{\theta\}=\begin{Bmatrix}w_{,x}\\ w_{,y}\end{Bmatrix} \tag{3.30}$$

Utilizing the definition of the slope matrix and vector of Eqs. (3.29-30), the strain due to large deflections may be expressed in terms of the generalized coordinates. Recognizing that the slope vector is the derivative of the bending shape functions, Eq. (3.28) becomes

$$\{\varepsilon_\theta^0\}=\frac{1}{2}[\theta]\begin{bmatrix}\lfloor H_w\rfloor_{,x}\\ \lfloor H_w\rfloor_{,y}\end{bmatrix}\{a\}=\frac{1}{2}[\theta][C_\theta]\{a\} \tag{3.31}$$

where $[C_\theta]$ results from the indicated differentiation and is given as

$$[C_\theta]=\begin{bmatrix}0 & 1 & 0 & 2x & y & 0 & 3x^2 & 2xy\\ 0 & 0 & 1 & 0 & x & 2y & 0 & x^2\end{bmatrix}$$

$$\begin{bmatrix}y^2 & 0 & 3x^2y & 2xy^2 & y^3 & 3x^2y^2 & 2xy^3 & 3x^2y^3\\ 2xy & 3y^2 & x^3 & 2x^2y & 3xy^2 & 2x^3y & 3x^2y^2 & 3x^3y^2\end{bmatrix} \tag{3.32}$$

Employing the coordinate transformation, the membrane strains can be expressed in terms of the nodal d.o.f.'s as

$$\{\varepsilon_\theta^0\} = \frac{1}{2}[\theta][C_\theta][T_b]\{w_b\} = \frac{1}{2}[\theta][B_\theta]\{w_b\} \tag{3.33}$$

Hence the strain-displacement relations described in Eq. (3.24) can be written in terms of the nodal d.o.f.'s as

$$\{\varepsilon\} = [B_m]\{w_m\} + \frac{1}{2}[\theta][B_\theta]\{w_b\} + z[B_b]\{w_b\} \tag{3.34}$$

3.3 Electric Field and Electric Displacement Density

In Section 3.2 the nodal displacement vector included a term described as the electrical degrees of freedom. The most general composite piezoelectric element may consist of many piezoelectric layers embedded within a laminated composite panel resulting in a electrical d.o.f. vector which contains an applied (or measured) voltage corresponding to each piezoelectric layer. The electrical d.o.f.'s can therefore be expressed as

$$\{w_\phi\} = \{V_1 \quad V_2 \quad \cdots \quad V_{np}\}^T \tag{3.35}$$

where *np* represents the number of piezoelectric layers presents.

The electrode of the piezoelectric layer establishes an equipotential boundary condition and the dielectric permittivity is assumed isotropic. The voltage establishes a linear electric displacement density and electric field through the thickness of the piezoelectric material. The electric field strength is the negative of the voltage or potential gradient, and is defined as

$$\mathrm{E} = -\nabla V \tag{3.36}$$

The piezoelectric material considered for this study is a thin rectangular plate and assumed to be isotropic, thus the stress/charge constants simplify to $d_{31} = d_{32}$. Since the electrodes are on the top and bottom of the piezoelectric plate, polarization occurs only in the *3*-direction. The stress/charge constant d_{33} is assumed to be constant throughout the thickness which results in an electric field in the *3*-direction only. A detailed explanation

of the stress/charge relations is provided in Appendix B. The total electric field due to all of the piezoelectric layers can therefore be expressed as

$$\{E_3\} = -[B_\phi]\{w_\phi\} \tag{3.37}$$

where the matrix $[B_\phi]$ is a diagonal matrix with elements consisting of the reciprocal of the thickness of each piezoelectric layer. Thus $[B_\phi]$ may be written as

$$[B_\phi] = \begin{bmatrix} \frac{1}{h_1} & \cdots & 0 \\ \vdots & \ddots & \vdots \\ 0 & \cdots & \frac{1}{h_{np}} \end{bmatrix} \tag{3.38}$$

where *np* represents the number of piezoelectric layers present.

Summarizing the above results, the generalized strain-displacement relations based on the small defection assumption can be obtained by combining Eqs. (3.24) and (3.37) as

$$\{\bar{\varepsilon}\} = \begin{Bmatrix} \varepsilon \\ E_3 \end{Bmatrix} = \begin{bmatrix} z[B_b] & [B_m] & 0 \\ 0 & 0 & -[B_\phi] \end{bmatrix} \begin{Bmatrix} w_b \\ w_m \\ w_\phi \end{Bmatrix} \tag{3.39}$$

Similarly, for large deflections, Eq. (3.39) can be modified by including the large deflection strain of Eq. (3.34) yielding

$$\{\tilde{\varepsilon}\} = \begin{Bmatrix} \varepsilon \\ E_3 \end{Bmatrix} = \begin{bmatrix} z[B_b] + \frac{1}{2}[\theta][B_\theta] & [B_m] & 0 \\ 0 & 0 & -[B_\phi] \end{bmatrix} \begin{Bmatrix} w_b \\ w_m \\ w_\phi \end{Bmatrix} \tag{3.40}$$

Since the electric displacement density is assumed to be generated along the polarization axis only (*3*-direction), Eq. (2.17) can be reduced to

$$D_3 = [d][Q](\{\varepsilon\} - E_3\{d\}) + \epsilon_{33}^{\sigma} E_3 \tag{3.41}$$

where the appropriate strain may be employed. The stress/charge coefficients $\{d\}$ are expressed as a vector, due to the geometrical assumptions made during the transformation of the piezoelectric constants described in Appendix B.

3.4 Constitutive Equations

The finite element equations of motion for the plate element used will be derived using classical laminate plate theory (CLPT). The CLPT is used, since in the simplest case a piezoceramic patch bonded to an isotropic substrate constitutes a laminate. In the most general case, a laminated composite element will consist of a typical lay-up with a number of alternating piezoelectric layers. A typical laminated composite with embedded piezoelectric layers is shown in Figure 3.2. A typical isotropic panel with symmetrically bonded surface piezoceramic patches is shown in Figure 3.3. The CLPT assumes that the piezoelectric is perfectly bonded and that each lamina is in a state of plane stress. For the thin plate considered, the rotary inertia and transverse shear deformation effects are assumed negligible.

The stress-strain relations of a specially orthotropic composite lamina and a piezoceramic layer is [18]

$$\begin{Bmatrix} \sigma_1 \\ \sigma_2 \\ \tau_{12} \end{Bmatrix}_s = \begin{bmatrix} Q_{11} & Q_{12} & 0 \\ Q_{12} & Q_{22} & 0 \\ 0 & 0 & Q_{66} \end{bmatrix}_s \begin{Bmatrix} \varepsilon_1 \\ \varepsilon_2 \\ \gamma_{12} \end{Bmatrix} \tag{3.42}$$

and

$$\begin{Bmatrix} \sigma_1 \\ \sigma_2 \\ \tau_{12} \end{Bmatrix}_p = \begin{bmatrix} Q_{11} & Q_{12} & 0 \\ Q_{12} & Q_{22} & 0 \\ 0 & 0 & Q_{66} \end{bmatrix}_p \left(\begin{Bmatrix} \varepsilon_1 \\ \varepsilon_2 \\ \gamma_{12} \end{Bmatrix} - E_{3p} \begin{Bmatrix} d_{31} \\ d_{32} \\ 0 \end{Bmatrix}_p \right) \tag{3.43}$$

where the subscripts s and p indicate the structural and piezoelectric lamina respectively. The piezoelectric material considered is assumed to be isotropic in the *1*- and *2*-directions therefore $d_{31}=d_{32}$. The polarization axis of the piezoceramic is assumed to be such that a positive strain or elongation in the *1*- and *2*-directions results from a "positive" applied voltage referenced to the electrode bonded to the plate.

The stress-strain relations for the k^{th} layer of a laminated composite is obtained by combining Eqs. (3.42) and (3.43) are

$$\begin{Bmatrix}\sigma_x\\ \sigma_y\\ \tau_{xy}\end{Bmatrix}_k = \begin{bmatrix}\overline{Q}_{11} & \overline{Q}_{12} & \overline{Q}_{16}\\ \overline{Q}_{12} & \overline{Q}_{22} & \overline{Q}_{26}\\ \overline{Q}_{16} & \overline{Q}_{26} & \overline{Q}_{66}\end{bmatrix}_k \left(\begin{Bmatrix}\varepsilon_x\\ \varepsilon_y\\ \gamma_{xy}\end{Bmatrix} - E_{3k}\begin{Bmatrix}d_x\\ d_y\\ d_{xy}\end{Bmatrix}_k \right) \tag{3.44}$$

where the transformed reduced lamina stiffness matrix $[\overline{Q}]_k$ is developed from the transformation of the principle material coordinates with respect to the global coordinates, similar transformations exist for the stress, strain, and the stress/charge constants. Appendix B provides a comprehensive derivation of the required principal material coordinate transformations.

For a general orthotropic piezoelectric layer, the generated electric displacement density along the polarization axis (*3*-direction) for the k^{th} layer may be written as

$$D_{3k} = \lfloor d_x \quad d_y \quad d_{xy} \rfloor_k \begin{bmatrix}\overline{Q}_{11} & \overline{Q}_{12} & \overline{Q}_{16}\\ \overline{Q}_{12} & \overline{Q}_{22} & \overline{Q}_{26}\\ \overline{Q}_{16} & \overline{Q}_{26} & \overline{Q}_{66}\end{bmatrix}_k \left(\begin{Bmatrix}\varepsilon_x\\ \varepsilon_y\\ \gamma_{xy}\end{Bmatrix} - E_{3k}\begin{Bmatrix}d_x\\ d_y\\ d_{xy}\end{Bmatrix}_k \right) + \epsilon^{\sigma}_{33k} E_{3k} \tag{3.45}$$

Eqs. (3.44-45) may be condensed in matrix form as

$$\{\sigma\}_k = [\overline{Q}]_k (\{\varepsilon\} - E_{3k}\{d\}_k) \tag{3.46}$$

$$D_{3k} = \{d\}_k^T [\overline{Q}]_k (\{\varepsilon\} - E_{3k}\{d\}_k) + \epsilon^{\sigma}_{33k} E_{3k} \tag{3.47}$$

where $[\overline{Q}]_k$ and $\{d\}_k$ are the lamina stiffness and stress/charge constants respectively for the k^{th} piezoelectric layer and are transformed to the global *x,y* coordinates. For a composite lamina without a piezoelectric layer, set $E_{3k} = \{d\}_k = 0$.

3.5 Equations of Motion

3.5.1 Generalized Hamilton's Principle

Finite element equations of motion for the laminated composite panel with fully coupled electrical-structural properties are derived utilizing the generalized Hamilton's principle [19] to obtain

$$\int_{t_1}^{t_2} \delta(T - U + W_e - W_m + W)dt = 0 \tag{3.48}$$

where T and U are the kinetic energy and strain energy of the system, W_e is the electrical energy, W_m is the magnetic energy, and W is the work done due to external forces and applied electric field. The magnetic energy is negligible for piezoceramic materials if no external magnetic fields are located near the specimen. The kinetic energy of plate element is defined as

$$T = \int_{V} \frac{1}{2}\rho\left(\{\dot{w}\}^T\{\dot{w}\} + \{\dot{u}\}^T\{\dot{u}\} + \{\dot{v}\}^T\{\dot{v}\}\right)dV \tag{3.49}$$

where $\dot{w}$, $\dot{u}$, and $\dot{v}$ are the transverse and membrane velocity components and ρ is the mass per unit volume, and V is the volume of the element. The potential and electrical energies are defined as

$$U = \int_{V} \frac{1}{2}\{\varepsilon\}^T\{\sigma\}dV \tag{3.50}$$

$$W_e = \int_{V} \frac{1}{2}\{E\}^T\{D\}dV \tag{3.51}$$

and the work done on the element by external sources is defined as

$$W = \int_{V} \{w\}^T\{F_b\}dV + \int_{S_1} \{w\}^T\{F_s\}dS + \{w\}^T\{F_c\} - \int_{S_2} V\rho_{cs}dS \tag{3.52}$$

where $\{F_b\}$ is the body force vector, $\{F_s\}$ the surface traction vector, $\{F_c\}$ is the concentrated loading vector, S_1 is the surface area of the applied traction, S_2 is the surface area of the piezoelectric material, V is the voltage applied to the piezoelectric, and ρ_{cs} is the surface charge density generated by the piezoelectric effect. The electrostatic energy results from the charging process of the equivalent piezoelectric capacitance, as described in Appendix C. In Hamilton's principle, all variations must vanish at the time $t = t_1$ and $t = t_2$. The Hamilton's variational statement may be written in the most general form as

$$\int_V \Big[\rho\big(\{\delta\dot{w}\}^T\{\dot{w}\}+\{\delta\dot{u}\}^T\{\dot{u}\}+\{\delta\dot{v}\}^T\{\dot{v}\}\big)$$

$$-\{\delta\varepsilon\}^T\{\sigma\}+\{\delta E\}^T\{D\}+\{\delta w\}^T\{F_b\}\Big]dV$$

$$+\int_{S_1}\{\delta w\}^T\{F_s\}dS-\int_{S_2}\delta V\rho_{cs}dS+\{\delta w\}^T\{F_c\}=0 \tag{3.53}$$

Evaluation of Eq. (3.53) leads to the development of the finite element matrices and the elemental equations of motions.

3.5.2 Resultant Forces and Moments

The stresses of each individual lamina are not necessarily equal, therefore Eq. (3.44) is not directly applicable since the curvatures are typically unknown and are very difficult if not impossible to measure experimentally. However the inplane strains and curvatures of Eq. (3.44) can be related to the applied forces and moments through the static equilibrium conditions thus making Eq. (3.44) more useful [18]. When working with laminated composite plates, it is however very convenient to consider the forces and moments per unit length. Such forces and moments are commonly referred to as the stress resultants. The stress resultants are determined by substituting Eq. (3.44) into the following integral

$$(\{N\},\{M\})=\int_{-h/2}^{h/2}\{\sigma\}_k(1,z)dz \tag{3.54}$$

Substituting Eqn. (3.34) for the k^{th} layer stresses in the above equation and performing the necessary integration leads to the stress resultants of a composite laminate panel as

$$\begin{Bmatrix}N\\M\end{Bmatrix}=\begin{bmatrix}[A] & [B]\\ [B] & [D]\end{bmatrix}\begin{Bmatrix}\varepsilon^0\\ \kappa\end{Bmatrix}-\begin{Bmatrix}N_\phi\\ M_\phi\end{Bmatrix} \tag{3.55}$$

where $[A]$, $[B]$, and $[D$ are the extensional, coupling and bending stiffness matrices of the laminate, respectively, which for an n-layer laminate are defined as

$$[A]=\sum_{k=1}^{n}[\overline{Q}]_k(z_{k+1}-z_k) \tag{3.56}$$

$$[B]=\sum_{k=1}^{n}\frac{1}{2}\left[\overline{Q}\right]_k\left(z_{k+1}^2-z_k^2\right) \tag{3.57}$$

$$[D]=\sum_{k=1}^{n}\frac{1}{3}\left[\overline{Q}\right]_k\left(z_{k+1}^3-z_k^3\right) \tag{3.58}$$

The force and moment vectors resulting from the piezoelectric effect are defined as

$$\left(\{N_\phi\},\{M_\phi\}\right)=\int_{-h/2}^{h/2}\left[\overline{Q}\right]_k\{d\}_k E_{3k}(1,z)dz \tag{3.59}$$

3.5.3 Stress Resultants for Small Deflections

The piezoelectric force and moment vectors will be subsequently examined in much greater detail in Section 3.5.5. Nevertheless, the overall force resultant vector may be expressed in terms of the nodal d.o.f.'s, and are given here for the linear small displacement approximation as

$$\begin{aligned}\{N\}&=[A][C_m][T_m]\{w_m\}+[B][C_b][T_b]\{w_b\}-\{N_\phi\}\\&=[A][B_m]\{w_m\}+[B][B_b]\{w_b\}-\{N_\phi\}\\&=\{N_m\}+\{N_b\}-\{N_\phi\}\end{aligned} \tag{3.60}$$

Similarly the resultant moment vector may also be expressed in terms of the nodal d.o.f.'s as

$$\begin{aligned}\{M\}&=[B][C_m][T_m]\{w_m\}+[D][C_b][T_b]\{w_b\}-\{M_\phi\}\\&=[B][B_m]\{w_m\}+[D][B_b]\{w_b\}-\{M_\phi\}\\&=\{M_m\}+\{M_b\}-\{M_\phi\}\end{aligned} \tag{3.61}$$

3.5.4 Stress Resultants for Large Deflection

The von Karman large deflection strain-displacement relations of Eq. (3.34) are substituted into Eq. (3.55) to determine the resultant force vector, hence

$$\begin{aligned}\{\widetilde{N}\} &= [A]\{\varepsilon_m^0\} + [A]\{\varepsilon_\theta^0\} + [B]\{\kappa\} - \{N_\phi\} \\ &= [A][C_m][T_m]\{w_m\} + \frac{1}{2}[A][\theta][C_\theta][T_b]\{w_b\} \\ &\quad + [B][C_b][T_b]\{w_b\} - \{N_\phi\} \\ &= [A][B_m]\{w_m\} + \frac{1}{2}[A][\theta][B_\theta]\{w_b\} \\ &\quad + [B][B_m]\{w_b\} - \{N_\phi\} \\ &= \{N_m\} + \{N_B\} + \{N_b\} - \{N_\phi\}\end{aligned} \tag{3.62}$$

Similarly the resultant moment vector may be determined as

$$\begin{aligned}\{\widetilde{M}\} &= [B]\{\varepsilon_m^0\} + [B]\{\varepsilon_\theta^0\} + [D]\{\kappa\} - \{M_\phi\} \\ &= [B][C_m][T_m]\{w_m\} + \frac{1}{2}[B][\theta][C_\theta][T_b]\{w_b\} \\ &\quad + [D][C_b][T_b]\{w_b\} - \{M_\phi\} \\ &= [B][B_m]\{w_m\} + \frac{1}{2}[B][\theta][B_\theta]\{w_b\} + [D][B_b]\{w_b\} - \{M_\phi\} \\ &= \{M_m\} + \{M_B\} + \{M_b\} - \{M_\phi\}\end{aligned} \tag{3.63}$$

Comparing Eqs. (3.62) and (3.63) with Eqs. (3.60) and (3.61), the resultant stress $\{N_B\}$ and $\{M_B\}$ are the components due to large deflections.

3.5.5 Piezoelectric Resultant Forces and Moments

Since each piezoelectric layer contributes to the total force resultant vector a summation over the range of *np* piezoelectric layers must be incorporated to account for each piezoelectric layer. Thus the piezoelectric force resultant vector is defined as

$$\{N_\phi\} = \sum_{k=1}^{np} \int_{z_k}^{z_{k+1}} [\overline{Q}]_k \{d\}_k E_{3k} dz \tag{3.64}$$

The lamina stiffness $[\overline{Q}]$, stress/charge constants $\{d\}$, and the electric field $\{E_3\}$ remain constant for each piezoelectric layer with respect to the *3*-direction and are also assumed to be isotropic in the *1*- and *2*- direction, thus the indicated integration reduces to

$$\{N_\phi\} = \sum_{k=1}^{np} [\overline{Q}]_k \{d\}_k h_k E_{3k}$$

$$= [[\overline{Q}]_1 \{d\}_1 h_1 \quad \cdots \quad [\overline{Q}]_k \{d\}_k h_k \quad \cdots \quad [\overline{Q}]_{np} \{d\}_{np} h_{np}] \{E_3\} \tag{3.65}$$

Furthermore Eq. (3.37) may be substituted for $\{E_3\}$ producing

$$\{N_\phi\} = -[[\overline{Q}]_1 \{d\}_1 h_1 \quad \cdots \quad [\overline{Q}]_k \{d\}_k h_k \quad \cdots \quad [\overline{Q}]_{np} \{d\}_{np} h_{np}] [B_\phi] \{w_\phi\} \tag{3.66}$$

$$\{N_\phi\} = -[P_N][B_\phi]\{w_\phi\} \tag{3.67}$$

where

$$[P_N] = [[\overline{Q}]_1 \{d\}_1 h_1 \quad \cdots \quad [\overline{Q}]_k \{d\}_k h_k \quad \cdots \quad [\overline{Q}]_{np} \{d\}_{np} h_{np}] \tag{3.68}$$

Similarly the piezoelectric moment resultant may be expressed as

$$\{M_\phi\} = -[P_M][B_\phi]\{w_\phi\} \tag{3.69}$$

where

$$[P_M] = \left[\frac{1}{2}[\overline{Q}]_1 \{d\}_1 h_1 (z_2 + z_1) \quad \cdots \quad \frac{1}{2}[\overline{Q}]_k \{d\}_k h_k (z_{k+1} + z_k) \quad \cdots \right.$$
$$\left. \frac{1}{2}[\overline{Q}]_{np} \{d\}_{np} h_{np} (z_{np+1} + z_{np})\right] \tag{3.70}$$

3.6 Element Matrices

3.6.1 Introduction

Evaluating the terms in the Hamilton's variational statement of Eq. (3.53) results in the finite element matrices. Variation of the potential and kinetic energies leads to the development of the element stiffness and mass matrices, respectively. During this investigation, body and concentrated forces are neglected.

3.6.2 Linear Stiffness Matrices

The finite element linear stiffness matrices will be determined first by evaluating the potential energy terms of Hamilton's variational statement Eq. (3.53). Thus the potential and electrical energy terms for the k^{th} layer of Eq. (3.53) may be expressed as

$$\int_V \left(\{\delta\varepsilon\}^T\{\sigma\} - \{\delta E\}^T\{D\}\right)dV$$

$$= \int_A \left[\int_{-h/2}^{h/2} \left(\{\delta\varepsilon^0\}^T + z\{\delta\kappa\}^T\right)\{\sigma\}_k\, dz - \int_{-h/2}^{h/2} (\delta E_{3k}) D_{3k}\, dz\right] dA \tag{3.71}$$

where the first integrand represents the strain energy and the second integrand represents the electrical energy due to the polarization properties of the piezoelectric in the *3*-direction only. Thus by applying the stress resultants of Eq. (3.54), the variational energy becomes

$$\int_A \left[\{\delta\varepsilon^0\}^T\{N\} + \{\delta\kappa\}^T\{M\} - \int_{-h/2}^{h/2} (\delta E_{3k}) D_{3k}\, dz\right] dA \tag{3.72}$$

The first term of Eq. (3.72) is evaluated by substituting the force resultant vector of Eq. (3.60) which yields

$$\int_A \{\delta\varepsilon^0\}^T\{N\}dA = \int_A \{\delta\varepsilon^0\}^T\left([A]\{\varepsilon^0\} + [B]\{\kappa\} - \{N_\phi\}\right)dA$$

$$= \int_A \{\delta w_m\}^T [T_m]^T [C_m]^T \left([A][C_m][T_m]\{w_m\}\right.$$

$$\left. + [B][C_b][T_b]\{w_b\} - [P_N]\{E_3\}\right)dA \tag{3.73}$$

Thus by applying the results of Eq. (3.73), the first term of Eq. (3.72) may be expressed in the form

$$\int_A \{\delta w_m\}^T [B_m]^T \left([A][B_m]\{w_m\} + [B][B_b]\{w_b\} + [P_N][B_\phi]\{w_\phi\}\right) dA \qquad (3.74)$$

Similarly by substituting the moment resultants of Eq. (3.61), the second term of Eq. (3.72) becomes

$$\begin{aligned} \int_A \{\delta\kappa\}^T \{M\} dA &= \int_A \{\delta\kappa\}^T \left([B]\{\varepsilon^0\} + [D]\{\kappa\} - \{M_\phi\}\right) dA \\ &= \int_A \{\delta w_b\}^T [T_b]^T [C_b]^T \left([B][C_m][T_m]\{w_m\}\right. \\ &\quad \left. + [D][C_b][T_b]\{w_b\} - [P_M]\{E_{3k}\}\right) dA \end{aligned} \qquad (3.75)$$

By collecting terms, Eq. (3.75) can be simplified as

$$\int_A \{\delta w_b\}^T [B_b]^T \left([B][B_m]\{w_m\} + [D][B_b]\{w_b\} + [P_M][B_\phi]\{w_\phi\}\right) dA \qquad (3.76)$$

The third term of Eq. (3.72) is evaluated by substituting Eq. (3.47) and Eq. (3.14) for the electric displacement density as

$$\int_A \left[\int_{-h/2}^{h/2} \left[(\delta E_{3k}) D_{3k}\, dz\right] dA = \right.$$

$$\int_A \left[\sum_{k=1}^{np} \int_{z_k}^{z_{k+1}} \left[(\delta E_{3k})\{d\}_k^T [\overline{Q}]_k \left(\{\varepsilon^0\} + z\{\kappa\} - E_{3k}\{d\}_k\right) + \epsilon_{33k}^{\sigma} E_{3k}\right] dz\right] dA \qquad (3.77)$$

Again integration of the piezoelectric lamina with respect to the thickness may be simplified by considering the geometric material assumptions previously mentioned. Thus Eq. (3.77) reduces to

$$\begin{aligned} \int_A \Bigg[\sum_{k=1}^{np} &\left[(\delta E_{3k})\{d\}_k^T [\overline{Q}]_k h_k \{\varepsilon^o\} + (\delta E_{3k})\{d\}_k^T [\overline{Q}]_k \{\kappa\} \frac{h_k}{2} (z_{k+1} + z_k)\right. \\ &\left. - (\delta E_{3k})\{d\}_k^T [\overline{Q}]_k \{d\}_k E_{3k} h_k + (\delta E_{3k}) \epsilon_{33k}^{\sigma} E_{3k} h_k\right] dA \end{aligned} \qquad (3.78)$$

By considering the laminate and utilizing matrix notation, Eq. (3.78) may be expressed as

$$\int_A [-\{\delta w_\phi\}^T [B_\phi]^T [P_N]^T [B_m]\{w_m\}$$

$$-\{\delta w_\phi\}^T [B_\phi]^T [P_M]^T [B_b]\{w_b\}$$

$$+\{\delta w_\phi\}^T [B_\phi]^T ([\epsilon_{33}^\sigma]-[\gamma])\{w_\phi\}]dA \tag{3.79}$$

where the matrices $[\epsilon_{33}^\sigma]$ and $[\gamma]$ are defined as

$$[\epsilon_{33}^\sigma]=\begin{bmatrix} \epsilon_{331}^\sigma & \cdots & 0 \\ \vdots & \epsilon_{33k}^\sigma & \vdots \\ 0 & \cdots & \epsilon_{33np}^\sigma \end{bmatrix} \tag{3.80}$$

$$[\gamma]=\begin{bmatrix} \{d\}_1^T [\overline{Q}]_1 \{d\}_1 & \cdots & 0 \\ \vdots & \{d\}_k^T [\overline{Q}]_k \{d\}_k & \vdots \\ 0 & \cdots & \{d\}_{np}^T [\overline{Q}]_{np} \{d\}_{np} \end{bmatrix} \tag{3.81}$$

Thus combining Eqs. (3.74), (3.76), (3.79) yields Hamilton's variational statement, less the kinetic energy terms, which can be expressed as

$$\int_A [\{\delta w_m\}^T [B_m]^T [A][B_m]\{w_m\} \tag{3.82a}$$

$$+\{\delta w_m\}^T [B_m]^T [B][B_b]\{w_b\} \tag{3.82b}$$

$$+\{\delta w_m\}^T [B_m]^T [P_N][B_\phi]\{w_\phi\} \tag{3.82c}$$

$$+\{\delta w_b\}^T [B_b]^T [B][B_m]\{w_m\} \tag{3.82d}$$

$$+\{\delta w_b\}^T [B_b]^T [D][B_b]\{w_b\} \tag{3.82e}$$

$$+\{\delta w_b\}^T [B_b]^T [P_M][B_\phi]\{w_\phi\} \tag{3.82f}$$

$$+\{\delta w_\phi\}^T[B_\phi]^T[P_M]^T[B_b]\{w_b\} \tag{3.82h}$$

$$+\{\delta w_\phi\}^T[B_\phi]^T([\gamma]-[\epsilon_{33}^\sigma])\{w_\phi\}]dA=0 \tag{3.82i}$$

The element stiffness matrices are determined from Eq. (3.82) and may be cast into a matrix form of

$$\begin{Bmatrix}\delta w_b\\ \delta w_m\\ \delta w_\phi\end{Bmatrix}^T\begin{bmatrix}[k_b] & [k_{bm}] & [k_{b\phi}]\\ [k_{mb}] & [k_m] & [k_{m\phi}]\\ [k_{\phi b}] & [k_{\phi m}] & [k_\phi]\end{bmatrix}\begin{Bmatrix}w_b\\ w_m\\ w_\phi\end{Bmatrix} \tag{3.83}$$

where the corresponding linear stiffness matrices are

$$[k_m]=\int_A[B_m]^T[A][B_m]dA \tag{3.84}$$

$$[k_{mb}]=\int_A[B_m]^T[B][B_b]dA \tag{3.85}$$

$$[k_{m\phi}]=\int_A[B_m]^T dA[P_N][B_\phi] \tag{3.86}$$

$$[k_{bm}]=\int_A[B_b]^T[B][B_m]dA \tag{3.87}$$

$$[k_b]=\int_A[B_b]^T[D][B_b]dA \tag{3.88}$$

$$[k_{b\phi}]=\int_A[B_b]^T dA[P_M][B_\phi] \tag{3.89}$$

$$[k_{\phi m}]=[B_\phi]^T[P_N]^T\int_A[B_m]dA \tag{3.90}$$

$$[k_{\phi b}]=[B_\phi]^T[P_M]^T\int_A[B_b]dA \tag{3.91}$$

$$[k_\phi]=[B_\phi]^T([\gamma]-[\epsilon_{33}^\sigma])A \tag{3.92}$$

3.6.3 Large Deflection Equations

The nonlinear element stiffness matrices are determined by following the same procedure outlined for the linear stiffness matrices in Section 3.6.2. In order to determine the nonlinear stiffness matrices, the von Karman large deflection strain must be included in the Hamilton's variational statement. The resulting variational potential and electrical energy statement, including the von Karman large deflection strain, may be expressed as

$$\int_A \Big[\int_{-h/2}^{h/2} \left(\{\delta\varepsilon^0\}^T + z\{\delta\kappa\}^T \right) \{\sigma\}_k \, dz$$

$$- \sum_{k=1}^{np} \int_{z_k}^{z_{k+1}} \left[(\delta E_{3k}) \left\{ \{d\}_k^T [\overline{Q}]_k \{\varepsilon^0\} + z\{\kappa\} - \{d\}_k E_{3k} + E_{3k} \epsilon_{33k}^{\sigma} \right\} \right] dz \Big] dA \tag{3.93}$$

Considering the stress resultants of Eq. (3.54) and substituting the results into the first integrand of Eq. (3.93) yields

$$\int_A \left[\{\delta\varepsilon^o\}^T \{\widetilde{N}\} + \{\delta\kappa\}^T \{\widetilde{M}\} \right] dA \tag{3.94}$$

Since the membrane strain and curvatures are independent of the plate thickness, the variations in Eq. (3.94) becomes

$$\{\delta\varepsilon^o\}^T = \{\delta w_m\}^T [B_m]^T + \{\delta w_b\}^T [B_\theta]^T [\theta]^T \tag{3.95}$$

$$\{\delta\kappa\}^T = \{\delta w_b\}^T [B_b]^T \tag{3.96}$$

where the following relation is utilized

$$\begin{aligned} \delta\left(\frac{1}{2} [\theta][B_\theta]\{w_b\} \right) &= \frac{1}{2} [\delta\theta][B_\theta]\{w_b\} + \frac{1}{2} [\theta][B_\theta]\{\delta w_b\} \\ &= [\theta][B_\theta]\{\delta w_b\} \end{aligned} \tag{3.97}$$

The second integrand of Eq. (3.93) may be similarly evaluated by substituting the von Karman large displacements of Eq. (3.34) and performing the variational operation described above in Eqs. (3.95) and (3.96). Evaluation of the linear terms follows the

procedure outlined in Eqs. (3.78) and (3.79). Hence the variational statement of Eq. (3.93) becomes

$$\int_A [\{\delta w_m\}^T [B_m]^T ([A][B_m]\{w_m\} + \frac{1}{2}[A][\theta][B_\theta]\{w_b\}$$

$$+ [B][B_b]\{w_b\} - \{N_\phi\})$$

$$+ \{\delta w_b\}^T [B_\theta]^T [\theta]^T ([A][B_m]\{w_m\} + \frac{1}{2}[A][\theta][B_\theta]\{w_b\}$$

$$+ [B][B_b]\{w_b\} - \{N_\phi\})$$

$$+ \{\delta w_b\}^T [B_b]^T ([B][B_m]\{w_m\} + \frac{1}{2}[B][\theta][B_\theta]\{w_b\}$$

$$+ [D][B_b]\{w_b\} - \{M_\phi\})$$

$$+ \{\delta w_\phi\}^T [B_\phi]^T [P_N]^T \left([B_m]\{w_m\} + \frac{1}{2}[\theta][B_\theta]\{w_b\} \right)$$

$$+ \{\delta w_\phi\}^T [B_\phi]^T [P_M]^T [B_b]\{w_b\}$$

$$+ \{\delta w_\phi\}^T [B_\phi]^T ([\gamma] - [\epsilon_{33}^\sigma])\{w_\phi\}] dA = 0 \qquad (3.98)$$

The variational statement contains identical terms which lead to the linear stiffness matrices, however nonlinear stiffness matrices resulting from the von Karman large deflection will appear and are indicated by the inclusion of the slope matrix. Thus the variational potential energy statement in Eq. (3.98) may be written as

$$\int_A [\{\delta w_m\}^T [B_m]^T [A][B_m]\{w_m\} \tag{3.99a}$$

$$+\frac{1}{2}\{\delta w_m\}^T [B_m]^T [A][\theta][B_\theta]\{w_b\} \tag{3.99b}$$

$$+\{\delta w_m\}^T [B_m]^T [B][B_b]\{w_b\} \tag{3.99c}$$

$$+\{\delta w_m\}^T [B_m]^T [P_N][B_\phi]\{w_\phi\} \tag{3.99d}$$

$$+\{\delta w_b\}^T [B_\theta]^T [\theta]^T [A][B_m]\{w_m\} \tag{3.99e}$$

$$+\frac{1}{2}\{\delta w_b\}^T [B_\theta]^T [\theta]^T [A][\theta][B_\theta]\{w_b\} \tag{3.99f}$$

$$+\{\delta w_b\}^T [B_\theta]^T [\theta]^T [B][B_b]\{w_b\} \tag{3.99g}$$

$$+\{\delta w_b\}^T [B_\theta]^T [\theta]^T [P_N][B_\phi]\{w_\phi\} \tag{3.99h}$$

$$+\{\delta w_b\}^T [B_b]^T [B][B_m]\{w_m\} \tag{3.99i}$$

$$+\frac{1}{2}\{\delta w_b\}^T [B_b]^T [B][\theta][B_\theta]\{w_b\} \tag{3.99j}$$

$$+\{\delta w_b\}^T [B_b]^T [D][B_b]\{w_b\} \tag{3.99k}$$

$$+\{\delta w_b\}^T [B_b]^T [P_M][B_\phi]\{w_\phi\} \tag{3.99l}$$

$$+\{\delta w_\phi\}^T [B_\phi]^T [P_N]^T [B_m]\{w_m\} \tag{3.99m}$$

$$+\frac{1}{2}\{\delta w_\phi\}^T [B_\phi]^T [P_N]^T [\theta][B_\theta]\{w_b\} \tag{3.99n}$$

$$+\{\delta w_\phi\}^T [B_\phi]^T [P_M]^T [B_b]\{w_b\} \tag{3.99o}$$

$$+\{\delta w_\phi\}^T [B_\phi]^T ([\gamma]-[\epsilon_{33}^\sigma])\{w_\phi\}]dA = 0 \tag{3.99p}$$

Note that the linear expressions indicated in Eqs. (3.99a, c, d, i, k, m, o, p) are identical to those of Eqs. (3.82a, b, c, d, e, g, h, i) respectively. The remaining expressions which contain the slope matrix will lead to the nonlinear stiffness matrices. The following transformation relationship is applicable for any force resultant vector and will be utilized to further simplify expressions for the nonlinear stiffness matrices. Thus the product of the transpose of the slope matrix and any force vector may be expressed as

$$[\theta]^T\{N_i\} = \begin{bmatrix} w_{,x} & 0 & w_{,y} \\ 0 & w_{,y} & w_{,x} \end{bmatrix} \begin{Bmatrix} N_x \\ N_y \\ N_{xy} \end{Bmatrix}_i = \begin{Bmatrix} N_x w_{,x} + N_{xy} w_{,y} \\ N_y w_{,y} + N_{xy} w_{,x} \end{Bmatrix}_i \tag{3.100}$$

likewise

$$[N_i]\{\theta\} = \begin{bmatrix} N_x & N_{xy} \\ N_{xy} & N_y \end{bmatrix}_i \begin{Bmatrix} w_{,x} \\ w_{,y} \end{Bmatrix} = \begin{Bmatrix} N_x w_{,x} + N_{xy} w_{,y} \\ N_y w_{,y} + N_{xy} w_{,x} \end{Bmatrix}_i \tag{3.101}$$

Thus by applying Eqs. (3.9) and (3.32), the above relation yields

$$[\theta]^T\{N_i\} = [N_i]\{\theta\} = [N_i][C_\theta]\{a\} = [N_i][B_\theta]\{w_b\} \qquad i = b, m, \theta, \phi \tag{3.102}$$

Equations (3.99e) and (3.99h) may be manipulated into a symmetrical form. Thus Eq. (3.99e) becomes

$$\{\delta w_b\}^T \int_A [B_\theta]^T [\theta]^T [A][B_m]\{w_m\} dA =$$

$$\frac{1}{2}\{\delta w_b\}^T \int_A [B_\theta]^T [\theta]^T \left[[A][B_m]\{w_m\} + [N_m][B_\theta]\{w_b\}\right] dA \tag{3.103}$$

and Eq. (3.99h) becomes

$$\{\delta w_b\}^T \int_A [B_\theta]^T [\theta]^T [P_N][B_\phi]\{w_\phi\} dA =$$

$$\frac{1}{2}\{\delta w_b\}^T \int_A [B_\theta]^T \left([\theta]^T [P_N][B_\phi]\{w_\phi\} - [N_\phi][B_\theta]\{w_b\}\right) dA \tag{3.104}$$

where the membrane force vectors of Eqs. (3.62) and (3.67) are used. Combining Eq. (3.103) with Eq. (3.99b) the resulting expression becomes

$$\int_A \Big[\frac{1}{2} \{\delta w_b\}^T [B_\theta]^T [\theta]^T [A][B_m]\{w_m\} + \frac{1}{2} \{\delta w_b\}^T [B_\theta]^T [N_m][B_\theta]\{w_b\} + \frac{1}{2} \{\delta w_m\}^T [B_m]^T [A][\theta][B_\theta]\{w_b\} \Big] dA \tag{3.105}$$

The above relationship may be expressed in terms of the first order nonlinear stiffness matrices as

$$\frac{1}{2} \left(\{\delta w_b\}^T [n1_{bm}]\{w_m\} + \{\delta w_b\}^T [n1_{Nm}]\{w_b\} + \{\delta w_m\}^T [n1_{mb}]\{w_b\} \right) \tag{3.106}$$

where the first-order nonlinear element stiffness matrices are given by

$$[n1_{bm}] = \int_A [B_\theta][\theta]^T [A][B_m] dA \tag{3.107}$$

$$[n1_{Nm}] = \int_A [B_\theta]^T [N_m][B_\theta] dA \tag{3.108}$$

$$[n1_{mb}] = \int_A [B_m]^T [A][\theta][B_\theta] dA \tag{3.109}$$

Equation (3.104) may be expressed as

$$\frac{1}{2} \left(\{\delta w_b\}^T [n1_{b\phi}]\{w_\phi\} + \{\delta w_b\}^T [n1_{N\phi}]\{w_b\} \right) \tag{3.110}$$

where

$$[n1_{b\phi}] = \int_A [B_\theta]^T [\theta]^T dA [P_N][B_\phi] \tag{3.111}$$

$$[n1_{N\phi}] = -\int_A [B_\theta]^T [N_\phi][B_\theta] dA \tag{3.112}$$

Similarly Eq. (3.99g) may be expressed symmetrically utilizing the bending force vector and adding it to Eq. (3.99j), hence

$$\int_A \left[\frac{1}{2} \{\delta w_b\}^T [B_\theta]^T [\theta]^T [B][B_b] \{w_b\} \right.$$

$$+ \frac{1}{2} \{\delta w_b\}^T [B_\theta]^T [N_B][B_\theta] \{w_b\}$$

$$\left. + \frac{1}{2} \{\delta w_b\}^T [B_b]^T [B][\theta][B_\theta] \{w_b\} \right] dA \tag{3.113}$$

Equation (3.113) can be expressed as the first-order nonlinear stiffness matrix due to the laminate coupling matrix $[B]$ and large deflection effects as

$$\frac{1}{2} \{\delta w_b\}^T [n1_{NB}] \{w_b\} \tag{3.114}$$

where

$$[n1_{NB}] = \int_A \left([B_\theta]^T [\theta]^T [B][B_b] + [B_\theta]^T [N_b][B_\theta] + [B_b]^T [B][\theta][B_\theta] \right) dA \tag{3.115}$$

The first-order nonlinear stiffness matrix due to electromechanical coupling can be determined from Eq. (3.99n) as

$$-\frac{1}{2} \{\delta w_\phi\}^T [n1_{\phi b}] \{w_b\} \tag{3.116}$$

where

$$[n1_{\phi b}] = [B_\phi]^T [P_N]^T \int_A [\theta][B_\theta] dA \tag{3.117}$$

The second-order nonlinear stiffness matrix is determined from Eq. (3.99f) as

$$\frac{1}{3} \{\delta w_b\}^T [n2_b] \{w_b\} \tag{3.118}$$

where

$$[n2_b] = \frac{3}{2} \int_A [B_\theta]^T [\theta]^T [A][\theta][B_\theta] dA \tag{3.119}$$

combining all the stiffness matrices the complete variation statement becomes

$$\int_V \left[\{\delta\varepsilon\}^T\{\sigma\} - \{\delta E\}^T\{D\}\right]dV = \int_A \Big(\{\delta w_m\}^T[k_m]\{w_m\} + \{\delta w_m\}^T\left([k_{mb}] + \frac{1}{2}[n1_{mb}]\right)\{w_b\}$$

$$+ \{\delta w_m\}^T[k_{m\phi}]\{w_\phi\} + \{\delta w_b\}^T\left([k_{bm}] + \frac{1}{2}[n1_{bm}]\{w_m\}\right)$$

$$+ \{\delta w_b\}^T\left([k_{b\phi}] + \frac{1}{2}[n1_{b\phi}]\right)\{w_\phi\} + \{\delta w_b\}^T([k_b] + \frac{1}{2}[n1_{Nm}]$$

$$-\frac{1}{2}[n1_{N\phi}] + \frac{1}{2}[n1_{NB}] + \frac{1}{3}[n2_b])\{w_b\}$$

$$+ \{\delta w_\phi\}^T[k_{\phi m}]\{w_m\}$$

$$+ \{\delta w_\phi\}^T[k_{\phi b}]\{w_b\}$$

$$+ \{\delta w_b\}^T[k_{b\phi}]\{w_\phi\}$$

$$+ \frac{1}{2}\{\delta w_b\}^T[n1_{b\phi}]\{w_\phi\}$$

$$+ \frac{1}{2}\{\delta w_\phi\}^T[n1_{\phi b}]\{w_b\}$$

$$+ \{\delta w_\phi\}^T[k_\phi]\{w_\phi\})dA \qquad (3.120)$$

The integrand on the right-hand side of Eq. (3.120) may be conveniently cast into matrix form as

$$\begin{Bmatrix}\delta w_b\\ \delta w_m\\ \delta w_\phi\end{Bmatrix}^T\left(\begin{bmatrix}[k_b] & [k_{bm}] & [k_{b\phi}]\\ [k_{mb}] & [k_m] & [k_{m\phi}]\\ [k_{\phi b}] & [k_{\phi m}] & [k_\phi]\end{bmatrix} + \frac{1}{3}\begin{bmatrix}[n2_b] & [0] & [0]\\ [0] & [0] & [0]\\ [0] & [0] & [0]\end{bmatrix} - \frac{1}{2}\begin{bmatrix}[n1_{N\phi}] & [0] & [0]\\ [0] & [0] & [0]\\ [0] & [0] & [0]\end{bmatrix}\right.$$

$$\left. + \frac{1}{2}\begin{bmatrix}[n1_{NB} + n1_{Nm}] & [n1_{bm}] & [n1_{b\phi}]\\ [n1_{mb}] & [0] & [0]\\ [n1_{\phi b}] & [0] & [0]\end{bmatrix}\right)\begin{Bmatrix}w_b\\ w_m\\ w_\phi\end{Bmatrix} \qquad (3.121)$$

3.6.4 Mass Matrices

The variation of the kinetic energy terms of Eq. (3.43) leads to the element mass matrices, which consist of mechanical quantities only, since the electrical d.o.f.'s do not have an equivalent inertial analogy. Thus the variational kinetic energy may be written as

$$\int_V \rho\left(\{\delta\dot{w}\}^T\{\dot{w}\} + \{\delta\dot{u}\}^T\{\dot{u}\} + \{\delta\dot{v}\}^T\{\dot{v}\}\right)dV$$

$$= -\int_V \rho\left(\{\delta w\}^T\{\ddot{w}\} + \{\delta u\}^T\{\ddot{u}\} + \{\delta v\}^T\{\ddot{v}\}\right)dV$$

$$= -\left(\{\delta w_b\}^T[m_b]\{\ddot{w}_b\} + \{\delta w_m\}^T[m_m]\{\ddot{w}_m\}\right) \tag{3.122}$$

where the element mass matrices are given by

$$[m_b] = [T_b]^T \int_A \{H_w\} h\rho(x,y) \lfloor H_w \rfloor dA [T_b] \tag{3.123}$$

$$[m_m] = [T_m]^T \left(\int_A \{H_u\} h\rho(x,y) \lfloor H_u \rfloor + \int_A \{H_v\} h\rho(x,y) \lfloor H_v \rfloor \right) dA [T_m] \tag{3.124}$$

3.6.5 External Force Vector

In completing the variations indicated in the Hamilton's variational statement of Eq. (3.43), the work done due to external forces, body forces and surface traction's were assumed negligible, however the electrostatic work due to the externally applied voltage must be included. The electrostatic work done as, described in Appendix C, is given by Eq. (C.23). Since the space charge within the volume of the piezoelectric is zero, only a surface charge accumulates on the electrode surfaces, hence the virtual electrostatic work done can be expressed as

$$\int_{S_2} \delta V \rho_{cs} dS = \int_{S_2} \{\delta w_\phi\}^T \{\rho_{cs}\} dA = -\{\delta w_\phi\}^T \{p_\phi\} \tag{3.125}$$

where

$$\{p_\phi\} = -\int_A \{\rho_{cs}\} dA \tag{3.126}$$

3.6.6 Element Equations of Motion

The element equations of motion may be formed by substituting Eqs. (3.120), (3.121), and (3.125) into Hamilton's variational statement Eq. (3.53), and collecting terms, resulting in

$$\begin{bmatrix} m_b & 0 & 0 \\ 0 & m_m & 0 \\ 0 & 0 & 0 \end{bmatrix} \begin{Bmatrix} \ddot{w}_b \\ \ddot{w}_m \\ \ddot{w}_\phi \end{Bmatrix} + \left(\begin{bmatrix} k_b & k_{bm} & k_{b\phi} \\ k_{mb} & k_m & k_{m\phi} \\ k_{\phi b} & k_{\phi m} & k_\phi \end{bmatrix} + \frac{1}{3} \begin{bmatrix} n2_b & 0 & 0 \\ 0 & 0 & 0 \\ 0 & 0 & 0 \end{bmatrix} - \frac{1}{2} \begin{bmatrix} n1_{N\phi} & 0 & 0 \\ 0 & 0 & 0 \\ 0 & 0 & 0 \end{bmatrix} \right.$$

$$\left. + \frac{1}{2} \begin{bmatrix} n1_{NB} + n1_{Nm} & n1_{bm} & n1_{b\phi} \\ n1_{mb} & 0 & 0 \\ n1_{\phi b} & 0 & 0 \end{bmatrix} \right) \begin{Bmatrix} w_b \\ w_m \\ w_\phi \end{Bmatrix} = \begin{Bmatrix} p_b \\ p_m \\ p_\phi \end{Bmatrix} \tag{3.127}$$

3.7 System Matrices

The element equations of motion Eq. (3.127), are a set of equations which describe the fully coupled structural and electrical properties. Application of Eq. (3.127) requires the implementation of an assembly procedure in accordance to the prescribed electrical and structural boundary conditions. The assembly process for the structural stiffness can be shown symbolically as

$$[K] = \sum [k] \tag{3.128}$$

where the global stiffness matrix $[K]$ has dimensions m x m for m structural and electrical d.o.f.'s and the element stiffness $[k]$ is of size (24+np)x(24+np). The assembly procedure can be visualized by first starting with a null global stiffness matrix, then subsequently adding to it $[k]$ of each element until all the elements are considered. Assembly of the mass matrix is accomplished using an identical procedure, however special attention is required for the piezoelectric elements and will be subsequently discussed in greater detail. Assembly of Eq. (3.127) yields the following fully coupled system of equations

$$\begin{bmatrix} M & 0 \\ 0 & 0 \end{bmatrix}\begin{Bmatrix} \ddot{W} \\ \ddot{W}_\phi \end{Bmatrix}+\left(\begin{bmatrix} K_w & K_{w\phi} \\ K_{\phi w} & K_\phi \end{bmatrix}+\frac{1}{2}\begin{bmatrix} N1 & 0 \\ 0 & 0 \end{bmatrix}+\frac{1}{3}\begin{bmatrix} N2 & 0 \\ 0 & 0 \end{bmatrix}\right.$$

$$\left.+\frac{1}{2}\begin{bmatrix} 0 & N1_{w\phi} \\ N1_{\phi w} & 0 \end{bmatrix}-\frac{1}{2}\begin{bmatrix} N1_{N\phi} & 0 \\ 0 & 0 \end{bmatrix}\right)\begin{Bmatrix} W \\ W_\phi \end{Bmatrix}=\begin{Bmatrix} P_w \\ P_\phi \end{Bmatrix} \tag{3.129}$$

where the system matrices and vectors are

$$[M]=\begin{bmatrix} [M_b] & [0] \\ [0] & [M_m] \end{bmatrix} \tag{3.130}$$

$$[K_w]=\begin{bmatrix} [K_b] & [K_{bm}] \\ [K_{mb}] & [K_m] \end{bmatrix} \tag{3.131}$$

$$[K_{W\phi}]=\begin{bmatrix} [K_{b\phi}] \\ [K_{m\phi}] \end{bmatrix} \tag{3.132}$$

$$[K_{\phi w}]=\begin{bmatrix} [K_{\phi b}] & [K_{\phi m}] \end{bmatrix} \tag{3.133}$$

$$[N1]=\begin{bmatrix} [N1_{NB}+N1_{Nm}] & [N1_{bm}] \\ [N1_{mb}] & [0] \end{bmatrix} \tag{3.134}$$

$$[N1_{w\phi}]=\begin{bmatrix} [N1_{b\phi}] \\ [0] \end{bmatrix} \tag{3.135}$$

$$[N1_{N\phi}]=\begin{bmatrix} [N1_{N\phi}] & [0] \\ [0] & [0] \end{bmatrix} \tag{3.136}$$

$$[N2]=\begin{bmatrix} [N2_b] & [0] \\ [0] & [0] \end{bmatrix} \tag{3.137}$$

$$\{W\}=\begin{Bmatrix} W_b \\ W_m \end{Bmatrix} \tag{3.138}$$

$$\{P_w\}=\begin{Bmatrix} P_b \\ P_m \end{Bmatrix} \tag{3.139}$$

If the given structure contains several piezoceramic patches, and each patch consists of n finite elements (Figure 3.4), the assembly process must be modified only for elements which contain piezoelectric material. The prescribed electric boundary conditions require that the electrode be maintained to an equipotential, therefore each patch must consist of one electrical d.o.f. and can be simply assembled as

$$\{W_\phi\} = \{\{w_\phi\}_1 \quad \cdots \quad \{w_\phi\}_k \cdots \quad \{w_\phi\}_N\}^T \tag{3.140}$$

where N is the number of patches and $\{w_\phi\}_k$ as defined in Eq. (3.35) is a npx1 vector representing np number of piezoceramic layers. The solution for the assembled system of equations in Eq. (3.129) may be obtained by utilizing the standard finite element solution procedure. Thus during the solution process there is no need to distinguish between structural or electrical quantities other than known or unknown quantities.

3.8 Solution of Static Sensor Equation

To determine the voltage produced by a single piezoelectric patch bonded to a panel subjected to a static uniform distributed load, Eq. (3.129) may be partitioned as

$$[M]\{\ddot{W}\} + \left([K_w] + \frac{1}{2}[N1] - \frac{1}{2}[N1_{N\phi}] + \frac{1}{3}[N2]\right)\{W\}$$

$$+ \left([K_{w\phi}] + \frac{1}{2}[N1_{w\phi}]\right)W_\phi = \{P_w\} \tag{3.141}$$

$$\left([K_{\phi w}] + \frac{1}{2}[N1_{\phi w}]\right)\{W\} + K_\phi W_\phi = 0 \tag{3.142}$$

where Eq. (3.142) may be solved in terms of the unknown voltage as

$$W_\phi = -K_\phi^{-1}\left([K_{\phi w}] + \frac{1}{2}[N1_{\phi w}]\right)\{W\} \tag{3.143}$$

where $\{P_\phi\} = 0$ since there is no externally applied voltage to sensor. Furthermore Eq. (3.143) may be substituted into Eq. (3.141) resulting in a system of equations which may

be solved for the structural d.o.f. in response to the structural loading. The structural d.o.f. may be subsequently applied to Eq. (3.143) in order to determine the voltage. Since the system under consideration is static, the inertial terms will be identically zero. In addition since there is no externally applied voltage, the first-order nonlinear electrically coupled stiffness $\left[N1_{N\phi}\right]$ will also be identically zero. Substituting Eq. (3.143) into Eq. (3.141) yields the following system of equations, which must be solved for the structural d.o.f. due to the static loading

$$\left([K_w]+\frac{1}{3}[N2]+\frac{1}{2}[N1]-[K_{w\phi}][K_\phi]^{-1}[K_{\phi w}]-\frac{1}{2}[K_{w\phi}][K_\phi]^{-1}[N1_{\phi w}]\right.$$

$$\left.-\frac{1}{2}[N1_{w\phi}][K_\phi]^{-1}[K_{\phi w}]-\frac{1}{4}[N1_{w\phi}][K_\phi]^{-1}[N1_{\phi w}]\right)\{W\}=\{P_w\} \qquad (3.144)$$

The Newton-Raphson iterative method is used to solve the nonlinear system of equations of Eq. (3.144). Recall that the first- and second-order nonlinear stiffness matrices are functions of the unknown displacements.

3.8.1 Newton-Raphson Iteration Method

The Newton-Raphson [20] iterative method is used to solve Eq. (3.144) by solving for an incremental deflection which is given by

$$\{W\}_{i+1}=\{W\}_i+\{\Delta W\}_i \qquad (3.145)$$

The iterative procedure is carried out until the incremental deflection $\{\Delta W\}$ approaches zero resulting in a converged static deflection $\{W\}$.

Equation (3.144) can be written as a function, which may be expressed in terms of a Taylor series expansion thus

$$\{\Psi(W)\} = ([K_w] + \frac{1}{3}[N2] + \frac{1}{2}[N1]$$

$$-[K_{w\phi}][K_\phi]^{-1}[K_{\phi w}] - \frac{1}{2}[K_{w\phi}][K_\phi]^{-1}[N1_{\phi w}]$$

$$-\frac{1}{2}[N1_{w\phi}][K_\phi]^{-1}[K_{\phi w}] - \frac{1}{4}[N1_{w\phi}][K_\phi]^{-1}[N1_{\phi w}])\{W\} - \{P_w\} = 0 \qquad (3.146)$$

The truncated Taylor series expansion is represented symbolically as

$$\{\Psi(W + \Delta W)\} = \{\Psi(W)\} + \left\{\frac{d\Psi(W)}{dW}\right\}\{\Delta W\} = \{0\} \qquad (3.147)$$

Differentiation of Eq. (3.146), referred to as the tangent stiffness, results in

$$d\Psi(W) = d[([K_w] + \frac{1}{3}[N2] + \frac{1}{2}[N1]$$

$$-[K_{w\phi}][K_\phi]^{-1}[K_{\phi w}] - \frac{1}{2}[K_{w\phi}][K_\phi]^{-1}[N1_{\phi w}]$$

$$-\frac{1}{2}[N1_{w\phi}][K_\phi]^{-1}[K_{\phi w}] - \frac{1}{4}[N1_{w\phi}][K_\phi]^{-1}[N1_{\phi w}])]\{W\} \qquad (3.148)$$

The indicated differentiation of the tangent stiffness in Eq. (3.148) is accomplished by a term by term evaluation, beginning with the first term, which is the linear structural stiffness matrix. Since the linear stiffness matrix is constant with respect to the structural d.o.f., the differentiation is a trivial operation resulting in

$$d([K_w]\{W\}) = [K_w]\{dW\} \qquad (3.149)$$

Differentiation of the first-order nonlinear stiffness matrices invokes a two-step approach since $[N1]$ is comprised of $[N1_{Nm}]$, $[N1_{bm}]$, $[N1_{mb}]$, and $[N1_{NB}]$. The first step will deal with $[N1_{Nm}]$, $[N1_{bm}]$, and $[N1_{bm}]$, and the second step will involve the differentiation of $[N1_{NB}]$. The differentiation must be performed on the element level stiffness matrices, thus $[n1]$ is expressed as

$$([n1])\{w\} = \left(\begin{bmatrix} [n1_{Nm}] & [n1_{bm}] \\ [[n1_{mb}]] & [0] \end{bmatrix} \right) \begin{Bmatrix} w_b \\ w_m \end{Bmatrix} \tag{3.150}$$

Thus the derivative of $[N1]$ can be performed on the partitioned element level definitions given in Eq. (3.150) as

$$d([n1_{Nm}]\{w_b\}) + d([n1_{bm}]\{w_m\}) \tag{3.151}$$

and

$$d([n1_{mb}]\{w_b\}) \tag{3.152}$$

Applying the definitions expressed in Eqs. (3.107) and (3.108) to Eqs. (3.151)and (3.152) yields

$$\frac{1}{2}([n1_{Nm}] + [n1_{mb}])\{w_b\} + \frac{1}{2}[n1_{bm}]\{w_m\} = \frac{1}{2}[T_m]^T \int_A [C_m]^T [A][\theta][C_\theta]\{a\}dA$$

$$+ [T_b]^T \int_A [C_\theta]^T [\theta]^T [A][C_m]\{b\}dA \tag{3.153}$$

where $[C_\theta]\{a\} = \{\theta\}$. Performing the required differentiation of Eq. (3.153) yields

$$\frac{1}{2}[T_m]^T \int_A [C_m]^T [A]([d\theta]\{\theta\} + [\theta]\{d\theta\})dA$$

$$+ [T_b]^T \int_A [C_\theta]^T [d\theta]^T [A][C_m]\{b\}dA$$

$$+ [T_b]^T \int_A [C_\theta]^T [\theta]^T [A][C_m]\{db\}dA \tag{3.154}$$

Simplification may be achieved in the above equation by considering the following relations

$$[d\theta]\{\theta\} = \begin{bmatrix} dw_{,x} & 0 \\ 0 & dw_{,y} \\ dw_{,y} & dw_{,x} \end{bmatrix} \begin{Bmatrix} w_{,x} \\ w_{,y} \end{Bmatrix} = \begin{Bmatrix} dw_{,x}\, w_{,x} \\ dw_{,y}\, w_{,x} \\ dw_{,y}\, w_{,x} + dw_{,x}\, w_{,y} \end{Bmatrix} \tag{3.155}$$

$$[\theta]\{d\theta\} = \begin{bmatrix} w_{,x} & 0 \\ 0 & w_{,y} \\ w_{,y} & w_{,x} \end{bmatrix} \begin{Bmatrix} dw_{,x} \\ dw_{,y} \end{Bmatrix} = \begin{Bmatrix} dw_{,x}\, w_{,x} \\ dw_{,y}\, w_{,x} \\ dw_{,y}\, w_{,x} + dw_{,x}\, w_{,y} \end{Bmatrix} \tag{3.156}$$

Therefore

$$[d\theta]\{\theta\} = [\theta]\{d\theta\} = [\theta][C_\theta]\{da\} \tag{3.157}$$

Thus Eq. (3.154) may be cast in the following form

$$\begin{aligned} &[T_m]^T \int_A [C_m]^T [A][\theta][C_\theta] dA\{da\} \\ &+ [T_b]^T \int_A [C_\theta]^T [N_m][C_\theta]\{da\} dA \\ &+ [T_b]^T \int_A [C_\theta]^T [\theta]^T [A][C_m] dA\{db\} \end{aligned} \tag{3.158}$$

Thus the differentiation procedure can be summarized as

$$\begin{aligned} &d\left\{\left(\frac{1}{2}[n1_{Nm}] + [n1_{mb}]\right)\{w_b\}\right\} + d\left(\frac{1}{2}[n1_{mb}]\{w_b\}\right) \\ &= [n1_{mb}]\{dw_b\} + [n1_{Nm}]\{dw_b\} + [n1_{bm}]\{dw_m\} \end{aligned} \tag{3.159}$$

The second step used to differentiate $[N1_{NB}]$ uses a similar approach involving Eqs. (3.114), (3.99g), and (3.99j) resulting in

$$\begin{aligned} \frac{1}{2}[n1_{NB}]\{w_b\} &= [T_b]^T \int_A [C_\theta]^T [\theta]^T [B][C_b]\{b\} dA \\ &+ \frac{1}{2}[T_b]^T \int_A [C_b]^T [B][\theta][C_\theta]\{\theta\} dA \end{aligned} \tag{3.160}$$

Performing the indicated differentiation yields

$$\begin{aligned} &[T_b]^T \int_A [C_\theta]^T [d\theta]^T [B][C_b]\{a\} dA + [T_b]^T \int_A [C_\theta]^T [\theta]^T [B][C_b]\{da\} dA \\ &+ [T_b]^T \int_A [C_b]^T [B][\theta]\{d\theta\} dA \end{aligned} \tag{3.161}$$

and by using the relations in Eq. (3.157) yields

$$[T_b]^T \int_A ([C_\theta]^T [N_b][C_\theta] + [C_\theta]^T [\theta]^T [B][C_b]$$

$$+ [C_b]^T [B][\theta][C_\theta]) dA\{da\} \tag{3.162}$$

which may be summarized as

$$d\left(\frac{1}{2}[n1_{NB}]\{w_b\}\right) = [n1_{NB}]\{dw_b\} \tag{3.163}$$

Combining the results of Eqs. (3.159) and (3.163) yields

$$d\left(\frac{1}{2}[N1]\{W\}\right) = [N1]\{dW\} \tag{3.164}$$

Similarly, differentiation of the second-order nonlinear stiffness matrix may be performed using the element expression in Eq. (3.119) and substituting $[C_\theta]\{a\} = \{\theta\}$, thus

$$\frac{1}{3}[n2_b]\{w_b\} = \frac{1}{2}[T_b]^T \int_A [C_\theta]^T [\theta]^T [A][\theta]\{\theta\} dA \tag{3.165}$$

Performing the indicated differentiation operation produces

$$d\left(\frac{1}{3}[n2_b]\{w_b\}\right) = \frac{3}{2}[T_b]^T \int_A [C_\theta]^T [\theta]^T [A][\theta][C_\theta] dA\{da\} = [n2_b]\{dw_b\} \tag{3.166}$$

which may be expressed as

$$d\left(\frac{1}{3}[N2]\{W\}\right) = [N2]\{dW\} \tag{3.167}$$

The next term in Eq. (3.148) involves differentiation of the linear electrical-structural coupling stiffness matrices, which is a trivial operation since the stiffness matrices are constant with respect to the structural d.o.f., hence

$$d\left(\left[K_{w\phi}\right]\left[K_{\phi}\right]^{-1}\left[K_{\phi w}\right]\{W\}\right)=\left[K_{w\phi}\right]\left[K_{\phi}\right]^{-1}\left[K_{\phi w}\right]\{dW\} \tag{3.168}$$

The next term of Eq. (3.148) involves differentiation of the nonlinear electrical-structural coupling stiffness matrix, which is a function of the bending displacement, thus the differentiation is indicated as

$$d\left(\frac{1}{2}\left[K_{w\phi}\right]\left[K_{\phi}\right]^{-1}\left[N1_{\phi w}\right]\{W\}\right) \tag{3.169}$$

which can be expressed in terms of the element level matrices as

$$\left(\frac{1}{2}\begin{bmatrix}[k_{b\phi}]\\ [k_{m\phi}]\end{bmatrix}\left[k_{\phi}\right]^{-1}\begin{bmatrix}[n1_{\phi b}]\\ [0]\end{bmatrix}\right)\begin{Bmatrix}w_b\\ w_m\end{Bmatrix} \tag{3.170}$$

by recalling Eq. (3.117), the first order nonlinear coupling stiffness term is defined as

$$\frac{1}{2}\left[n1_{\phi b}\right]\{w_b\}=\left[B_{\phi}\right]^T\left[P_N\right]^T\int_A[\theta][C_{\theta}]dA[T_b]\{w_b\} \tag{3.171}$$

since it was previously shown that the linear stiffness matrices are constant matrices they are not affected by the differentiation indicated in Eq. (3.169). Thus differentiation may be accomplished by differentiating Eq. (3.171), which results in

$$\left[B_{\phi}\right]^T\left[P_N\right]^T\int_A[d\theta][C_{\theta}]dA[T_b]\{w_b\}+\left[B_{\phi}\right]^T\left[P_N\right]^T\int_A[\theta][C_{\theta}]dA[T_b] \tag{3.172}$$

by using the fact that $\{a\}=[T_b]\{w_b\}$. The relations of Eq. (3.157), Eq. (3.172) may be reduced to

$$\left[B_{\phi}\right]^T\left[P_N\right]^T\int_A[\theta][C_{\theta}]dA[T_b] \tag{3.173}$$

Thus the differentiation indicated in Eq. (3.169) can be summarized as

$$\left[K_{w\phi}\right]\left[K_{\phi}\right]^{-1}\left[N1_{\phi w}\right]\{dW\} \tag{3.174}$$

The next term of Eq. (3.148) requiring differentiation is the matrix transpose equation of Eq. (3.169)

$$d\left(\frac{1}{2}[N1_{w\phi}][K_{\phi}]^{-1}[K_{\phi w}]\{W\}\right) \tag{3.175}$$

thus neglecting the linear stiffness matrices differentiation of the first order nonlinear coupling matrix is simply the matrix transpose of Eq. (3.172) and is given by

$$[T_b]^T \int_A [C_\theta]^T [d\theta]^T dA[P_N][B_\phi]\{w_b\} + \frac{1}{2}[T_b]^T \int_A [C_\theta]^T [\theta]^T dA[P_N][B_\phi] \tag{3.176}$$

thus differentiation results in

$$d\left(\frac{1}{2}[N1_{w\phi}][K_{\phi}]^{-1}[K_{\phi w}]\{W\}\right) = [N1_{w\phi}][K_{\phi}]^{-1}[K_{\phi w}]\{dW\} \tag{3.177}$$

The next term of Eq. (3.148) involves the product of two nonlinear coupling matrices

$$d\left(\frac{1}{4}[N1_{w\phi}][K_{\phi}]^{-1}[N1_{\phi w}]\{W\}\right) \tag{3.178}$$

which is expressed at the element level as

$$\frac{1}{4}\begin{bmatrix}[n1_{b\phi}]\\ [0]\end{bmatrix}[k_{\phi}]^{-1}\begin{bmatrix}[n1_{\phi b}] \\ [0]\end{bmatrix}\begin{Bmatrix} w_b \\ w_m\end{Bmatrix} \tag{3.179}$$

This results in a differential with respect to the bending displacement only, resulting in

$$d\left(\frac{1}{4}[n1_{b\phi}][k_{\phi}]^{-1}[n1_{\phi b}]\{w_b\}\right) \tag{3.180}$$

where

$$[n1_{b\phi}] = [T_b]^T \int_A [C_\theta]^T [\theta]^T dA[P_N][B_\phi] = [n1_{\phi b}]^T \tag{3.181}$$

Once again the linear stiffness matrix is constant and unaffected by differentiation. Thus the differentiation is performed on the product of the first-order nonlinear stiffness matrices only resulting in

$$\frac{1}{4}[T_b]^T \int_A [C_\theta]^T [d\theta]^T dA [P_N][B_\phi][k_\phi]^{-1}[B_\phi]^T [P_N]^T \int_A [\theta][C_\theta] dA [T_b]\{w_b\}$$

$$+\frac{1}{4}[T_b]^T \int_A [C_\theta]^T [\theta] dA [P_N][B_\phi][k_\phi]^{-1}[B_\phi]^T [P_N]^T \int_A [\theta][C_\theta] dA [T_b]\{w_b\}$$

$$+\frac{1}{4}[T_b]^T \int_A [C_\theta]^T [\theta] dA [P_N][B_\phi][k_\phi]^{-1}[B_\phi]^T [P_N]^T \int_A [\theta][C_\theta] dA [T_b] \tag{3.182}$$

which is simplified by employing the relations of Eq. (3.157) resulting in

$$d\left(\frac{1}{4}[n1_{b\phi}][k_\phi]^{-1}[n1_{\phi b}]\{w_b\}\right) = \frac{3}{4}[n1_{b\phi}][k_\phi]^{-1}[n1_{\phi b}]\{w_b\} \tag{3.183}$$

Reassembling the system matrices yields

$$d\left(\frac{1}{4}[N1_{w\phi}][K_\phi]^{-1}[N1_{\phi w}]\{W\}\right) = \frac{3}{4}[N1_{w\phi}][K_\phi]^{-1}[N1_{\phi w}]\{dW\} \tag{3.184}$$

and collecting all terms yields the tangent stiffness matrix given by

$$\left\{\frac{\Psi(W)}{dW}\right\} = [K_{tan}]$$

$$= [K_w] + [N2] + [N1] - [K_{w\phi}][K_\phi]^{-1}[K_{\phi w}]$$

$$-[K_{w\phi}][K_\phi]^{-1}[K_{\phi w}] - [N1_{w\phi}][K_\phi]^{-1}[K_{\phi w}] - \frac{3}{4}[N1_{w\phi}][K_\phi]^{-1}[N1_{\phi w}] \tag{3.185}$$

Thus Eq. (3.147) becomes the nonlinear static equation where

$$[K_{tan}]\{\Delta W\} = \{\Delta P_w\} \tag{3.186}$$

The incremental right-hand side vector is

$$\{\Delta P_w\} = \{P_w\} - ([K_w] + \frac{1}{3}[N2] + \frac{1}{2}[N1]$$

$$-[K_{w\phi}][K_\phi]^{-1}[K_{\phi w}] - \frac{1}{2}[K_{w\phi}][K_\phi]^{-1}[N1_{\phi w}]$$

$$-\frac{1}{2}[N1_{w\phi}][K_\phi]^{-1}[K_{\phi w}] - \frac{1}{4}[N1_{w\phi}][K_\phi]^{-1}[N1_{\phi w}])\{W\} \qquad (3.187)$$

In the Newton-Raphson iteration, the initial nonlinear stiffness matrices are determined from the linear static displacements. Once the incremental load vector and tangent stiffness matrix are assembled, the Newton-Raphson tangent equation shown in Eq. (3.185) is solved to determine $\{\Delta P_w\}$, which is subsequently used to update the static deflections. During the iterative process, the incremental load vector and the incremental deflection will approach zero, resulting in a converged deflection solution.

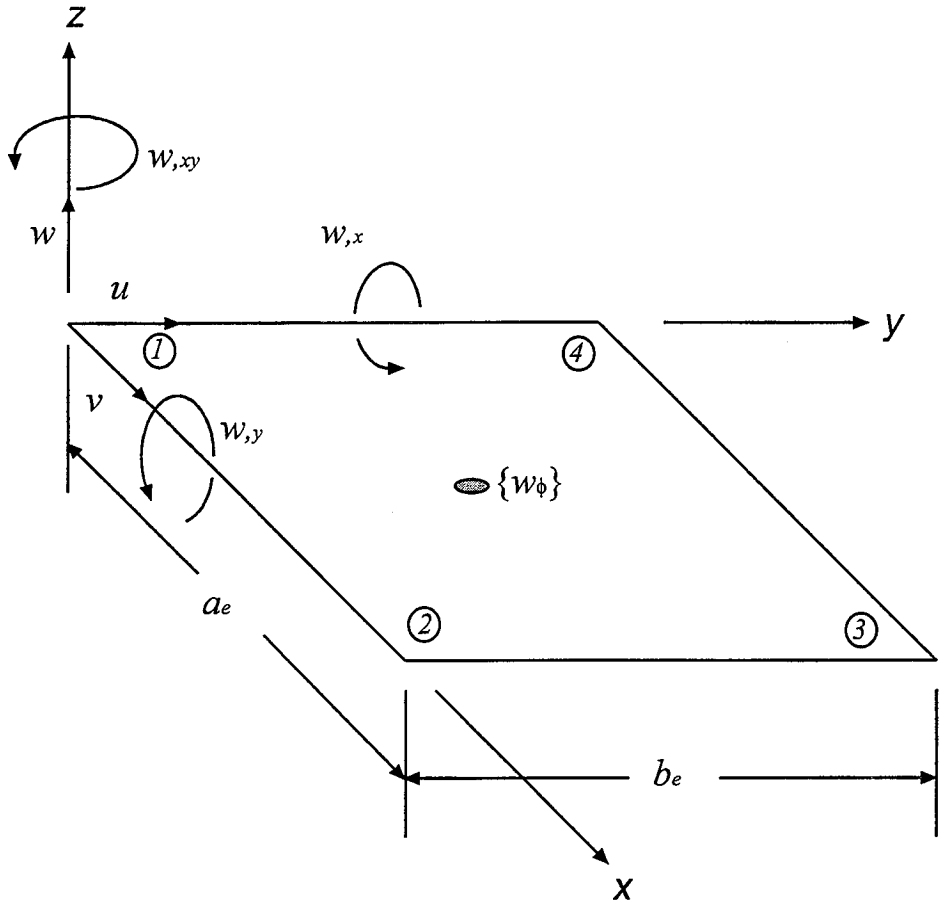

Fig. 3.1 Nodal degrees of freedom of a piezoelectric element

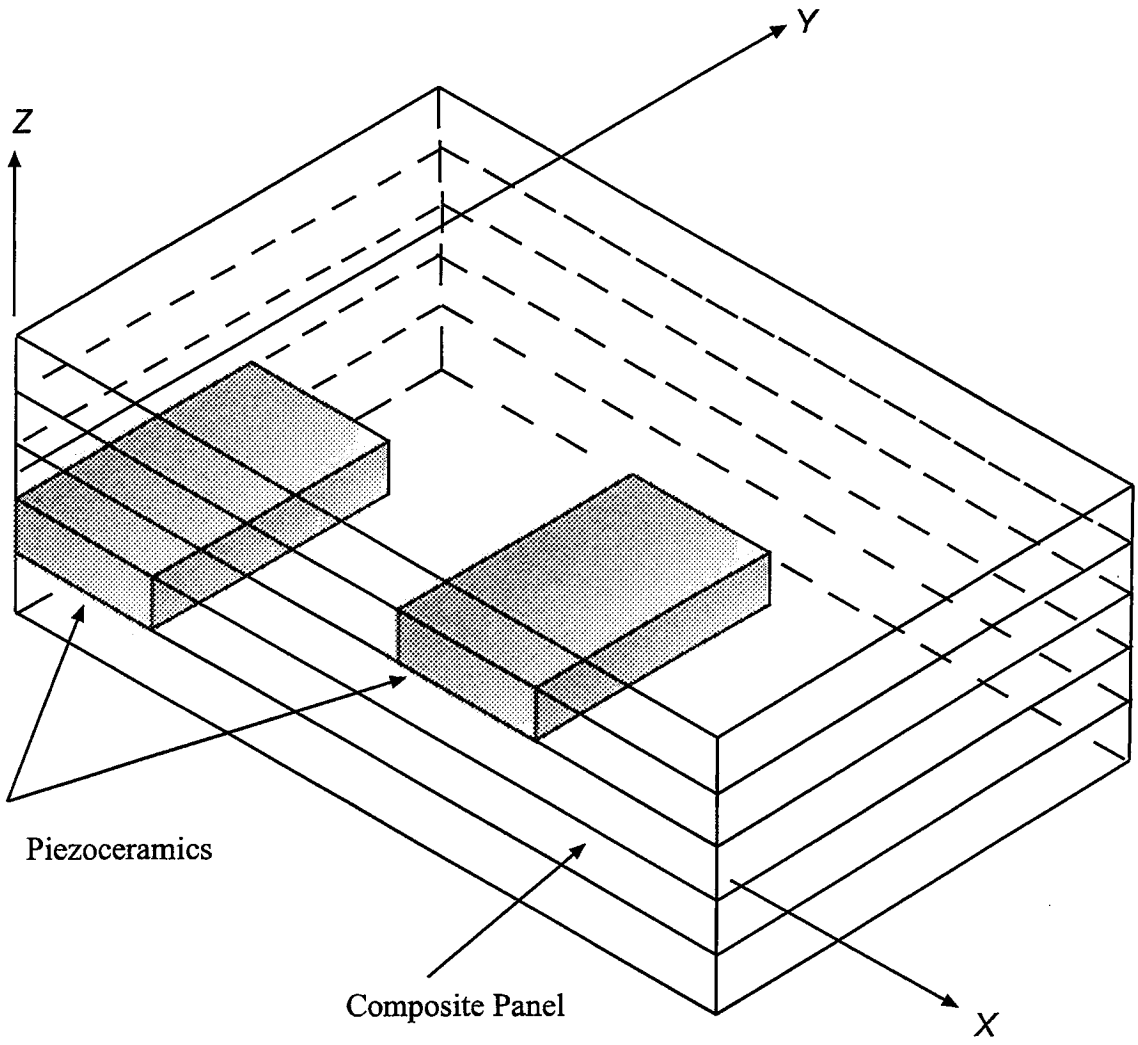

Fig. 3.2 Geometry of a laminate with embedded piezoceramics

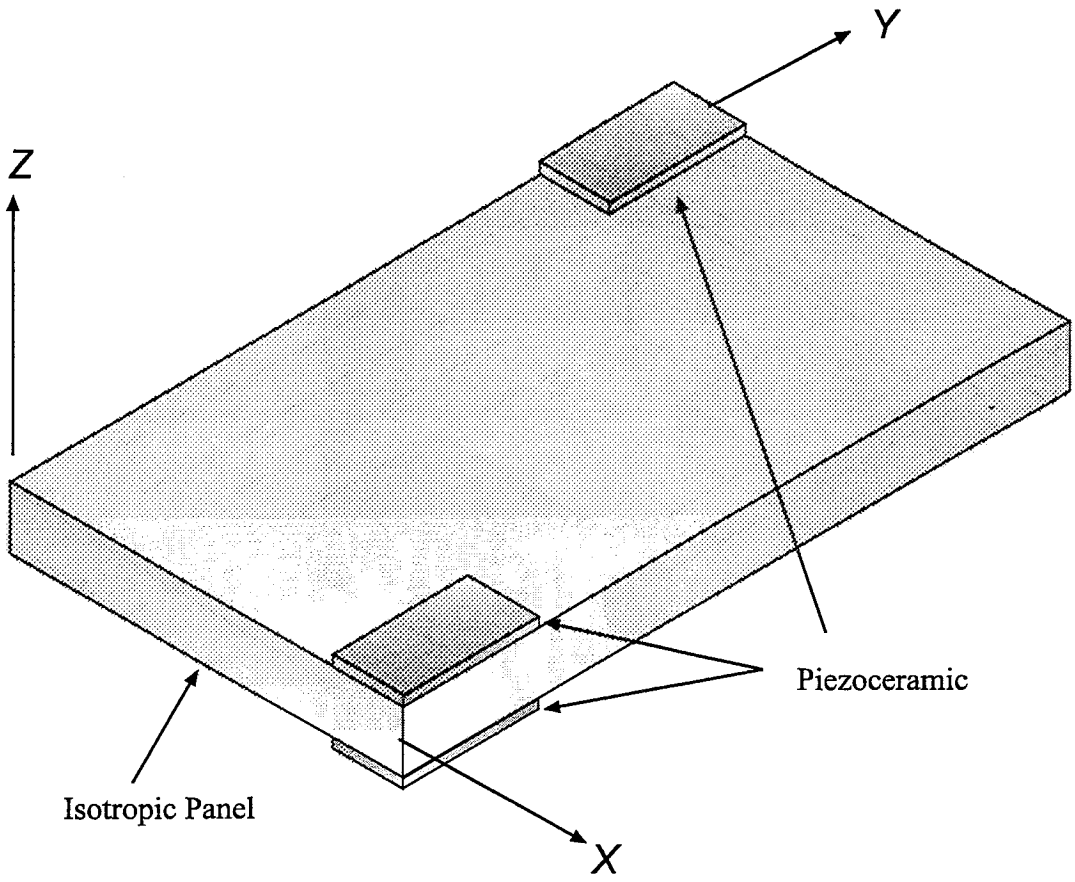

Fig. 3.3 Isotropic panel with surface mounted piezoceramics

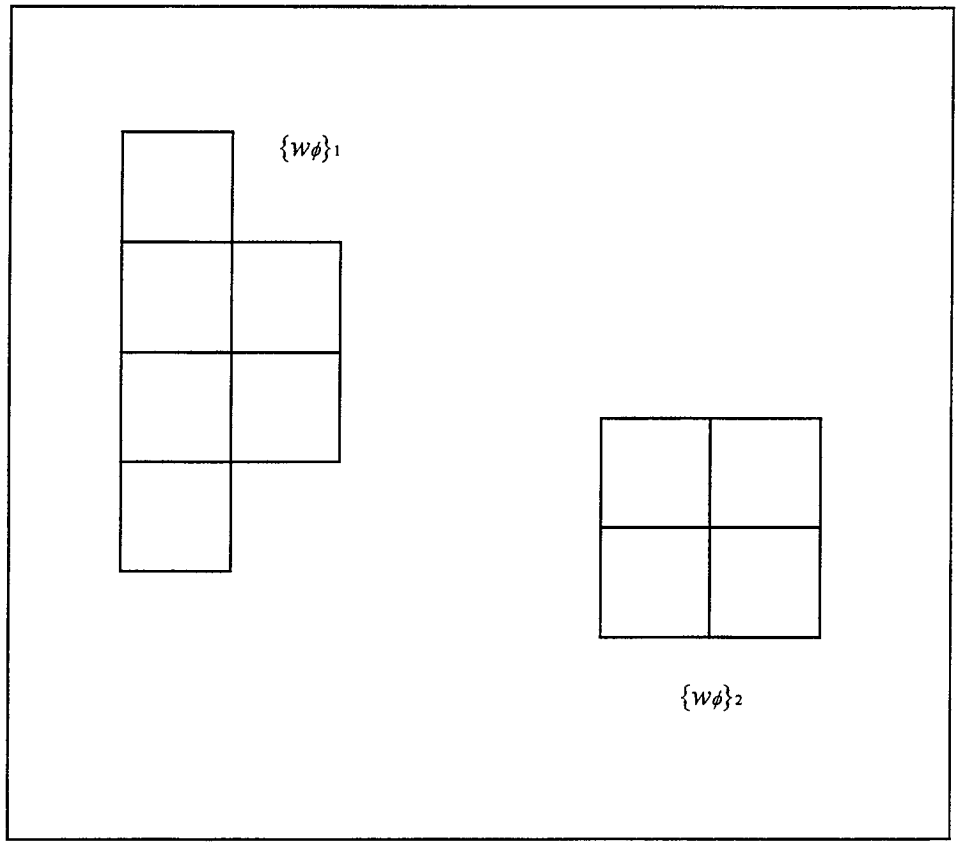

Fig. 3.4 Piezoceramic elements for two patches

CHAPTER IV

EXPERIMENTAL SETUP

4.1 Introduction

It was desired that a typical representative aircraft structural panel be tested, and the experimental results compared to the finite element analysis. Therefore a 14"x10"x0.040" aluminum panel was selected for the experiments. For a panel of this size, it was much easier to construct a test fixture that achieves approximate clamped boundary conditions as opposed to simply supported boundary conditions.

4.2 Establishment of Clamped Boundary Conditions

A clamping fixture consisting of two aluminum plates of size 25"x20"x1", with a rectangular 14"x10" hole machined out of the center, was manufactured to achieve the clamped boundary conditions as shown in Figure 4.1. The rectangular cut-out was centered such that there was a minimum of four inches of clamping surface around the perimeter of the 14"x10" panel cut-out. The mating surfaces of the clamping fixture were measured to be within ±0.002" flatness. A series of 26 pilot holes for 1/4" cap screws were drilled in an evenly spaced pattern 1/2" beyond the perimeter of the panel cut-out. Another series of 8 pilot holes were spaced evenly around the outer perimeter of the fixture 3/4" from the edges and sized to accommodate the 3/8" cap screws. The 0.040" test panel specimen was cut to 25"x20" so as to fit the overall clamping fixture. Two 1/4" alignment pins were placed at opposite corners to assure repeatable and consistent assembly. Wooden support blocks were placed on the bottom of the panel to support the clamping fixture in a vertical fashion. The clamping fixture was assembled with grade-8, high strength hex head cap screws, washers, and nuts. The 1/4" and 3/8" cap screws were tightened to 15 and 20 ft-lb respectively in 5 ft-lb increments. The tightening sequence followed is depicted in Figure 4.2.

4.3 Piezoelectric Wafer Preparation

A single 2.5"x1.5"x0.010" piezoelectric wafer was bonded to the panel 3/4" from the boundary, symmetrically on the centerline (see Figure 4.3). Before the wafer can be attached to the panel, electrical leads must be attached to the wafer electrodes to facilitate the instrumentation. Since the piezoelectric wafer was polarized in the *3*-direction the electrodes are on the top and bottom surfaces. The piezoelectric is a polarized dielectric, therefore if any residual electrode material is attached to any of the edges in the *2*- or *3*-direction, a complete or near short circuit will adversely affect the piezoelectric process, if not completely inhibit it. In addition, since the electric field is the gradient of the electrical potential as shown in Eq. (3.36) a very large electric field, or potential gradient will exist. This condition could cause dielectric breakdown of the piezoelectric resulting in a short circuit condition. This adverse condition may be minimized if the piezoelectric edges are straight and perpendicular. To assess the quality of the piezoelectric edges the resistance and capacitance can be measured with a high quality multimeter and comparing the results to the manufacturer's specifications. If an ill-conditioned edge is detected, as indicated by a low resistance or capacitance, then the edges may be gently scraped or sanded with a very fine machinist wet abrasive paper. If the specified resistance cannot be obtained then the piezoelectric wafer should not be used.

4.4 Piezoelectric Lead Attachment

Electrical leads must be soldered to the electrodes of the piezoelectric wafer. Traditionally to obtain a good electrically conductive and mechanically reliable solder bond both the substrate and the lead being attached must be raised to a temperature greater than the melting point of the solder. This technique will adversely affect the piezoelectric wafer since depolarization will occur if subjected to temperatures in excess of the Curie point which is 365^{o}C for PZT-5A [21]. The depolarization may occur locally within the piezoelectric, thereby altering the overall charge constants. A complete depolarization rendering the piezoelectric inoperative is unlikely, therefore extreme care

must be taken to assure that the piezoelectric properties are not altered during the soldering process.

The piezoelectric wafer is a polarized dielectric, and since thermal conductivity is proportional to electrical conductivity [22], the piezoelectric wafer is a thermal insulator. Hence the heat applied during soldering will not readily dissipate through the wafer. On the other hand the electrodes are nickel and are highly conductive, however since they are only 0.00005 - 0.0002" thick their thermal capacity is very small. The only other thermal member remaining is the lead to be attached. The lead size should be selected to minimize its thermal capacity so that it does not act as a heat sink and direct the heat away from the wafer, thus increasing the soldering time. The leads used were copper foil 2"x1/16"x0.001". A temperature selectable thermostaticly controlled soldering iron fitted with a small pencil tip was used and set to 360^{o}F. The electrodes of the piezoelectric wafer were cleaned with alcohol and a small amount of liquid flux applied. The lead was cleaned, fluxed, and tinned with solder. After the lead cooled additional flux was applied to the lead and placed on the substrate, then with light pressure, a tinned soldering iron was placed on top of the lead until the solder between the lead and electrode melted. The soldering iron was removed within five seconds as recommended by the piezoceramic manufacturer.

4.5 Piezoelectric Wafer Bonding

The piezoelectric wafer attachment is carried out in a two step process to ensure both electrical isolation and mechanical bonding. A strain gage epoxy adhesive system was used to bond the wafer to the aluminum panel [23]. The electrical isolation is obtained by applying a thin layer of adhesive to the panel prior to the application of the wafer. Initially the panel is cleaned with alcohol to remove any dirt and oil. The piezoelectric location was measured and marked within 1/64" using a sharpened mechanical lead holder. The scribe lines were extended three inches beyond the actual location for future reference since excess adhesive will cover the lines as indicated in Figure 4.4. Mylar

adhesive tape was applied 1/16" beyond the scribe lines creating a rectangular mold which will be filled with adhesive. Additional mylar tape was used to cover and protect the scribe lines remaining outside the frame, see Figure 4.5. The framed area was wet sanded with alcohol and abrasive cloth, wiped clean and treated with a micro-abrasive metal conditioner. Next a semipermiable Teflon cloth and mylar sheet were cut and placed over the area to be glued and one edge was attached to the panel with mylar tape. The adhesive is mixed and a thin layer is applied to the framed area, the Teflon cloth was placed over the adhesive and covered with the mylar sheet and a vacuum pad was attached and activated. The vacuum pad will provide a uniform pressure permitting excess adhesive to penetrate the Teflon cloth. The adhesive was permitted to cure overnight since the minimum curing time was six hours.

Once the adhesive cured the vacuum pad was removed along with the mylar tape. The Teflon cloth provided an abraded surface texture however the adhesive should be uniform without any voids or bumps. Using the original exact scribe lines reapply the mylar tape to create a frame which will be exactly the size of the piezoelectric wafer. The adhesive surface and the piezoelectric wafer were cleaned with alcohol and a thin layer of adhesive was applied to the existing base coat on the panel. The piezoelectric wafer was placed on the adhesive and covered with a thin layer of foam and the vacuum pad placed over it and allowed to cure over night. It should be noted that the electrical lead on the wafer should be as thin as possible including any residual solder. If however the piezoelectric wafer is very thin, and subjected to an excessive vacuum loading, the lead may crack the piezoelectric wafer. For a flat horizontal application, only a slight vacuum loading is required, to ensure a uniform distributed load during the curing process.

4.6 Uniform Distributed Loading

To assess the static piezoelectric sensor a uniform distributed load was applied to the panel. However, since piezoelectrics cannot sustain a static charge the uniform distributed load must be applied instantaneously. To achieve the instantaneous load the

test clamping fixture was modified to include a 14"x16"x1/4" plate on one side, thus creating a vacuum chamber. The vacuum plate was attached using the existing fixture bolts and was sealed with a vacuum grease. Three fittings facilitated a vacuum pump, vacuum gage, and a quick-release ball valve as indicated in Figure 4.6. To conduct the static sensor experiment the vacuum was applied and the maximum plate deflection was measured using a dial indicator. Once the desired deflection was achieved the vacuum was held by closing the valve and noting the corresponding pressure. With the plate in a deformed state, the residual charge was allowed to dissipate. At this time, the ball valve was opened quickly and the sensor voltage was measured by recording the time history using a fast Fourier analyzer.

4.7 Material Properties

The experiments conducted for this research were performed on a rectangular isotropic aluminum panel with a single bonded piezoceramic patch. Various static and dynamic experiments were conducted in order to obtain data that was compared to finite element analysis which will be discussed subsequently in Chapter IV. The piezoceramic used herein was PZT-5A manufactured by Morgan Matroc [21]. Table 4.1 provides the physical material properties. The physical properties of the aluminum panel used for the experiments may be found in Table 4.2.

PZT-5A			
Charge Constants	d_{31}	-171e-12	m/V
Permittivity	ϵ_r	1700	
Density	ρ	7700	kg/m^3
Length	L	0.0762	m
Width	W	0.0381	m
Thickness	h	254e-6	m
Young's Modulus	E	6.9e10	N/m^2
Poisson's Ratio	ν	0.31	

Table 4.1 Piezoceramic Properties

Aluminum Panel			
Density	ρ	2702	kg/m^3
Length	L	0.356	m
Width	W	0.254	m
Thickness	h	1.02e-3	m
Young's Modulus	E	6.1e10	N/m^2
Poisson's Ratio	ν	0.31	

Table 4.2 Aluminum Panel Properties

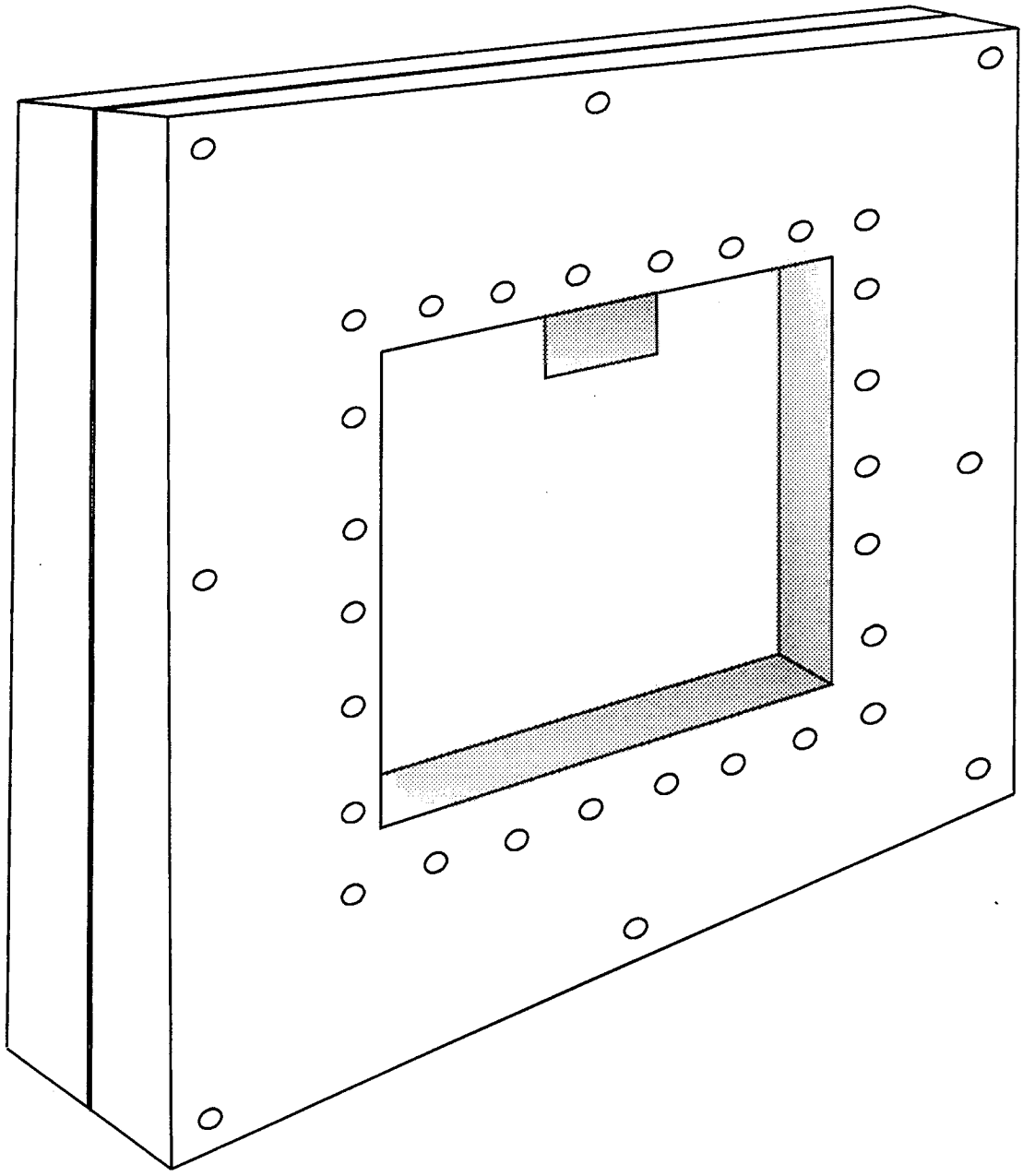

Fig. 4.1 Plate clamping fixture

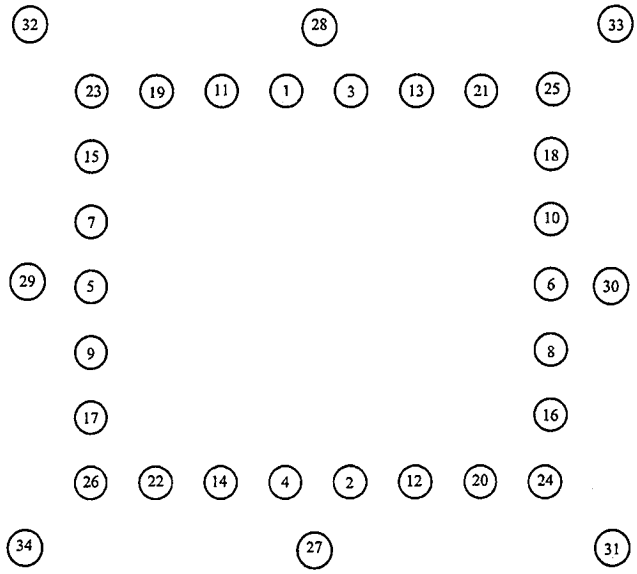

Fig. 4.2 Bolt tightening sequence

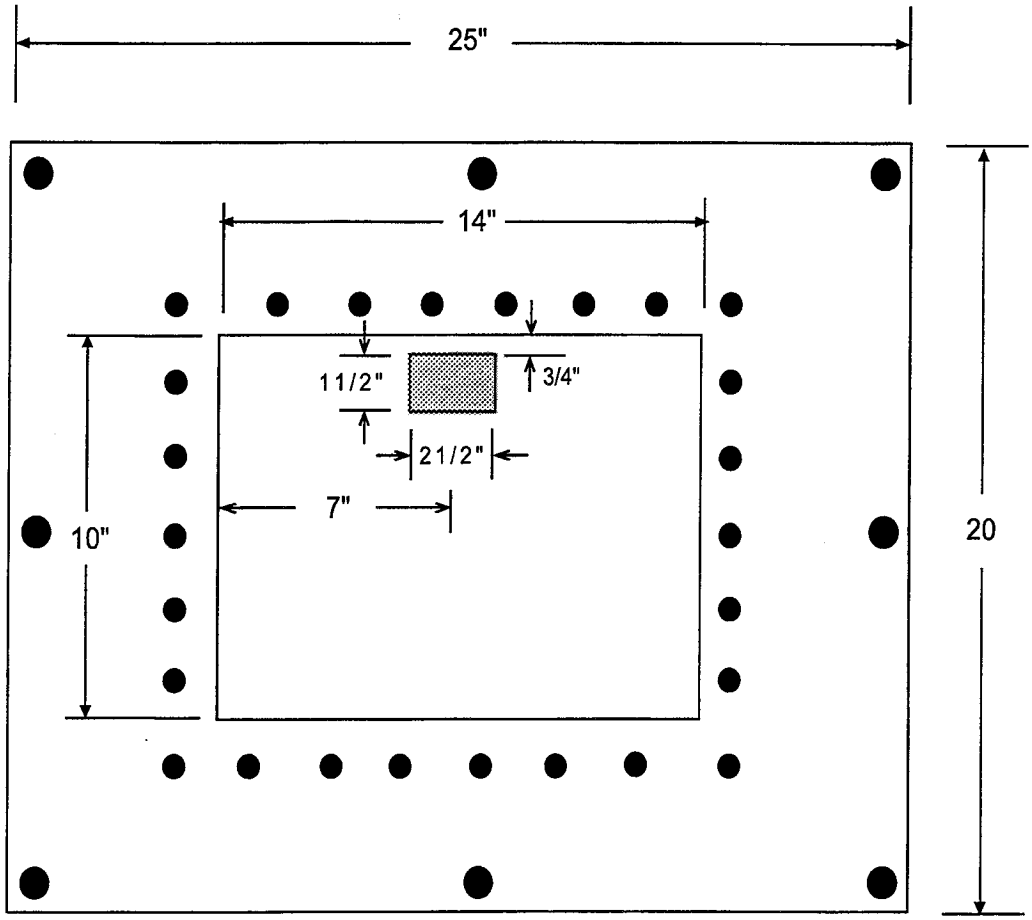

Fig. 4.3 Piezoceramic location

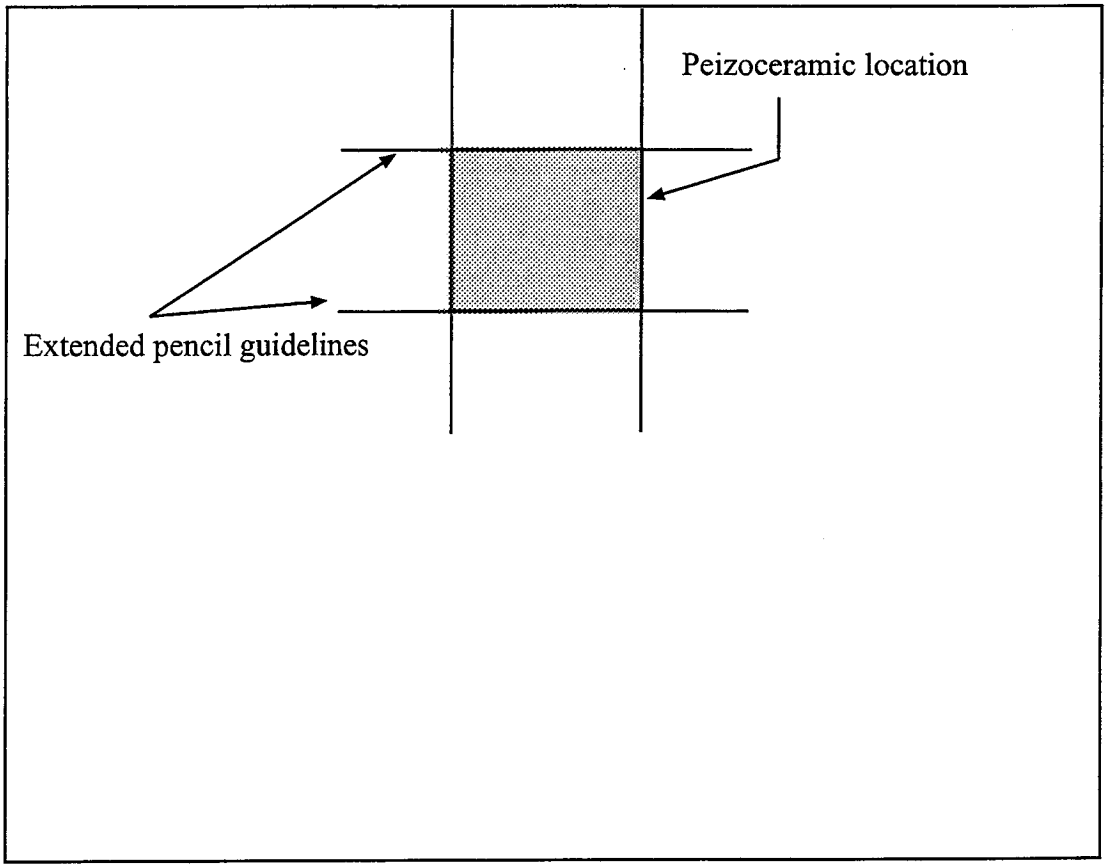

Fig. 4.4 Piezoceramic mounting preparation

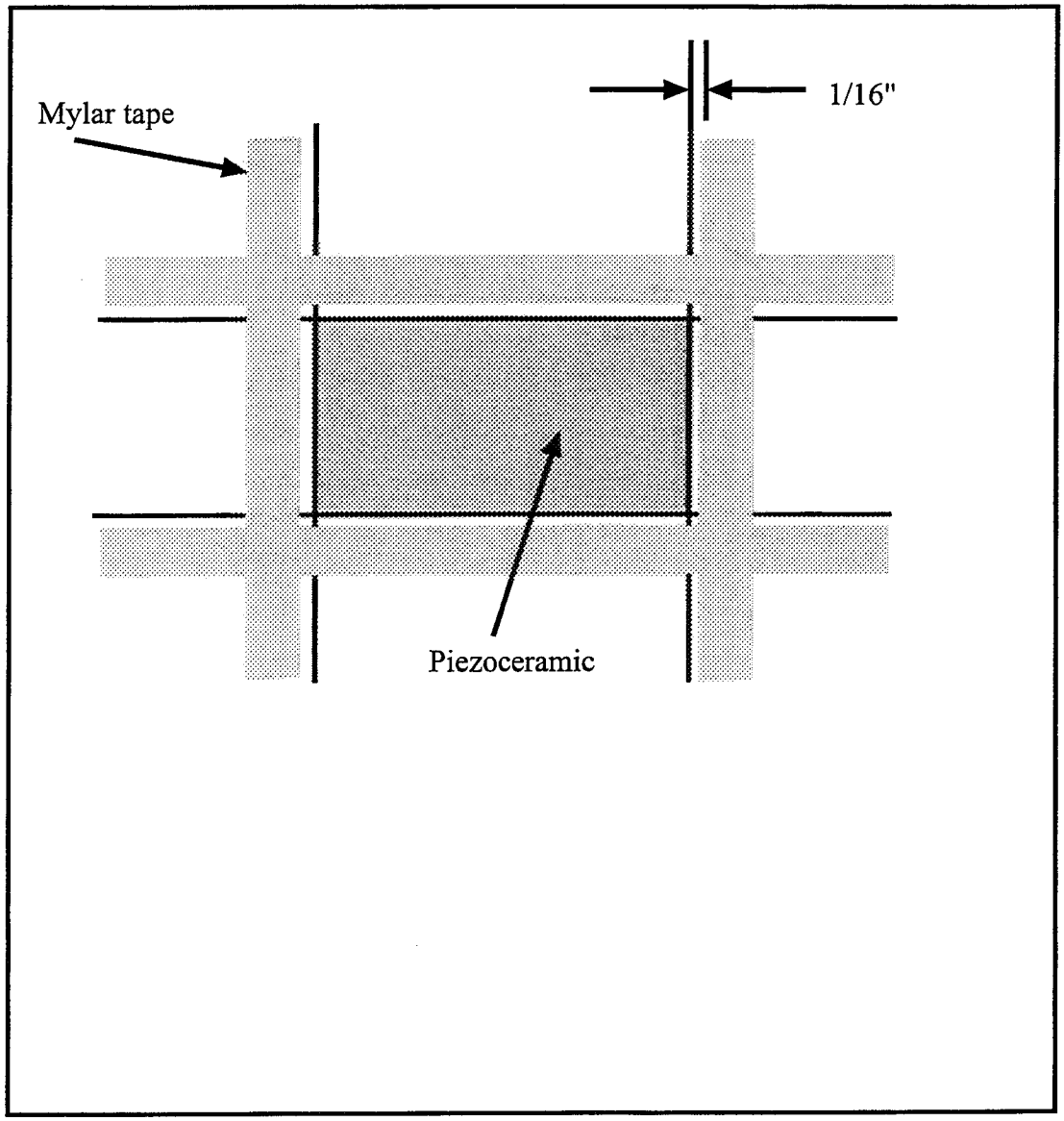

Fig. 4.5 Piezoceramic adhesive preparation

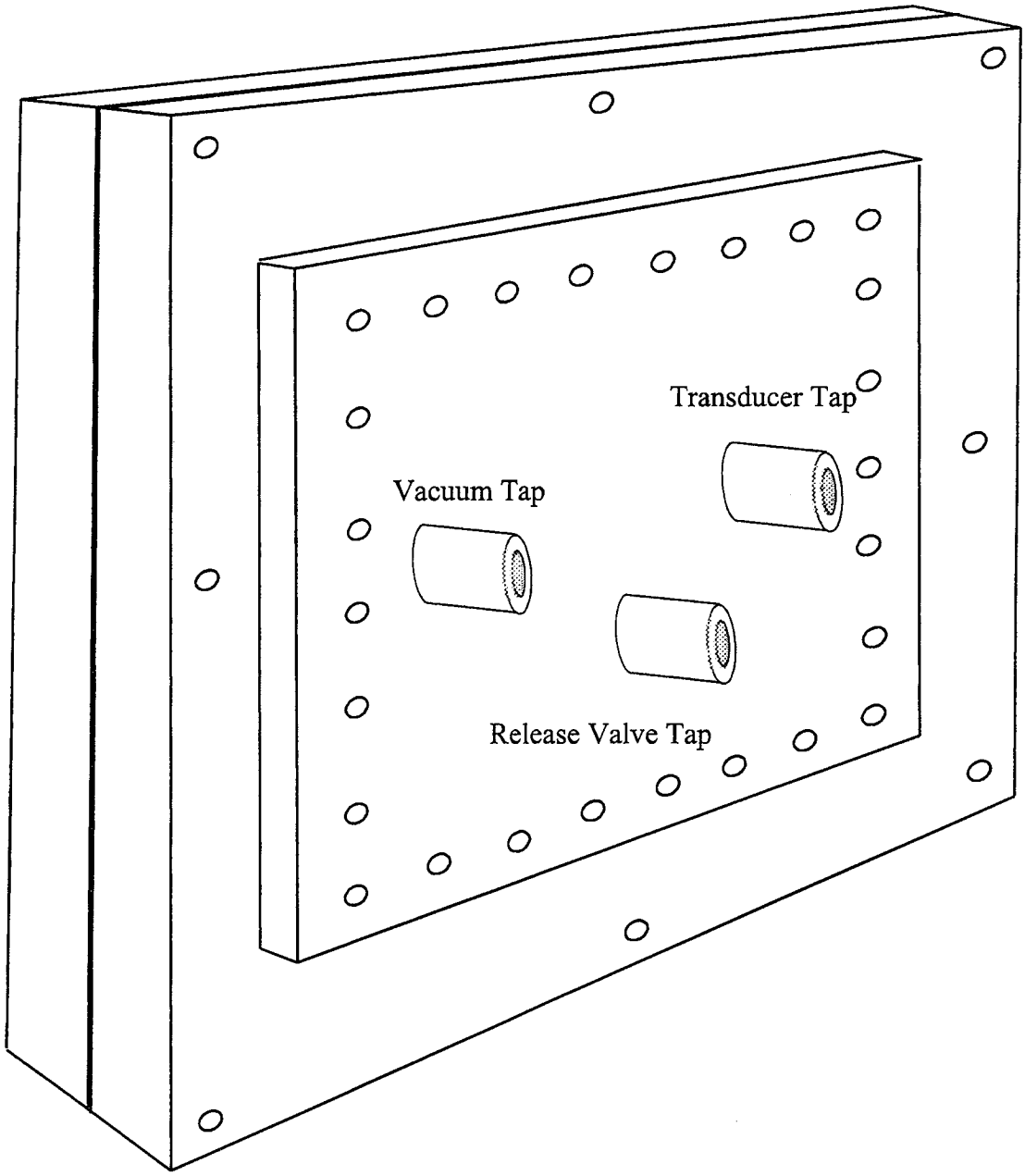

Fig. 4.6 Vacuum plate

CHAPTER V

NUMERICAL AND EXPERIMENTAL RESULTS

5.1 Introduction

The verification of the linear finite element model was conducted by considering a simply supported square panel. Initially, an isotropic panel is considered where the maximum transverse deflection was compared to the classical solution. Next a bonded piezoelectric patch is included and the predicted sensor voltage resulting from a uniform distributed load is compared to a voltage determined using a classical solution method. The large deflection finite element model was verified by comparing results to a single mode classical solution for moderately large deflections of a square clamped plate. Subsequently, finite element results are presented and compared to experimental results obtained from a clamped rectangular panel. Results include static and dynamic sensor applications and dynamic actuation.

5.1.1 Static Small Deflection

In order to verify the finite element model formulation, a simply supported isotropic panel subjected to a uniformly distributed load is considered. The small deflection approximation is used in the finite element formulation. The Navier solution for a simply supported rectangular plate is computed and used to validate the finite element model. The Navier solution for the transverse deflection of a simply supported plate under a uniform load is given by [24]

$$w(x,y)=\frac{16q_o}{\pi^6 D}\sum_{m=1}^{\infty}\sum_{n=1}^{\infty}\frac{1}{mn\left(\frac{m^2}{a^2}+\frac{n^2}{b^2}\right)^2}\sin\left(\frac{m\pi x}{a}\right)\sin\left(\frac{n\pi x}{b}\right) \tag{5.1}$$

where $m=1,3,5,\cdots\infty$ and $n=1,3,5,\cdots\infty$. Thus the maximum deflection can be found by substituting $x=a/2$ and $y=b/2$. Figure 5.1 provides the finite element analysis non-dimensional maximum deflection compared to the classic Navier solution of a

10"x10"x0.040" simply supported plate subjected to uniform loads. The accuracy of the finite-element, small-deflection formulation has thus been established.

5.1.2 Static Large Deflection

To verify the large deflection finite element model formulation a clamped square panel subjected to a uniform distributed load is considered. A single mode classical solution for moderately large transverse deflections is given by Chia [25] as

$$\left(\frac{w_{11}}{h}\right)^3 + 0.2522\frac{w_{11}}{h} = 0.0001333\frac{q_o a^4}{Dh} \tag{5.2}$$

where $w_{max} = 2.5223 w_{11}$, h is the panel thickness, D is the bending rigidity, q_O is the uniform distributed loading, and a is the width of the panel. Comparison of the large deflection finite element formulation non-dimensional displacement and the single mode solution is shown in Figure 5.2. Excellent agreement was obtained for the large defection formulation, thus establishing the accuracy of the finite element model.

5.1.3 Static Sensor

In order to validate the static sensor formulation an isotropic plate with a single piezoelectric patch bonded to the surface is considered using a classical voltage solution method. The classic solution applies Gauss's law to determine the charge enclosed within a surface and is given as

$$q = \int_S \mathrm{D} \cdot d\mathrm{a} \tag{5.3}$$

where **D** is the electric displacement density and $d\mathbf{a}$ is the differential normal vector of the surface S. However, the space charge within a dielectric is identically zero, thus Eq. (5.3) cannot be directly applied to piezoceramics. Since the charge generated by the k^{th} piezoceramic layer is accumulated at the electrodes (top and bottom surfaces of the k^{th} piezoceramic layer), Eq. (5.3) may be expanded to determine the effective charge such that

$$q_k = \frac{1}{2}\left(\iint_{S^1(z=z_{k+1})} D_3 dxdy + \iint_{S^2(z=z_k)} D_3 dxdy \right) \tag{5.4}$$

Substituting Eq. (2.12) into Eq. (5.4), setting the applied electric field to zero for the sensor application, and considering an effective or average electrode surface area yields

$$q_k = \iint_{S^e} [e](\{\varepsilon\} + z\{\kappa\}) dxdy \tag{5.5}$$

Substituting the strain-displacement relationships of Eqs. (3.16) and (3.17) yields

$$q_k = \iint_{S^e} \left(e_{31}(u_{,x} - zw_{,xx}) + e_{32}(v_{,y} - zw_{,yy}) + e_{36}(u_{,y} + v_{,x} - z2w_{,xy}) \right) dxdy \tag{5.6}$$

Neglecting the inplane strain, since the small displacement approximation was used, Eq. (5.6) may be simplified as

$$q_k = \iint_{s^e} -z\left[e_{31} w_{,xx} + e_{32} w_{,yy} + 2e_{36} w_{,xy} \right] dxdy \tag{5.7}$$

Utilizing the Navier solution of Eq. (5.1) for the transverse deflection and setting $e_{36} = 0$, the charge of Eq. (5.7) becomes

$$q_k = \frac{16 q_o b}{\pi^6 Da} e_{31} Z_p \sum_{m=1}^{\infty} \sum_{n=1}^{\infty} \frac{1}{n^2 \left(\frac{m^2}{a^2} + \frac{n^2}{b^2} \right)^2} \cos\left(\frac{m\pi x}{a} \right) \Bigg|_{x_1}^{x_2} \cos\left(\frac{n\pi y}{b} \right) \Bigg|_{y_1}^{y_2} +$$

$$\frac{16 q_o a}{\pi^6 Db} e_{32} Z_p \sum_{m=1}^{\infty} \sum_{n=1}^{\infty} \frac{1}{m^2 \left(\frac{m^2}{a^2} + \frac{n^2}{b^2} \right)^2} \cos\left(\frac{m\pi x}{a} \right) \Bigg|_{x_1}^{x_2} \cos\left(\frac{n\pi y}{b} \right) \Bigg|_{y_1}^{y_2} \tag{5.8}$$

where Z_p represents the distance of the mid plane of the k^{th} piezoceramic layer and is the effective electrode area as shown in Figure 5.3. The effective electrode area establishes the electrical boundary conditions to facilitate the electric displacement density. The classic and finite element voltages due to various pressure loading applied to a simply supported 10"x10" plate is shown in Figure 5.4. The excellent agreement indicates that the finite element formulation will accurately predict piezoelectric sensor voltages.

5.2 Experimental and Analytical Comparison

The experiment was conducted using a rectangular aluminum plate with a single piezoceramic patch bonded to the top surface. The validated finite element model was modified to include clamped boundary conditions. A full analytical model was used to model the complete experimental plate by using a 10x8 mesh which includes 4 piezoceramic elements and is shown in Figure 5.5. By employing a high input impedance charge amplifier, the charge signal may be recovered and related to the voltage generated by the piezoceramic through the intrinsic piezoelectric capacitance as $V=q/C$, as described in Appendix C. Since a charge amplifier was used during the experimental test (refer to Appendix E) the charge was converted to volts during the analysis. It should be mentioned that if a rate of strain is desired, then a current amplifier must be used in lieu of a charge amplifier.

The finite element simulation requires modal damping values of the plate, so they were determined experimentally along with the natural frequencies and are shown in Table 5.1. In the following Sections, a complete comparison of experimental and analytical results of the static and dynamic sensor and dynamic actuation is provided.

Experiment	Analysis	
Frequency Hz.	Modal Damping	Frequency Hz.
103.06	0.034	106.71
164.56	0.0047	173.0
236.1	0.0095	256.47
268.81	0.0007	282.58
298.94	0.004	316.70
392.9	0.0031	422.65
412.2	0.0057	433.65
488.5	0.0034	491.73

Table 5.1 Natural Frequencies and Damping Values

5.2.1 Static Sensor

The static sensor analysis was conducted in two steps. The first step implements the small deflection assumption, however in order to accurately predict the experimental results, a second approach including the large deflection approximation is performed. The linear piezoelectric theory accurately predicts the sensor voltage for small pressure loading, however for higher pressures the geometrical nonlinearities dictate the plate deflection and thereby affect the sensor voltage. Given the fully coupled electrical-structural formulation, the large deflection assumption includes the nonlinear electrical-structural stiffness matrices of Eq. (3.143). It should be noted however, that there is no nonlinear stiffness associated with the uncoupled electrical d.o.f. since the linear piezoelectric theory assumption is maintained.

The small deflection analysis and experimental sensor voltages of a 14"x10"x0.040" clamped plate due to uniform distributed loads are shown in Figure 5.6. Note that for small pressure loading, the small deflection analysis results coincide with the test results.

Thus for small pressure loading the small deflection analysis is valid. However it should be noted that for high speed flight vehicles it is not uncommon to experience differential pressures in the range of 3-5 psi, thus the experimental loading considered is not unreasonably high. The non-dimensional deflection due to the large deflection analysis is shown in conjunction with the experimental results of a 14"x10"x0.040" clamped plate in Figure 5.7, and excellent agreement between the large deflection analysis and the test data is achieved. Similarly the experimental and analytical sensor voltage based on the large deflection analysis is shown in Figure 5.8. The agreement for the sensor voltage between the analysis and the measured experimental results is not as close as the maximum deflection. Deflections and sensor voltages from the small deflection analysis are clearly not agreeable with the test data. The static sensor analysis was based on the assumption that the uniform distributed loading may be modeled as a step function triggered at some time t_O. Analytically, the piezoceramic is capable of producing a static charge, however real piezoceramics are not physically able to sustain a charge to a true DC response [26]. The static sensor experiment used was constructed to approximate a step response by establishing a distributed load and then allowing the generated charge to dissipate, then a ball valve was opened quickly thereby releasing the distributed load. Thus the pressure loading is actually a transient response with a finite rise time. As the distributed loading was increased the slope of the pressure discharge became more critical indicating that the discharge time could no longer be assumed to be instantaneous. Therefore improved analytical results may be obtained by simulating the transient response numerically and computing the subsequent response through Duhamel's integral.

5.2.2 Dynamic Sensor

The dynamic sensor analysis is based on the small deflection assumption since the applied loading was within the linear analysis range. However modal damping values are required and thus determined experimentally and are shown in Table 5.1. The experimental tests were conducted using a point load provided by an electrodynamic

shaker attached to the center of the panel as shown in Figure 5.9. A sinusoidal excitation signal was applied to the shaker and the subsequent piezoceramic voltage was measured and recorded. For the steady state dynamic sensor analysis the structural d.o.f. are transformed into modal coordinates by

$$\{W\} = \sum_{r=1}^{n} q_r(t)\{\psi\}_r = [\psi]\{q\} \tag{5.9}$$

where the $q's$ are the modal coordinates and $[\psi]$ is a reduced set of mode shapes. The small deflection equations of motion may be obtained by substituting Eq. (3.143) into Eq. (3.141) resulting in

$$[M]\{\ddot{W}\} + \left([K_w] - [K_{w\phi}][K_\phi]^{-1}[K_{\phi w}]\right)\{W\} = \{P_W\} \tag{5.10}$$

The equations of motion in Eq. (5.10) may be reduced to a set of uncoupled modal equations of much smaller d.o.f., by utilizing the modal transformation of Eq. (5.9), thus resulting in

$$m_r\ddot{q}_r + c_r\dot{q}_r + k_r q_r = f_r \qquad r = 1,2,\ldots,n \tag{5.11}$$

where the small deflection assumption was imposed resulting in the linear equations of motion. The uncoupled equation of motion of Eq. (5.11) may be written in the following form as

$$\ddot{q}_r + 2\zeta_r\omega_r\dot{q}_r + \omega_r^2 q_r = \frac{f_r}{m_r} \tag{5.12}$$

The modal mass, stiffness and force are obtained from

$$\{\psi\}^T([M],[K])\{\psi\} = (m_r, k_r) \tag{5.13}$$

where

$$[K] = \left([K_w] - [K_{w\phi}][K_\phi]^{-1}[K_{\phi w}]\right) \tag{5.14a}$$

$$\{\psi\}^T\{P_w\} = f_r \tag{5.14b}$$

The modal damping ζ_r ratios were determined experimentally, and are shown in Table 5.1. Thus the modal coordinates q_i in Eq. (5.12) may be determined and substituted into Eq. (5.9) to determine the nodal d.o.f., which are then substituted into Eq. (3.143) to determine the sensor voltage. Note that the first order nonlinear coupling stiffness of Eq. (3.143) is identically zero since the small deflection assumption has been applied. The dynamic analytical sensor voltage due to a sinusoidal point load applied to a 14"x10"x0.040" clamped plate is compared with the dynamic experimental sensor voltage in Figure 5.10. Similarly, the predicted and measured displacements of the plate center are compared in Figure 5.11. Excellent agreement between the experimental results and the analytical predictions are obtained for both the sensor voltage and the plate displacement as expected, given the linear static sensor results for small deflections. The dynamic analysis was computed using the reduced modal data set for the first eight modes shown in Table 5.1.

5.2.3 Dynamic Actuator

Since a single piezoelectric patch was used for the experiments, and it was observed that the resulting plate deflections were small due to piezoelectric actuation, the small deflection analysis was employed in the dynamic actuator formulation. In the experiment, a 120 Hz sinusoidal excitation signal voltage was amplified to 20 volts and supplied to the piezoceramic patch. The resulting acceleration at the panel center was measured as a time history on a fast fourier analyzer. The time domain acceleration signal was transformed in the frequency domain and integrated twice to determine the center plate displacement. The frequency domain integration was performed during post processing using Matlab©.

The actuator equation can be determined from Eq. (3.129) as

$$[M]\{\ddot{W}\}+\left([K_w]-\frac{1}{2}[N1_{N\phi}]-[K_{w\phi}][K_\phi]^{-1}[K_{\phi w}]\right)\{W\}=-[K_{w\phi}][K_\phi]^{-1}\{P_\phi\} \qquad (5.15)$$

where $\{P_\phi\}$ is the electrical loading determined from Eq. (3.126). Similarly the modal coordinate transformation shown in Section 5.2.2 can be applied to Eq. (5.15) resulting in

$$m_r\ddot{q}_r + c_r\dot{q}_r + k_r q_r = f_r \tag{5.16}$$

$$\ddot{q}_r + 2\zeta_r\omega_r\dot{q}_r + \omega_r^2 q_r = \frac{f_r}{m_r} \tag{5.17}$$

The modal mass, stiffness and force are obtained from

$$\{\psi\}_r^T([M],[K])\{\psi\}_r = (m_r, k_r) \tag{5.18}$$

where

$$[K] = \left([K_w] - \frac{1}{2}[N1_{N\phi}] - [K_{w\phi}][K_\phi]^{-1}[K_{\phi w}]\right) \tag{5.19a}$$

$$-\{\psi\}_r^T[K_{w\phi}][K_\phi]^{-1}\{P_\phi\} = f_r \tag{5.19b}$$

and f_r is the applied electrical load determined in Eq. (3.126). Note that even though the small deflection assumption is employed, in the actuation formulation the $[N1_{N\phi}]$ term is included since it is comprised of known quantities shown in Eq. (3.112).

The actuation voltage used in the analysis to determine P_ϕ was applied to a single piezoceramic actuator attached to a 14"x10"x0.040" clamped plate is shown in Figure 5.12. The actuation signal used in the experiment was a 20-volt sine wave of 120 hertz obtained from a signal generator. The predicted and measured displacement of the plate are compared in Figure 5.13 and excellent agreement between the predicted displacement and test data is obtained. Since the displacement of test data is small, the signal-to-noise ratio of the accelerometer was less than ideal resulting in the excessive noise present on the displacement signal.

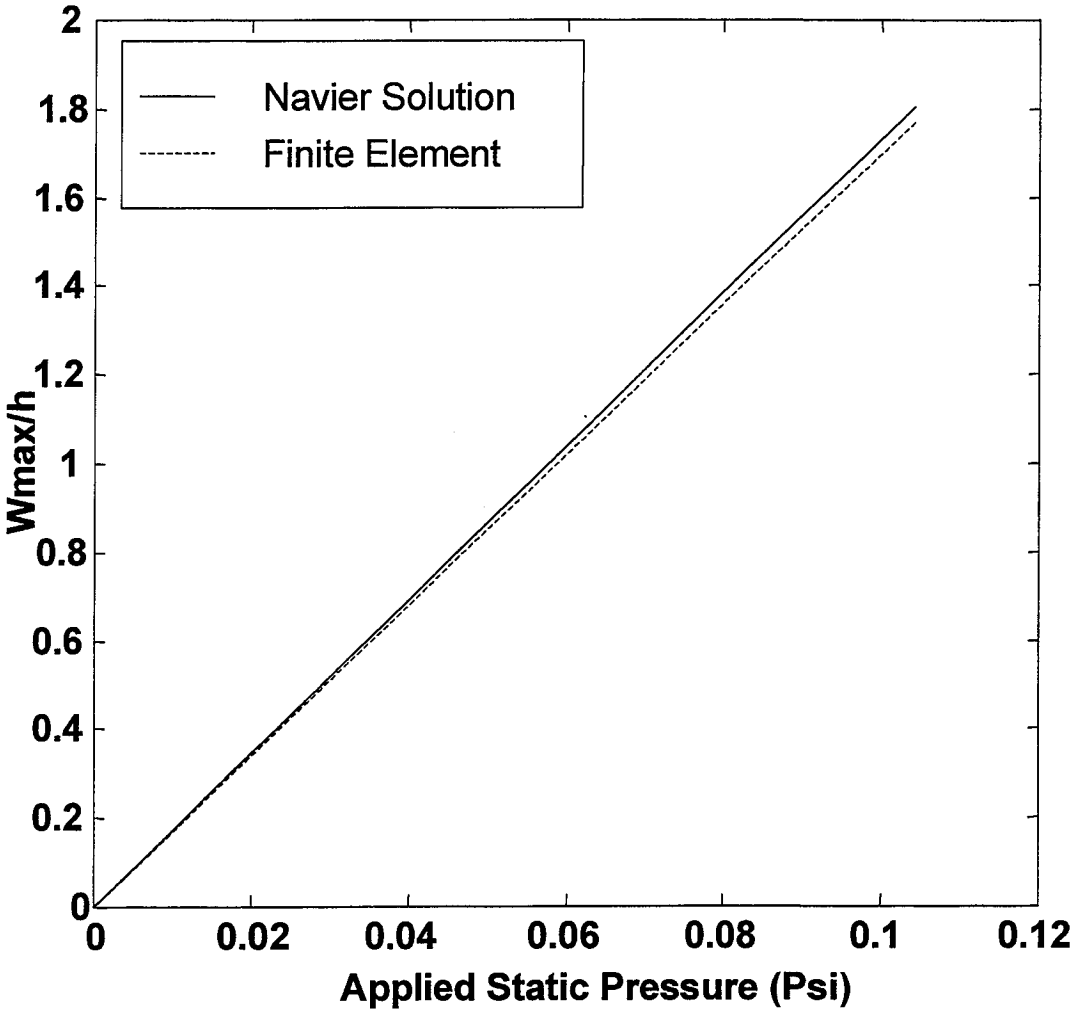

Fig. 5.1 Navier solution vs. finite element analysis non-dimensional displacement

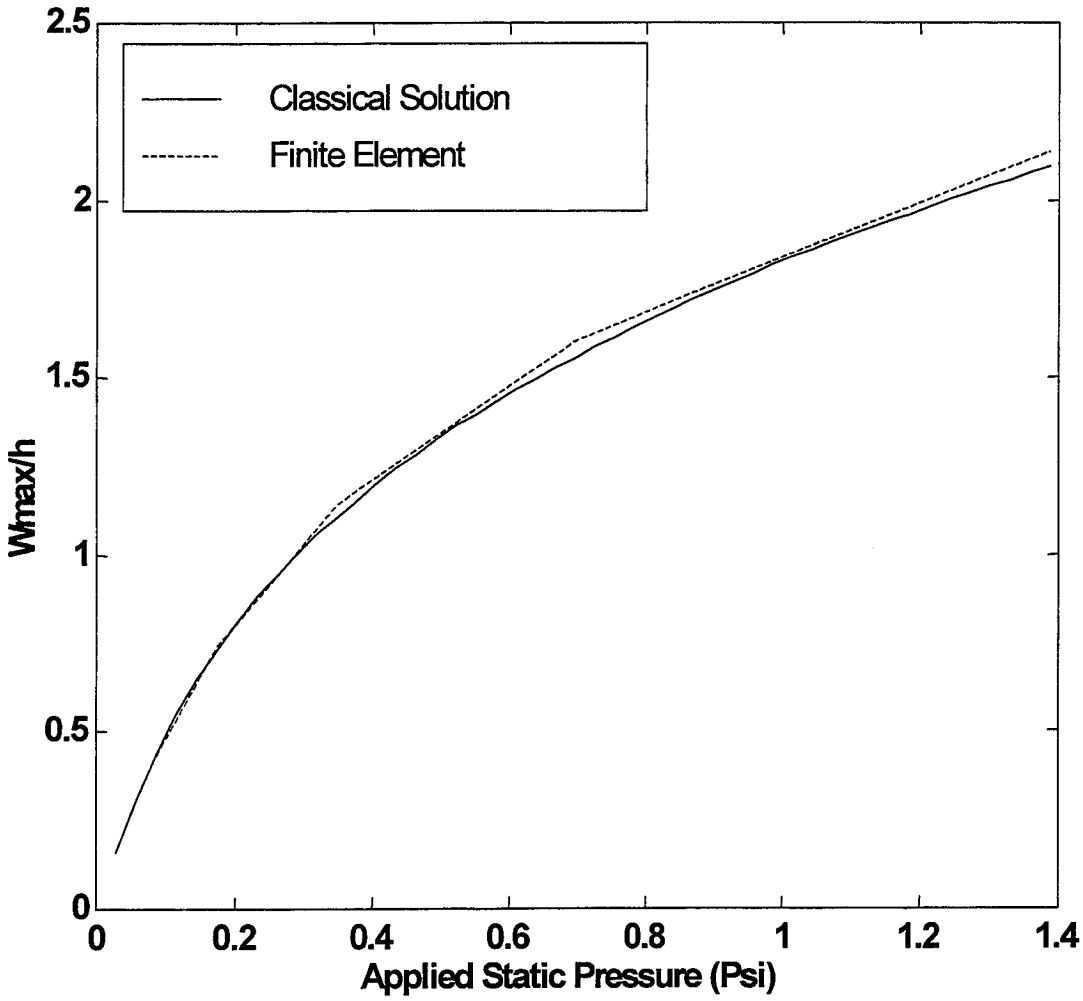

Fig. 5.2 Single mode solution vs. finite element analysis non-dimensional displacement

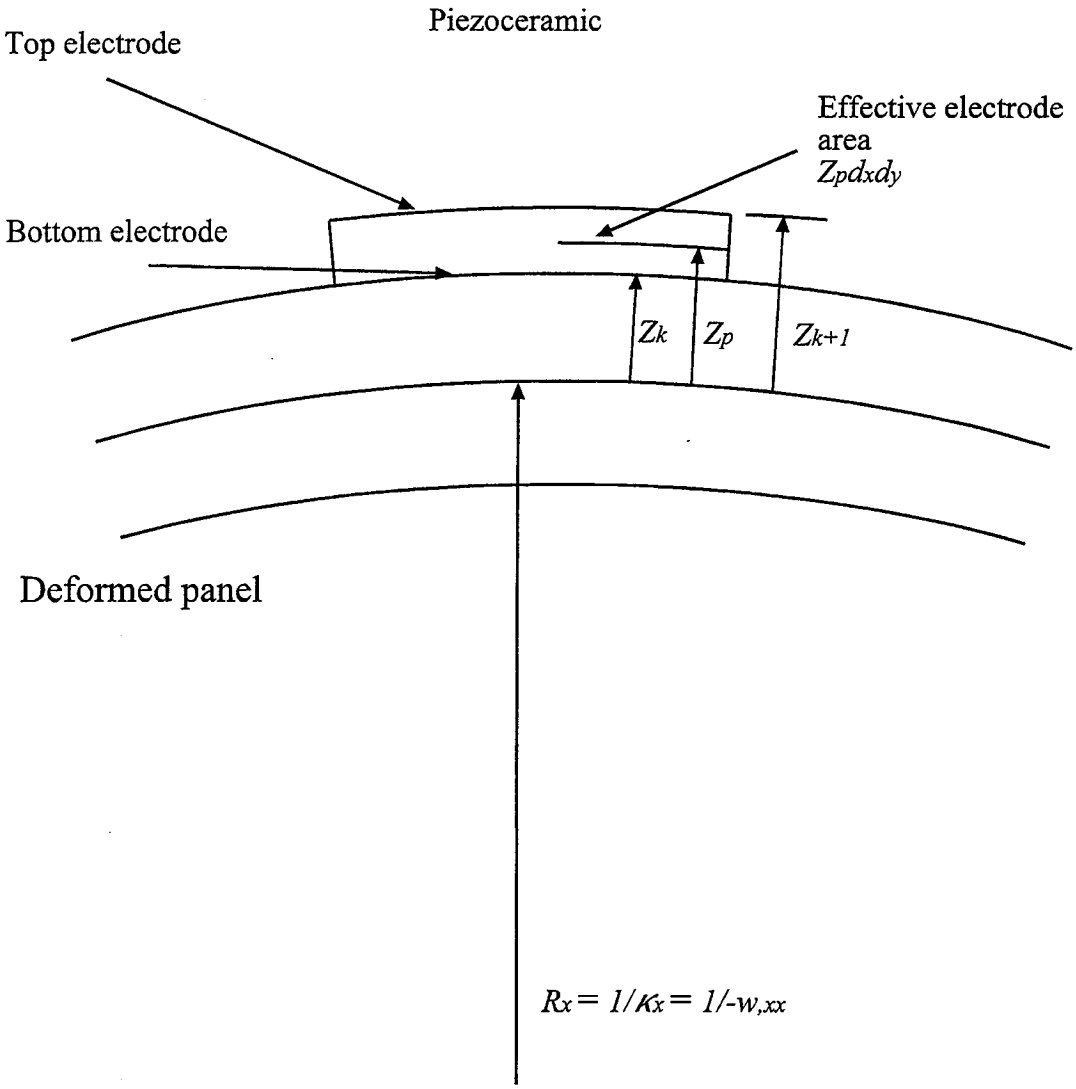

Fig. 5.3 Effective electrode area

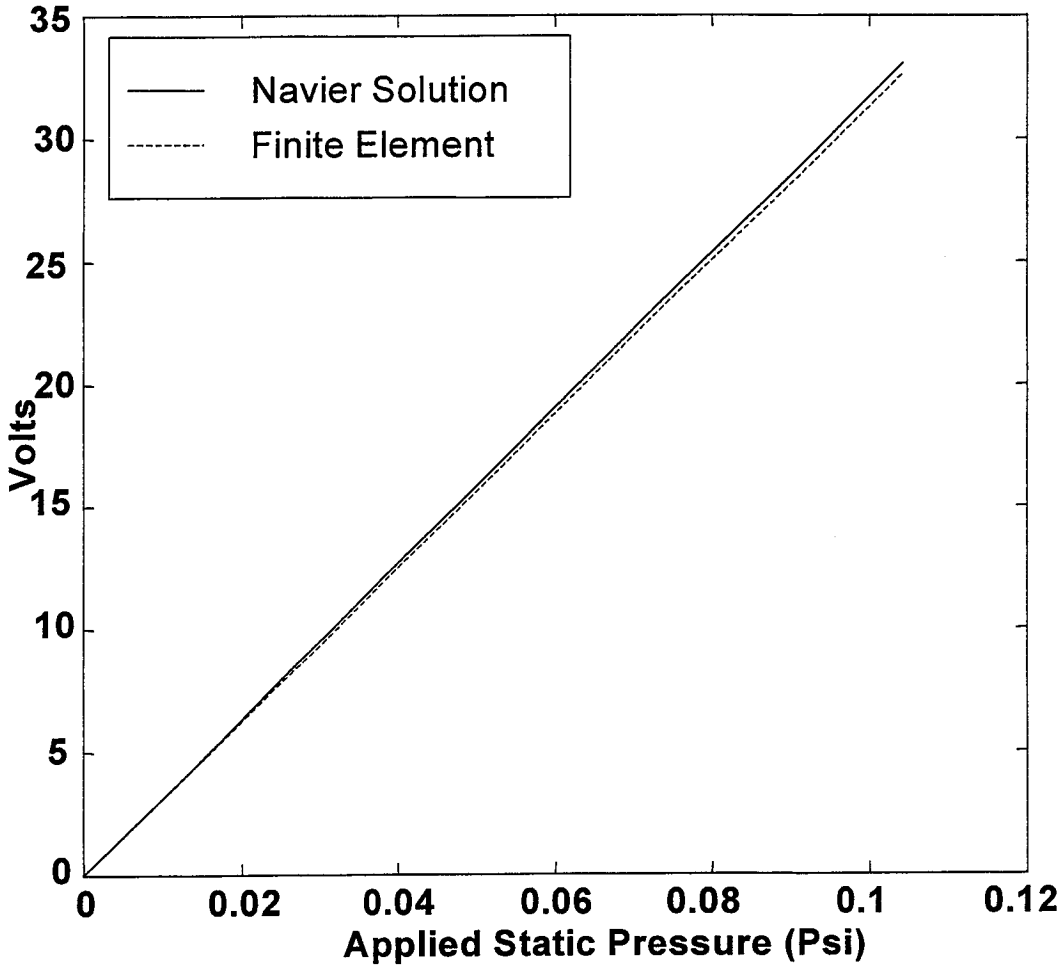

Fig. 5.4 Navier solution vs. finite element analysis sensor voltage

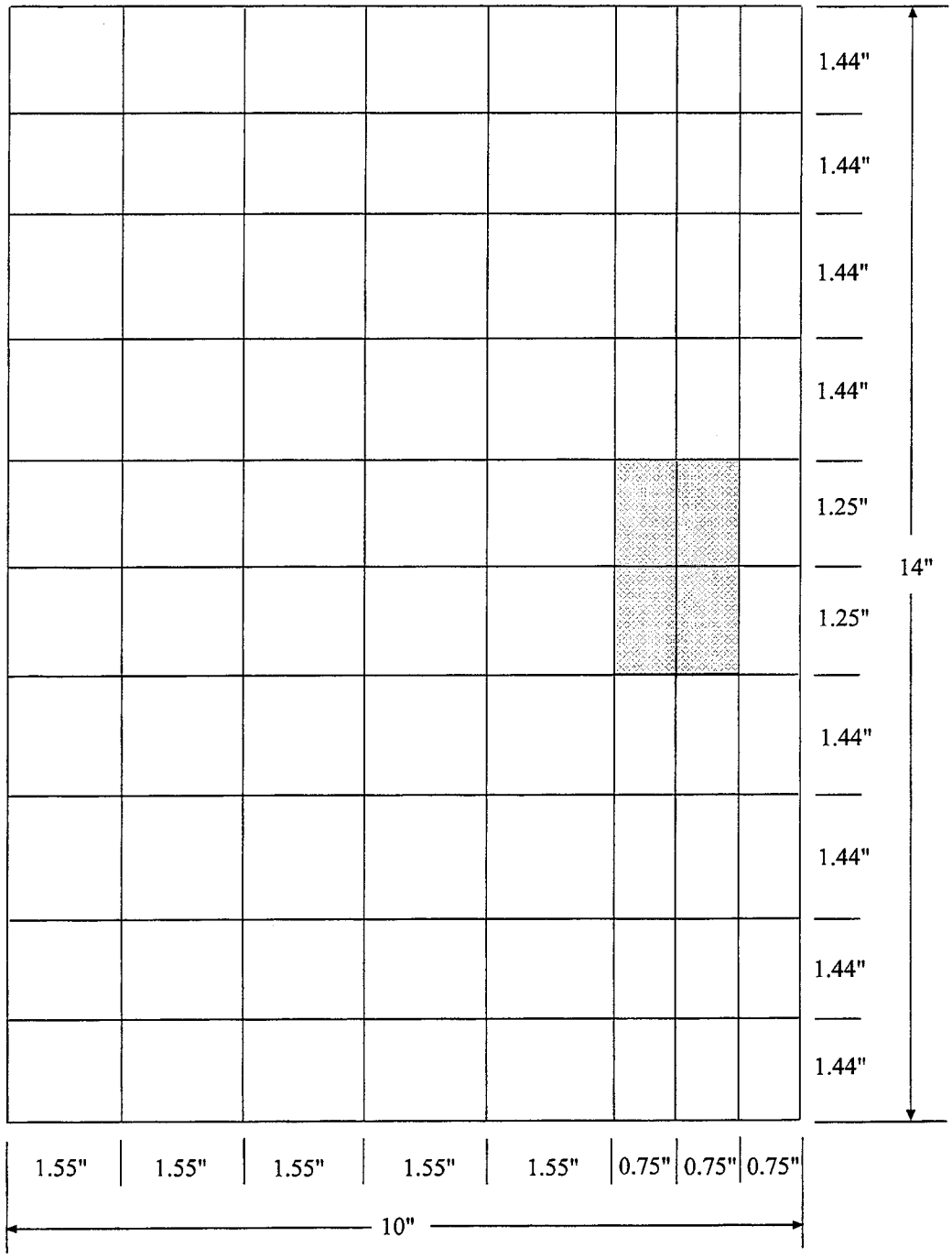

Fig. 5.5 Finite element mesh used for comparison with experiment

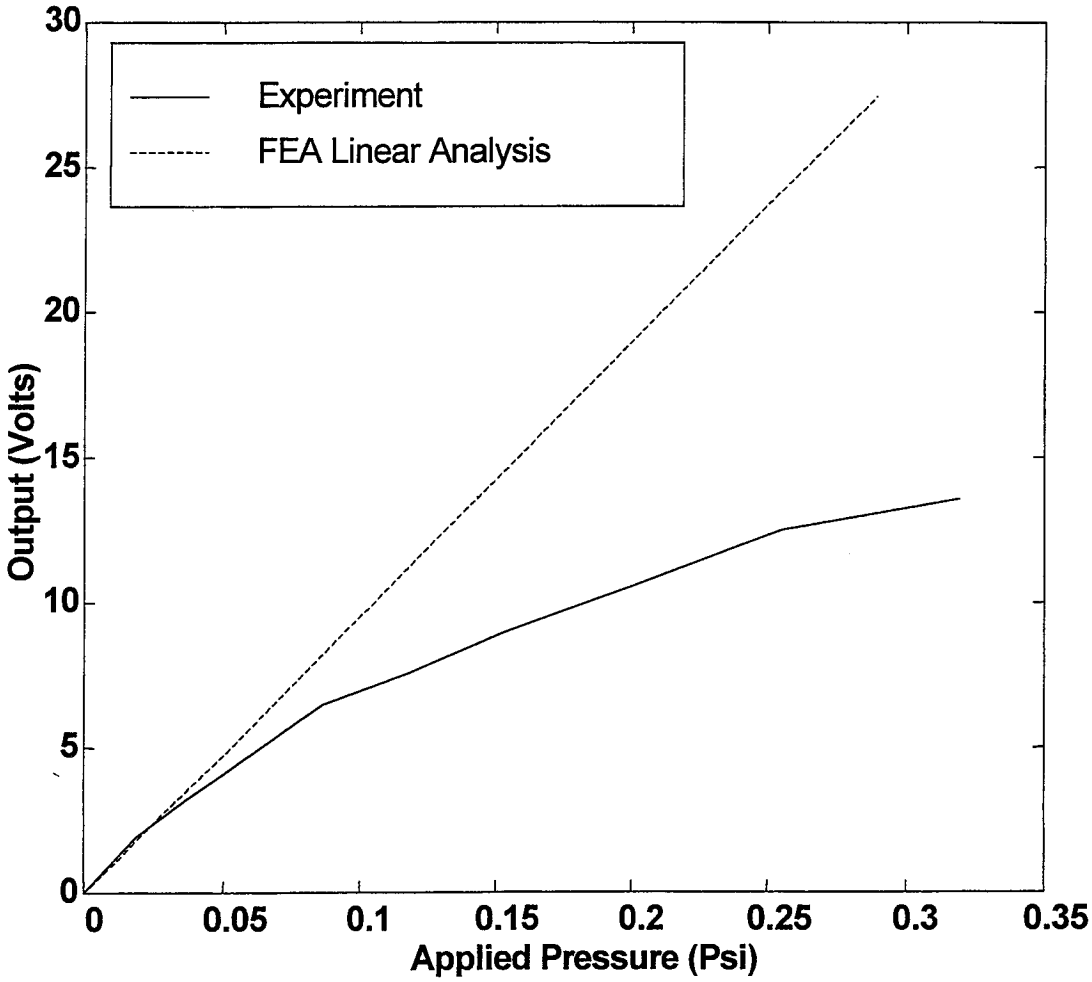

Fig. 5.6 Comparison of static sensor voltage from linear finite element analysis and experiment

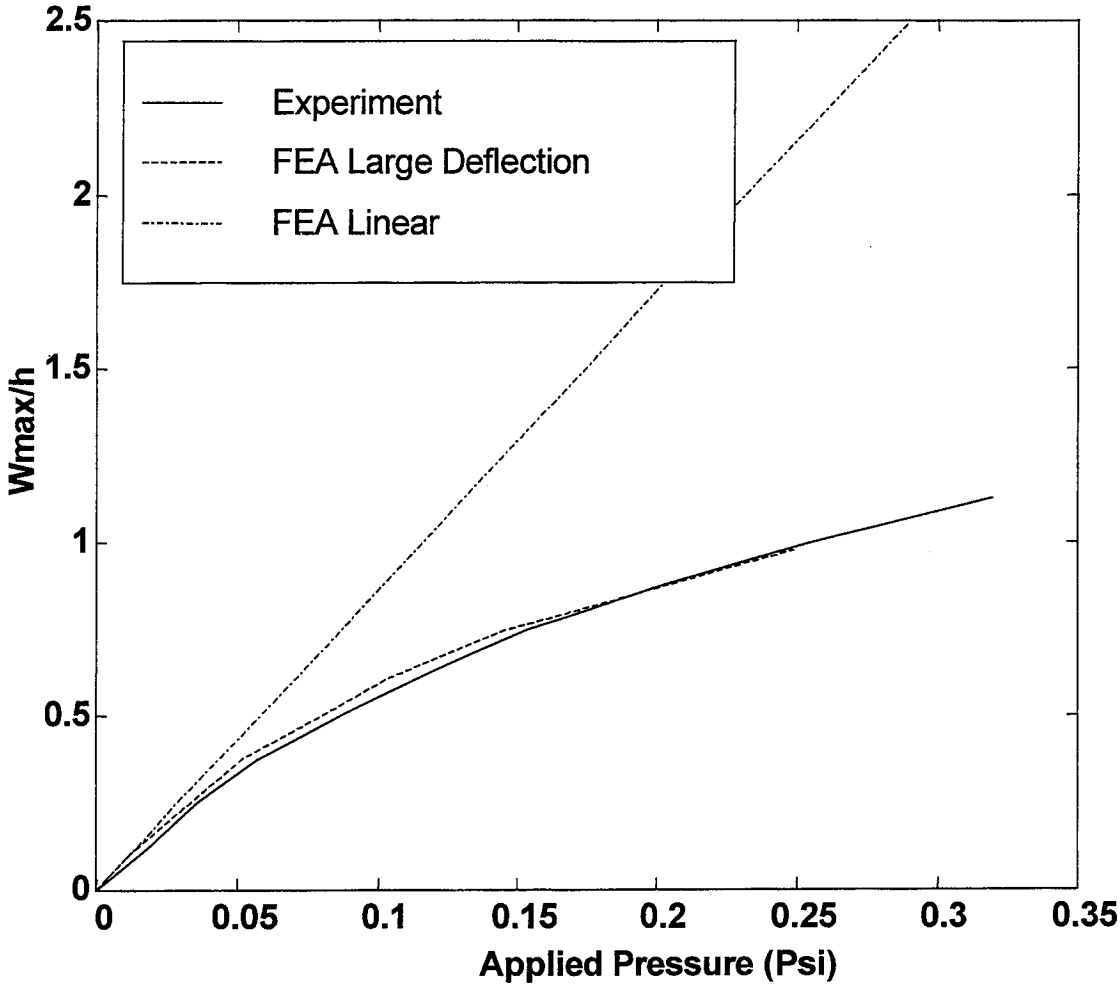

Fig. 5.7 Comparison of non-dimensional displacement from nonlinear finite element and experiment

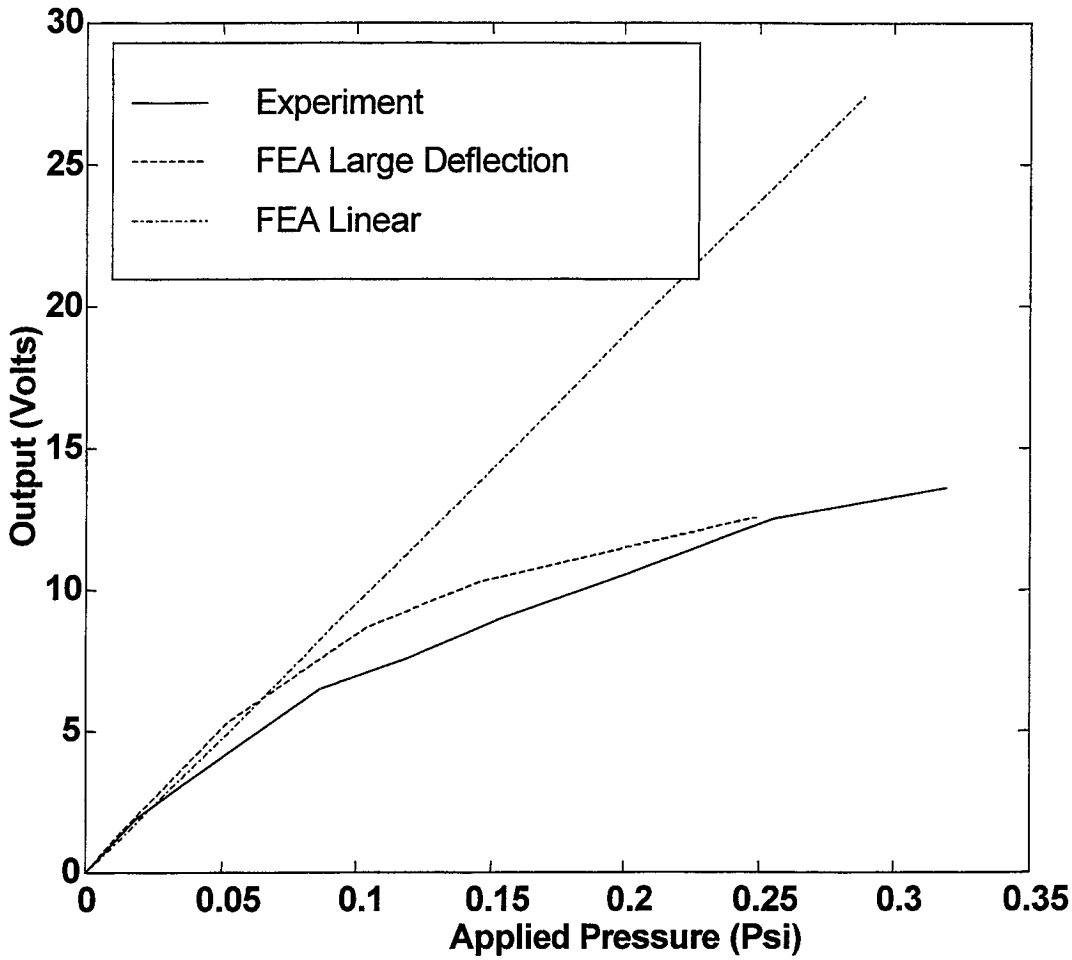

Fig. 5.8 Comparison of large deflection static sensor voltage from nonlinear finite element and experiment

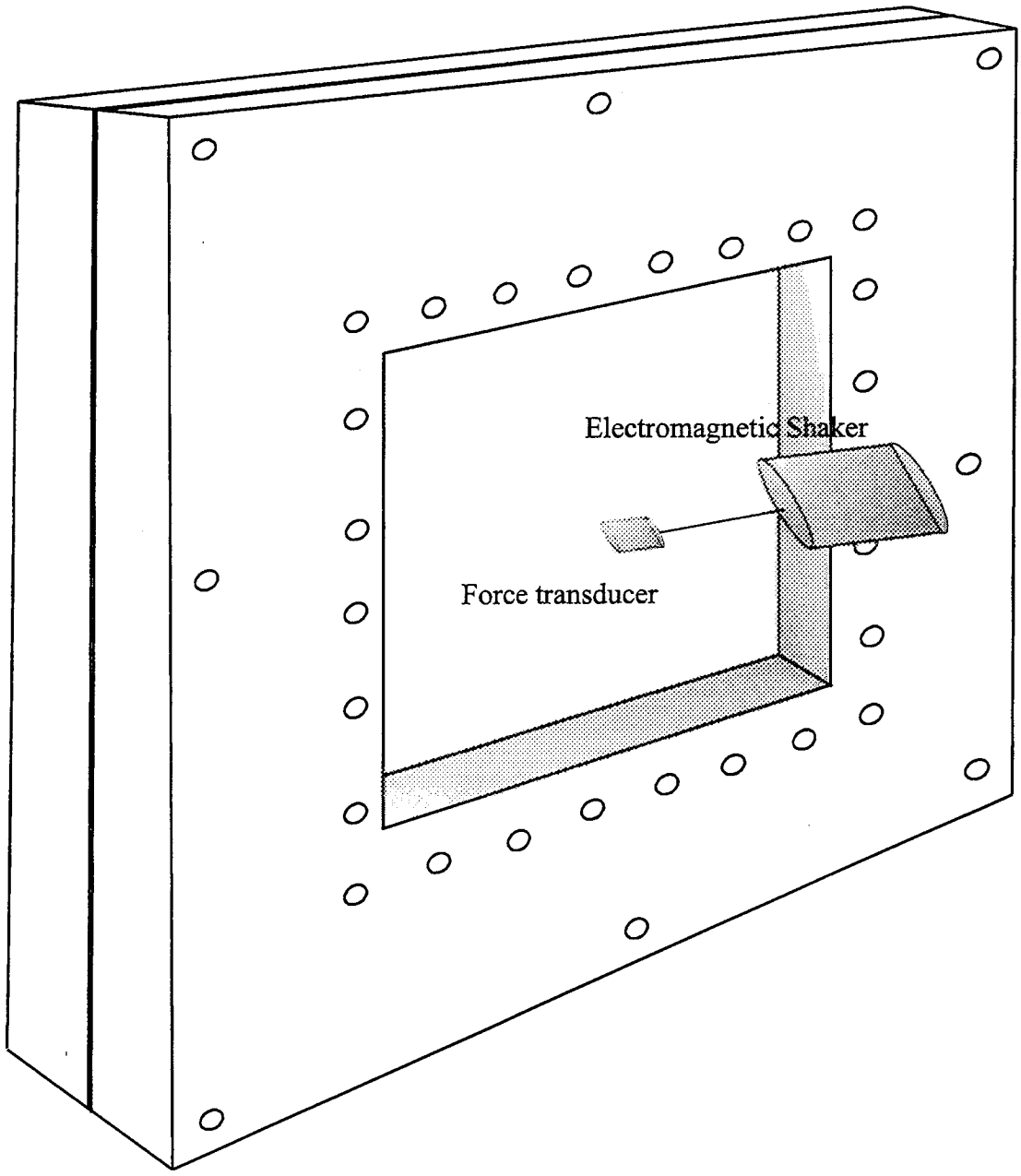

Fig. 5.9 Shaker location

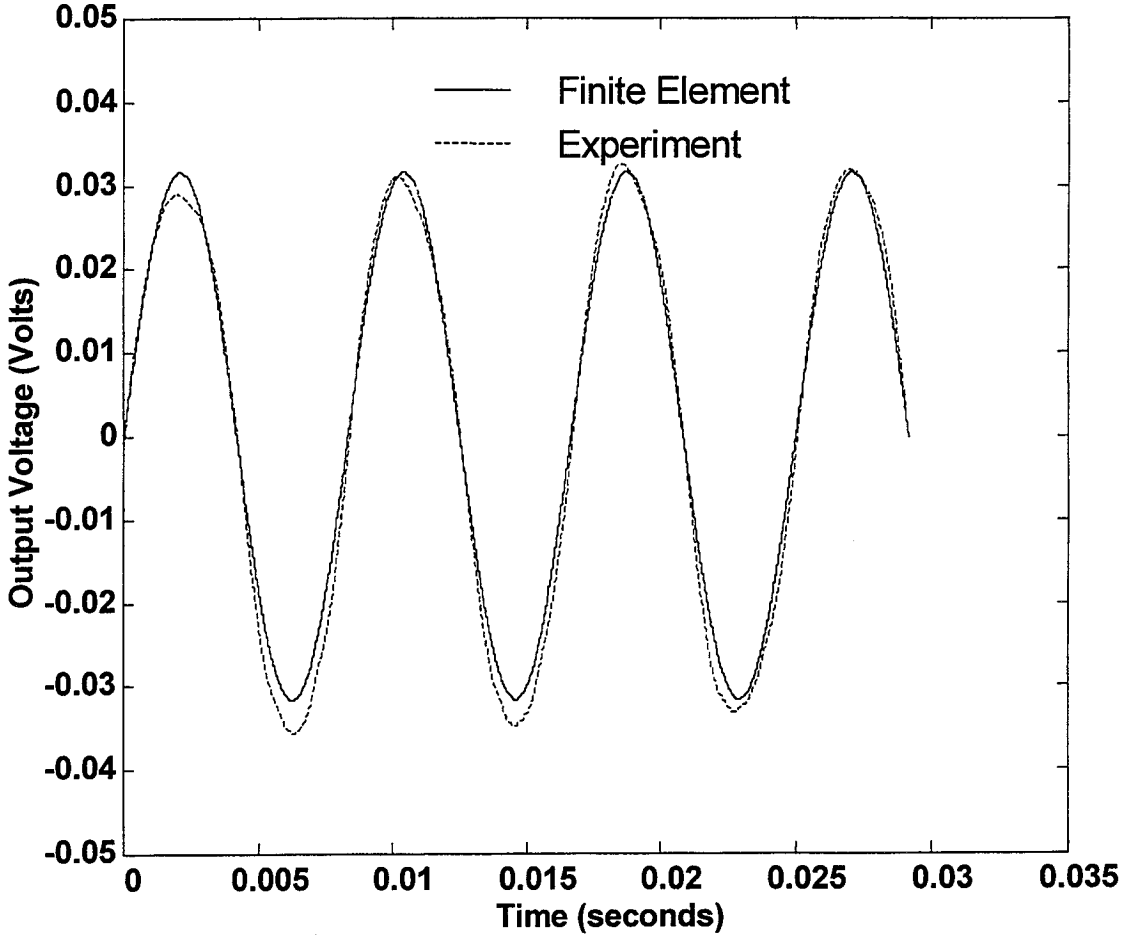

Fig. 5.10 Comparison of dynamic sensor voltage output from finite element analysis and experiment

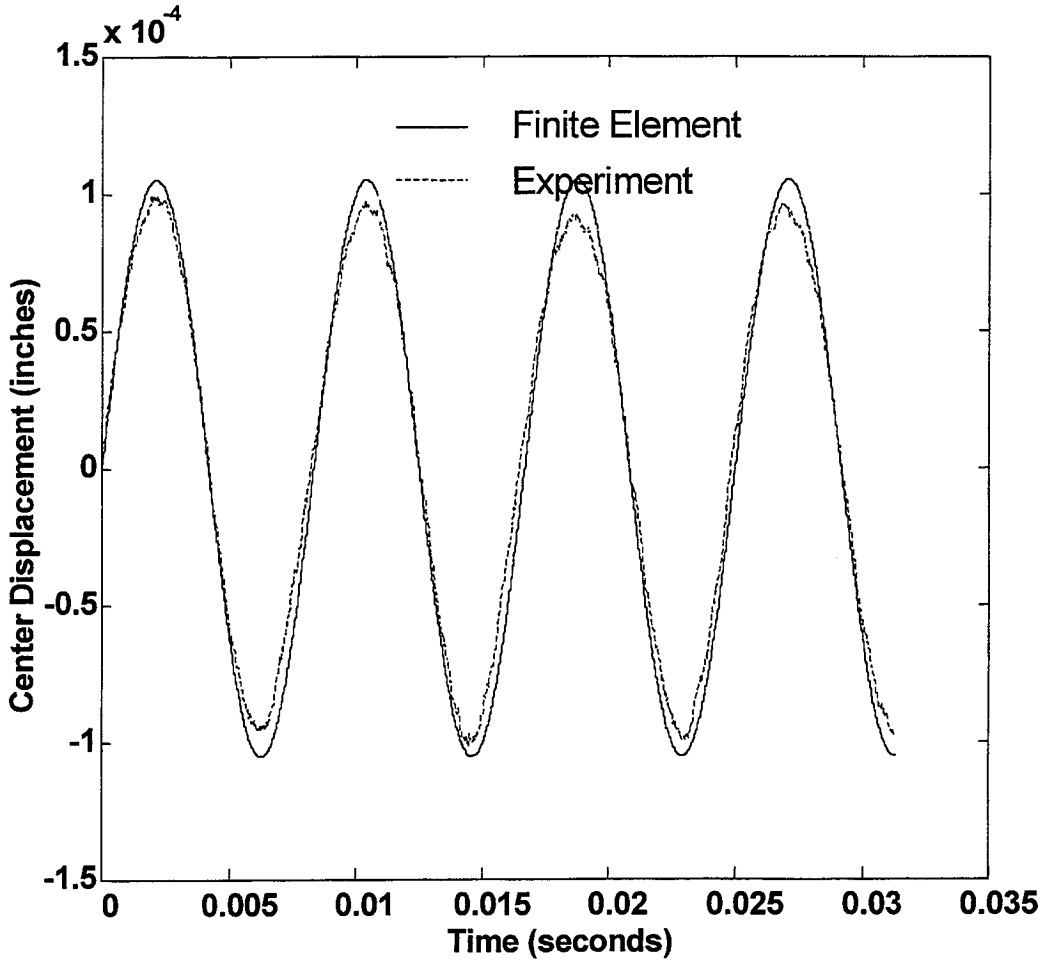

Fig. 5.11 Comparison of dynamic plate displacement from finite element analysis and experiment

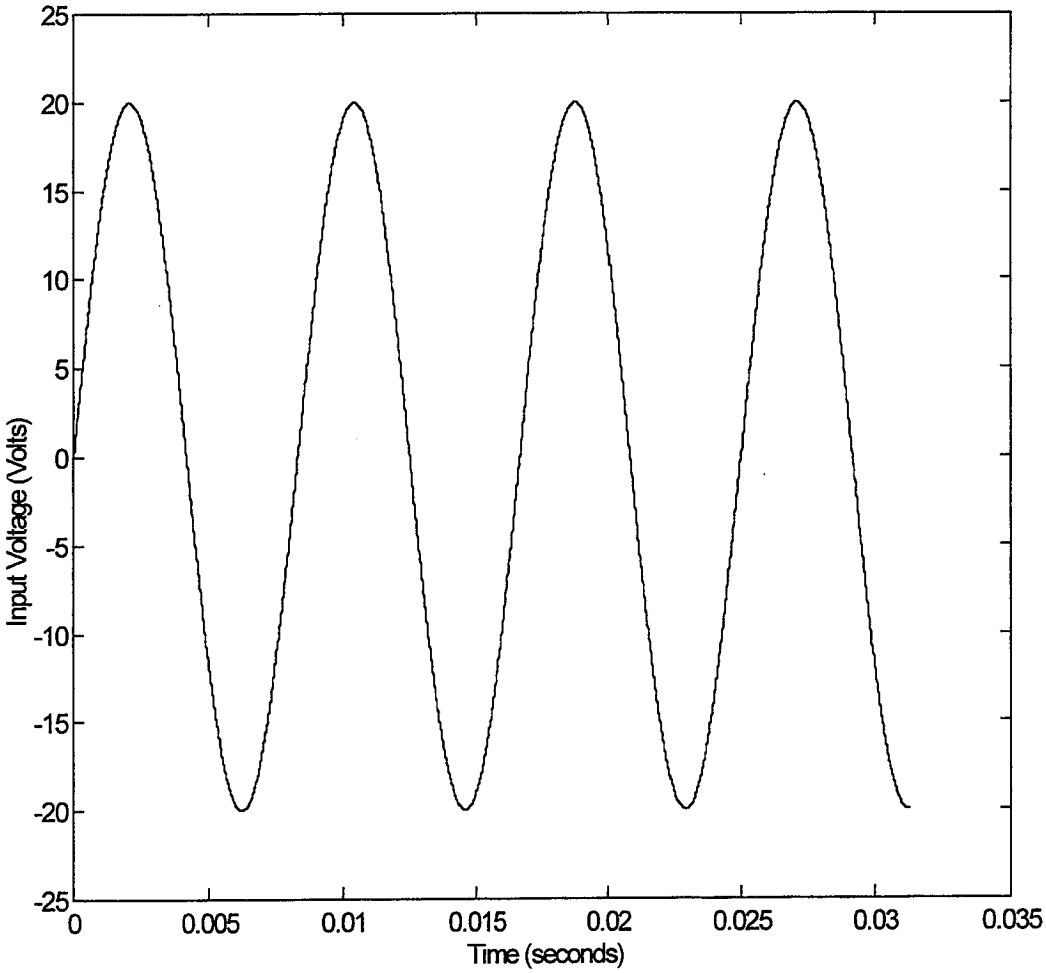

Fig. 5.12 Time history of electrical actuator signal used in the finite element analysis

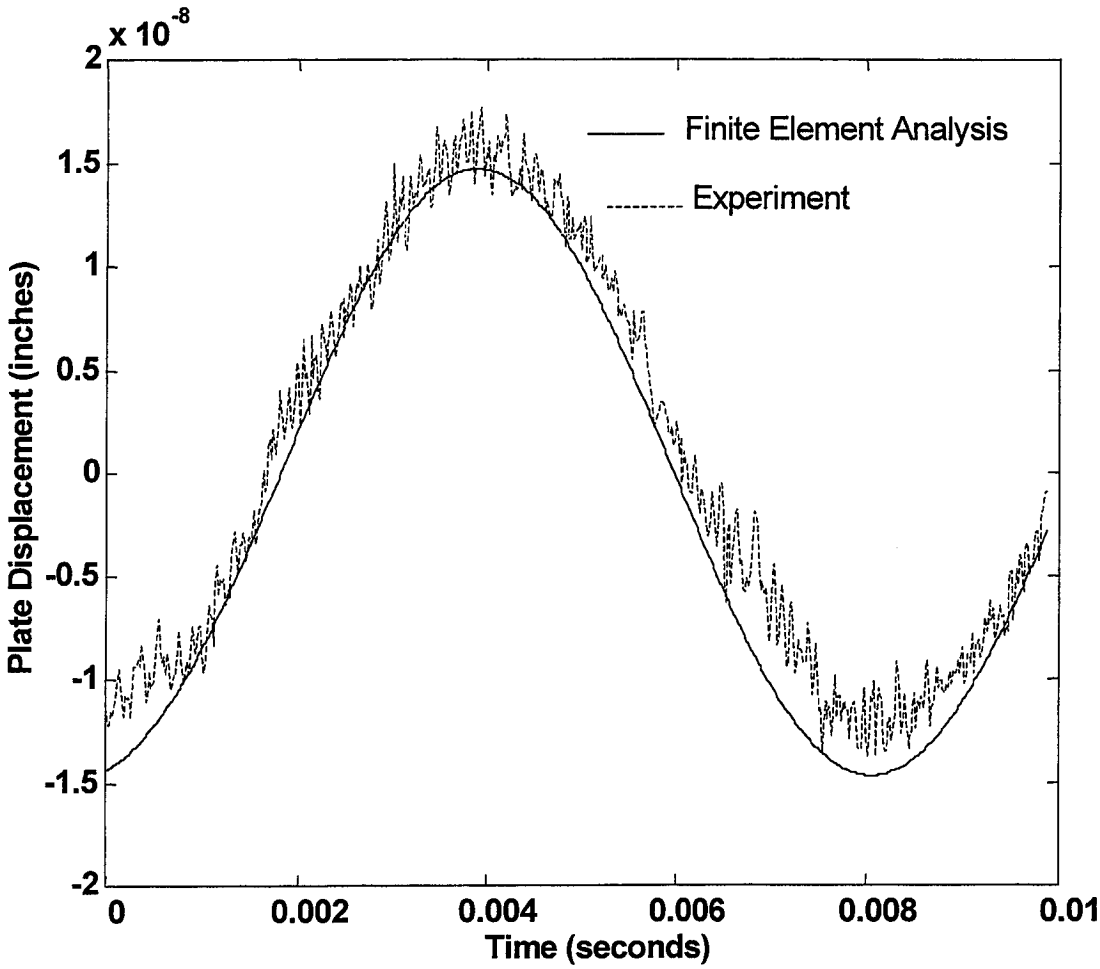

Fig. 5.13 Comparison of actuator plate displacement from finite element and experiment

CHAPTER VI

CONCLUSIONS

A finite element formulation exploiting the inherent electrical-structural coupled nature of piezoelectric materials is presented and compared to experimental test results. To verify the analytical model several tests were performed which included static uniform distributed loading, dynamic mechanical point loading, and dynamic piezoelectric actuation of a thin clamped plate with a bonded piezoceramic patch. The objective was to utilize linear piezoelectric theory in conjunction with the small deflection assumption in the finite element formulation, however the experimental tests indicated that the uniform distributed loading of the panel resulted in geometrical nonlinear transverse deflection. The predicted results obtained using small deflections were in excellent agreement with the test results for small pressure loading, however they were unacceptable for larger load values. The experimental pressure loading considered is not unreasonably high considering typical high speed flight vehicles experience pressures within the 3-5 psi range. Since the panel was selected to represent a typical aerodynamic structure, the finite element formulation was updated to include the von Karman large deflection theory which subsequently lead to coupled nonlinear electrical-structural stiffness. The predicted sensor voltages using the large deflection assumptions were in good agreement when compared to the experimental results. The sensor voltages obtained using the large deflection assumption were not as good as the predicted large deflection displacements, however the small deflection results are clearly unacceptable for the larger pressure loading. Excellent agreement between the predicted results and the dynamic test results were obtained utilizing the small displacement assumption since the experimental test used small dynamic loads.

It was discovered that the electrical-structural coupling of the piezoceramic leads to coupled linear and nonlinear electrical-structural stiffnesses in the large deflection static sensor. The coupled stiffness appears in the Newton-Raphson tangent stiffness

formulation. Thus, even though linear piezoelectric theory was utilized the electrical-structural coupling was sustained through the large deflection geometric nonlinearity.

Experimental measurement error was introduced since a charge attenuation circuit was required due to the large charge signal generated by the piezoceramic patch. The additional capacitance alters the low frequency response of the piezoceramic charge amplifier by decreasing the overall time constant thus, the measurement error may be reduced by modeling the effects of the charge attenuator during analysis. The charge attenuator may be eliminated from the experiment by utilizing a smaller piezoceramic sensor, thus compromising actuator performance, or utilizing a source follower to measure a proportional rate of strain in lieu of a proportional displacement measurement.

A more accurate model of conductors and insulators would improve the electric field formulation in the large deflection static sensor finite element formulation. Improvements can be made to include more elements to accurately model the piezoceramic while utilizing a symmetrical finite element model. However, it was observed that it is important to properly model the electrical boundary conditions when using a symmetrical model. Since the static sensor experiment used a pressure load that approximated a step function, the static sensor results could be improved by simulating the actual transient pressure loading and computing the results through numerical integration. In addition a more accurate method of measuring the static plate deflection should be used in lieu of the dial indicator used.

Future work may be applied in the area of incorporating piezoelectric thermal properties in the analysis or considering the application of control theory to the results. The piezoceramic physical properties show a strong temperature dependency which may be incorporated in the piezoceramic constitutive relations. Thus, a fully coupled electrical, structural, and thermal finite element model can be formulated. The finite element formulation was implemented in Matlab© which permits future opportunity to incorporate control and simulation analysis.

REFERENCES

1. Mason, W. P. *Piezoelectric Crystals and Their Application to Ultrasonics,* D. Van Nostrand Company, Inc., New Jersey, 1950, pp. 2-4.

2. Deresiewicz, H., Bieniek, M. P., Dimaggio, F. L., *The Collected Papers on Raymond D. Mindlin Volume II*, Springer-Verlag, New York, 1989, p. XV.

3. Tzou, H. S., Anderson, G. L., *Intelligent Structural Systems*, Kluwer Academic Publishers, Netherlands, 1992, p. vii.

4. Crawley, E. F., "Intelligent Structures for Aerospace: A Technology Overview and Assessment", *AIAA J.*, Vol. 32, No. 8, 1994, pp. 1689-1699.

5. IEEE Standard 176, "Piezoelectricity", IEEE, New York, 1978.

6. Lee, C. K., "Theory of Laminated Piezoelectric Plates for the Design of Distributed Sensor/Actuators. Part I: Governing Equations and Reciprocal Relationships", *J. Acoustical Society of America*, 87 (3), March 1990, pp. 1144-1158.

7. Dosch, J. J., Inman, D. J., Garcia, E., "A Self-sensing Piezoelectric Actuator for Collocated Control", *J. of Intelligent Material System and Structure*, Vol. 3, Jan. 1992, pp. 166-185.

8. Callahan, J., Baruh, H., "Modal Analysis Using Segmented Piezoelectric Sensors", *AIAA J.*, Vol. 33, No. 12, 1995, pp. 2371-2378.

9. Clark, R. L., Cole, D. G., "Active Damping of Enclosed Sound Fields Through Direct Rate Feedback Control", *J. Acoustical Society of America*, 97 (3), March 1995, pp. 1710-1716.

10. Lai, Z., "Vibration Control with Piezoelectric Actuation Applied to Nonlinear Panel Flutter Suppression", Ph. D. Dissertation, Old Dominion University, Norfolk, Virginia, 1994.

11. Allik, H., Hughes, T. Jr., "Finite Element Method for Piezoelectric Vibration", *International J. for Numerical Methods in Engineering*, Vol. 2, pp. 151-157, 1970.

12. Tzou, H. S., *Piezoelectric Shells*, Kluwer Academic Publishers, Netherlands, 1993, p. 462.

13. Zhou, R. C., "Finite Element Analysis For Nonlinear flutter Suppression of Composites Panels at Elevated Temperatures Using Piezoelectric Materials", Ph. D. Dissertation, Old Dominion University, Norfolk, Virginia, 1994.

14. Zhedudev, I. S., *Physics of Crystalline Dielectrics, Vol. 2 Electrical Properties*, Plenum Press, New York, 1971, pp. 600-601.

15. Anderson, E. H., Hagood, N. W., "Simultaneous Sensing/Actuation: Analysis and Application to Controlled Structures", *J. of Sound and Vibration*, 1994, 174(5), pp. 617-639.

16. Jordan, E. C., Balmain, K. G., *Electromagnetic Waves and Radiating Systems*, Prentice-Hall Inc., New Jersey, 1968, pp. 101-102.

17. Tiersten, H. F., *Linear Piezoelectric Plate Vibration*, Plenum Press, New York, 1969, p. 34.

18. Gibson, R. F., *Principles of Composite Material Mechanics*, McGraw-Hill Inc., New York, 1994, p. 47.

19. Eer Nisse, E. P., "Variational Method for Electroelastic Vibration Analysis", IEEE Transactions On Sonics and Ultrasonics, Vol. SU-14, No. 4, October 1967, pp. 153-160.

20. Dixon, I. R., "Finite Element Analysis of Nonlinear Panel Flutter of Rectangular Composite Plates Under a Uniform Thermal Load", M. S. Thesis, Old Dominion University, Norfolk, Virginia, 1991, pp. 42-48.

21. Product Catalog, Morgan-Matroc Inc., Electro Ceramics Division, Bedford, Ohio, 1993.

22. Halliday, D., Resnick, R., *Fundamentals of Physics*, John Wiley and Sons, New York, 1974, pp. 510-513.

23. Instruction Bulletin B-137-15, Micro-Measurements Division, Measurements Group, Inc., Raleigh, North Carolina.

24. Timoshenko, S., Woinowsky-Krieger, S., *Theory of Plates and Shells*, McGraw-Hill Inc., New York, 1959, p. 110.

25. Chia, C. Y., *Nonlinear Analysis of Plates*, McGraw-Hill Inc., New York, 1980, pp. 65-69.

26. Serridge, M., Licht, T. R., *Piezoelectric Accelerometer and Vibration Preamplifier Handbook*, Brüel & Kjær, Denmark, 1987

27. Product Catalog, PCB Piezotronics, Inc., Depew, New York.

APPENDIX A

TRANSFORMATION MATRICES

The element used in the finite element model is a rectangular element consisting of twenty four structural degrees of freedom, accounting for bending and membrane displacements plus an additional electrical degree of freedom for each piezoelectric layer. The rectangular element consists of four corner nodes with displacements *w, u, v* and their derivatives w_x, w_y, w_{xy}. The electrical d.o.f.'s are represented by the voltage V uniformly distributed over one side of the piezoelectric electrode, see Figure 3.1.

Coordinate transformations are required to relate the local element coordinates to the global structural coordinates. The membrane nodal displacements, given by

$$\{w_m\}^T = \lfloor u_1 \quad u_2 \quad u_3 \quad u_4 \quad v_1 \quad v_2 \quad v_3 \quad v_4 \rfloor \tag{A1}$$

are obtained using the bilinear approximation functions in Eq. (3.6). The nodal membrane displacements can be obtained by substituting the element nodal coordinates into the appropriate approximation functions. Thus the membrane nodal displacements become

$$u_1(0,0,t) = b_1 \tag{A1}$$

$$u_2(a_e,0,t) = b_1 + b_2 a_e \tag{A2}$$

$$u_3(a_e,b_e,t) = b_1 + b_2 a_e + b_3 b_e + b_4 a_e b_e \tag{A3}$$

$$u_4(0,b_e,t) = b_1 + b_3 b_e \tag{A4}$$

$$v_1(0,0,t) = b_5 \tag{A5}$$

$$v_2(a_e,0,t) = b_5 + b_6 a_e \tag{A6}$$

$$v_3(a_e,b_e,t) = b_5 + b_6 a_e + b_7 b_e + b_8 a_e b_e \tag{A7}$$

$$v_4(0,b_e,t)=b_5+b_7b_e \tag{A8}$$

where the element length and width are a_e and b_e respectively and the generalized coordinates are represented by the b coefficients.

The membrane displacements in Eqs. (A1-A8) may be written in matrix notation as

$$\begin{Bmatrix} u_1 \\ u_3 \\ u_3 \\ u_4 \\ v_1 \\ v_2 \\ v_3 \\ v_4 \end{Bmatrix} = \begin{bmatrix} 1 & 0 & 0 & 0 & 0 & 0 & 0 & 0 \\ 1 & a_e & 0 & 0 & 0 & 0 & 0 & 0 \\ 1 & a_e & b_e & a_eb_e & 0 & 0 & 0 & 0 \\ 1 & 0 & b_e & 0 & 0 & 0 & 0 & 0 \\ 0 & 0 & 0 & 0 & 1 & 0 & 0 & 0 \\ 0 & 0 & 0 & 0 & 1 & a_e & 0 & 0 \\ 0 & 0 & 0 & 0 & 1 & a_e & b_e & a_eb_e \\ 0 & 0 & 0 & 0 & 1 & 0 & b_e & 0 \end{bmatrix} \begin{Bmatrix} b_1 \\ b_2 \\ b_3 \\ b_4 \\ b_5 \\ b_6 \\ b_7 \\ b_8 \end{Bmatrix} \tag{A9}$$

Similarly the bending transformation is determined using sixteen d.o.f. Thus the sixteen bending nodal displacements are

$$\begin{aligned} \{w_b\}^T = \{ & w_1 \quad w_2 \quad w_3 \quad w_4 \quad w_{,x1} \quad w_{,x2} \quad w_{,x3} \quad w_{,x4} \\ & w_{,y1} \quad w_{,y2} \quad w_{,y3} \quad w_{,y4} \quad w_{,xy1} \quad w_{,xy2} \quad w_{,xy3} \quad w_{,xy4} \end{aligned} \tag{A10}$$

The displacements are approximated using the cubic polynomial defined by Eq. (3.4). Thus, the derivative expressions are given by

$$\begin{aligned} w_{,x} = {} & a_2+2a_4x+a_5y+3a_7x^2+2a_8xy+a_9y^2+3a_{11}x^2y \\ & +2a_{12}xy^2+a_{13}y^3+3a_{14}x^2y^2+2a_{15}xy^3+3a_{16}x^2y^3 \end{aligned} \tag{A11}$$

$$\begin{aligned} w_{,y} = {} & a_3+a_5x+2a_6y+a_8x^2+2a_9xy+3a_{10}y^2+a_{11}x^3 \\ & +2a_{12}x^2y+3a_{13}xy^2+2a_{14}x^3y+3a_{15}x^2y^2+3a_{16}x^3y^2 \end{aligned} \tag{A12}$$

$$w_{,xy} = a_5 + 2a_8 x + 2a_9 y + 3a_{11} x^2 + 4a_{12} xy$$

$$+ 3a_{13} y^2 + 6a_{14} x^2 y + 6a_{15} xy^2 + 9a_{16} x^2 y^2 + 3a_{16} x^3 y^2 \qquad \text{(A13)}$$

The nodal bending displacements are obtained by substituting the nodal coordinates into Eq. (3.4) and Eqs. (A4-A6). Thus the transverse displacements are given as

$$w_1(0,0,t) = a_1 \qquad \text{(A14)}$$

$$w_2(a_e,0,t) = a_1 + a_2 a_e + a_4 a_e^2 + a_7 a_e^3 \qquad \text{(A15)}$$

$$w_3(a_e,b_e,t) = a_1 + a_2 a_e + a_3 b_e + a_4 a_e^2 + a_5 a_e b_e + a_6 b_e^2$$

$$+ a_9 a_e b_e^2 + a_{10} b_e^3 + a_{11} a_e^3 b_e + a_{12} a_e^2 b_e^2$$

$$+ a_{13} a_e b_e^3 + a_{14} a_e^3 b_e^2 + a_{15} a_e^2 b_e^3 \qquad \text{(A16)}$$

$$w_4(0,b_e,t) = a_1 + a_3 b_e^3 + a_6 b_e^2 + a_{10} b_e^3 \qquad \text{(A17)}$$

Likewise, the slopes with respect to the x-axis are

$$w_{,x1}(0,0,t) = a_2 \qquad \text{(A18)}$$

$$w_{,x2}(a_e,0,t) = a_2 + 2a_4 a_e + 3a_7 a_e^2 \qquad \text{(A19)}$$

$$w_{,x3}(a_e,b_e,t) = a_2 + 2a_4 a_e + a_5 b_e + 3a_7 a_e^2 + 2a_8 a_e b_e$$

$$+ a_9 b_e^2 + 3a_{11} a_e^2 b_e + 2a_{12} a_e b_e^{12} + a_{13} b_e^3$$

$$+ 3a_{14} a_e^2 b_e^2 + 2a_{15} a_e b_e^3 + a_{16} a_e^2 b_e^3 \qquad \text{(A20)}$$

$$w_{,x4}(0,b_e,t) = a_2 + a_5 b_e + a_9 b_e^2 + a_{13} b_e^3 \qquad \text{(A21)}$$

The slopes with respect to the y-axis are

$$w_{,y1}(0,0,t) = a_3 \tag{A22}$$

$$w_{,y2}(a_e,0,t) = a_3 + a_5 a_e + a_8 a_e^2 + a_{11} a_e^3 \tag{A23}$$

$$\begin{aligned} w_{,y3}(a_e,b_e,t) = {} & a_3 + a_5 a_e + 2a_6 b_e + a_8 a_e^2 + 2a_9 a_e b_e \\ & + 3a_{10} b_e^2 + a_{11} a_e^3 + 2a_{12} a_e^2 b_e + 3a_{13} b_e^2 \\ & + 2a_{14} a_e^3 b_e + 3a_{15} a_e^2 b_e^2 + 3a_{16} a_e^3 b_e^2 \end{aligned} \tag{A24}$$

$$w_{,y4}(0,b_e,t) = a_3 + 2a_6 b_e + 3a_{10} b_e^2 \tag{A25}$$

The rotations about the *z*-axis are

$$w_{,xy1}(0,0,t) = a_5 \tag{A26}$$

$$w_{,xy2}(a_e,0,t) = a_5 + 2a_8 a_e + 3a_{11} a_e^2 \tag{A27}$$

$$\begin{aligned} w_{,xy3}(a_e,b_e,t) = {} & a_5 + 2a_8 a_e + 2a_9 b_e + 3a_{11} a_e^2 \\ & + 4a_{12} a_e b_e + 3a_{13} b_e^2 + 6a_{14} e_e^2 b_e \\ & + 6a_{15} a_e b_e^{12} + 9a_{16} a_e^2 b_e^2 \end{aligned} \tag{A28}$$

$$w_{,xy4}(0,b_e,t) = a_5 + 2a_9 b_e + 3a_{13} b_e^2 \tag{A29}$$

Equation (A14-22) may be expressed in matrix notion as $\{w_b\} = [T_b]^{-1}\{a\}$ where $[T_b]^{-1}$ is defined as

$$[T_b]^{-1} = \begin{bmatrix}
1 & 0 & 0 & 0 & 0 & 0 & 0 & 0 & 0 & 0 & 0 & 0 & 0 & 0 & 0 & 0 \\
1 & a_e & 0 & a_e^2 & 0 & 0 & a_e^3 & 0 & 0 & 0 & 0 & 0 & 0 & 0 & 0 & 0 \\
1 & a_e & b_e & a_e^2 & a_e b_e & b_e^2 & a_e^3 & a_e^2 b_e & a_e b_e^2 & b_e^3 & a_e^3 b_e & a_e^2 b_e^2 & a_e b_e^3 & a_e^3 b_e^2 & a_e^2 b_e^3 & a_e^3 b_e^3 \\
1 & 0 & b_e & 0 & 0 & b_e^2 & 0 & 0 & 0 & b_e^3 & 0 & 0 & 0 & 0 & 0 & 0 \\
0 & 1 & 0 & 0 & 0 & 0 & 0 & 0 & 0 & 0 & 0 & 0 & 0 & 0 & 0 & 0 \\
0 & 1 & 0 & 2a_e & 0 & 0 & 3a_e^2 & 0 & 0 & 0 & 0 & 0 & 0 & 0 & 0 & 0 \\
0 & 1 & 0 & 2a_e & b_e & 0 & 3a_e^2 & 2a_e b_e & b_e^2 & 0 & 3a_e^2 b_e & 2a_e b_e^2 & b_e^3 & 3a_e^2 b_e^2 & 2a_e b_e^3 & 3a_e^2 b_e^3 \\
0 & 1 & 0 & 0 & b_e & 0 & 0 & 0 & b_e^2 & 0 & 0 & 0 & b_e^3 & 0 & 0 & 0 \\
0 & 0 & 1 & 0 & 0 & 0 & 0 & 0 & 0 & 0 & 0 & 0 & 0 & 0 & 0 & 0 \\
0 & 0 & 1 & 0 & a_e & 0 & 0 & a_e^2 & 0 & 0 & a_e^3 & 0 & 0 & 0 & 0 & 0 \\
0 & 0 & 1 & 0 & a_e & 2b_e & 0 & a_e^2 & 2a_e b_e & 3b_e^2 & a_e^3 & 2a_e^2 b_e & 3a_e b_e^2 & 2a_e^3 b_e & 3a_e^2 b_e^2 & 3a_e^3 b_e^2 \\
0 & 0 & 1 & 0 & 0 & 2b_e & 0 & 0 & 0 & 3b_e^2 & 0 & 0 & 0 & 0 & 0 & 0 \\
0 & 0 & 0 & 0 & 1 & 0 & 0 & 0 & 0 & 0 & 0 & 0 & 0 & 0 & 0 & 0 \\
0 & 0 & 0 & 0 & 1 & 0 & 0 & 2a_e & 0 & 0 & 3a_e^2 & 0 & 0 & 0 & 0 & 0 \\
0 & 0 & 0 & 0 & 1 & 0 & 0 & 2a_e & 2b_e & 0 & 3a_e^2 & 4a_e b_e & 3b_e^2 & 6a_e^2 b_e & 6a_e b_e^2 & 9a_e^2 b_e^2 \\
0 & 0 & 0 & 0 & 1 & 0 & 0 & 0 & 2b_e & 0 & 0 & 0 & 3b_e^2 & 0 & 0 & 0
\end{bmatrix} \quad \text{(A30}$$

the bending transformation matrix $[T_b]$ therefore is obtained by inverting the matrix in Eq. (A30).

APPENDIX B

COORDINATE TRANSFORMATION

B.1 Transformed Reduced Stiffness Matrix

The stress-strain relations for a thin orthotropic layer are of the form

$$\begin{Bmatrix}\sigma_1\\ \sigma_2\\ \tau_{12}\end{Bmatrix}=\begin{bmatrix}Q_{11} & Q_{12} & 0\\ Q_{12} & Q_{22} & 0\\ 0 & 0 & Q_{66}\end{bmatrix}\begin{Bmatrix}\varepsilon_1\\ \varepsilon_2\\ \gamma_{12}\end{Bmatrix} \tag{B1}$$

where the subscripts *1* and *2* refer to material coordinate directions. The reduced stiffness matrix, $[Q]$ is a function of engineering constants as follows

$$Q_{11}=\frac{E_1}{1-\nu_{12}\nu_{21}} \tag{B2}$$

$$Q_{12}=\frac{\nu_{12}E_2}{1-\nu_{12}\nu_{21}} \tag{B3}$$

$$Q_{22}=\frac{E_2}{1-\nu_{12}\nu_{21}} \tag{B4}$$

$$Q_{66}=G_{12} \tag{B5}$$

The stresses in the material coordinate system can be transformed into the global *x-y* coordinate system by

$$\begin{Bmatrix}\sigma_x\\ \sigma_y\\ \tau_{xy}\end{Bmatrix}=\begin{bmatrix}\cos^2\theta & sin^2\theta & -2sin\theta\cos\theta\\ sin^2\theta & \cos^2\theta & 2sin\theta\cos\theta\\ sin\theta\cos\theta & -sin\theta\cos\theta & \cos^2\theta-sin^2\theta\end{bmatrix}\begin{Bmatrix}\sigma_1\\ \sigma_2\\ \tau_{12}\end{Bmatrix}$$

$$=[T_\sigma(\theta)]\begin{Bmatrix}\sigma_x\\ \sigma_y\\ \tau_{xy}\end{Bmatrix} \tag{B6}$$

The strain transformation can be expressed as

$$\begin{Bmatrix} \varepsilon_x \\ \varepsilon_y \\ \gamma_{xy} \end{Bmatrix} = \begin{bmatrix} cos^2\theta & sin^2\theta & sin\theta cos\theta \\ sin^2\theta & cos^2\theta & -sin\theta cos\theta \\ -2sin\theta cos\theta & 2sin\theta cos\theta & cos^2\theta - sin^2\theta \end{bmatrix} \begin{Bmatrix} \varepsilon_1 \\ \varepsilon_2 \\ \gamma_{12} \end{Bmatrix}$$

$$= [T_\varepsilon(\theta)] \begin{Bmatrix} \varepsilon_1 \\ \varepsilon_2 \\ \gamma_3 \end{Bmatrix} \tag{B7}$$

where θ is the lamination fiber angle with positive rotation from the x-axis with respect to the principal material coordinate *1*-axis as shown in Figure B1. Combining Eqs. (B1-B7) yields the laminate transformed reduced stiffness matrix

$$\begin{Bmatrix} \sigma_x \\ \sigma_y \\ \tau_{xy} \end{Bmatrix} = \begin{bmatrix} \overline{Q}_{11} & \overline{Q}_{12} & \overline{Q}_{16} \\ \overline{Q}_{12} & \overline{Q}_{22} & \overline{Q}_{26} \\ \overline{Q}_{16} & \overline{Q}_{26} & \overline{Q}_{66} \end{bmatrix} \begin{Bmatrix} \varepsilon_x \\ \varepsilon_y \\ \gamma_{xy} \end{Bmatrix} \tag{B8}$$

where

$$[\overline{Q}] = [T_\sigma(\theta)]^{-1}[Q][T_\varepsilon(\theta)] \tag{B9}$$

B.2 Transformation of Piezoelectric "*d*" Constants

Actuation strain shown in the stress-strain relations is proportional to the piezoelectric *d* constants and are presented in matrix form

$$[d] = \begin{bmatrix} 0 & 0 & 0 & 0 & d_{15} & 0 \\ 0 & 0 & 0 & d_{15} & 0 & 0 \\ d_{31} & d_{32} & d_{33} & 0 & 0 & 0 \end{bmatrix} \tag{B10}$$

This research assumes thin piezoelectric layers polarized in the *3*-direction and isotropic in the *1*- and *2*-directions. Thus the piezoelectric constant matrix is reduced to

$$[d] = \begin{bmatrix} 0 & 0 & 0 \\ 0 & 0 & 0 \\ d_{31} & d_{32} & 0 \end{bmatrix} \tag{B11}$$

The actuation strain may be represented as

$$\{\varepsilon_\phi\} = [d]^T \{E\} = E_3 \begin{Bmatrix} d_{31} \\ d_{32} \\ 0 \end{Bmatrix} \tag{B12}$$

Transformation of the principal material coordinates of the d constants to the global coordinates may be accomplished by utilizing the strain transformation

$$\begin{Bmatrix} d_x \\ d_y \\ d_{xy} \end{Bmatrix} = [T_\varepsilon(\theta)] \begin{Bmatrix} d_{31} \\ d_{32} \\ 0 \end{Bmatrix} \tag{B13}$$

Thus for the isotropic assumption of the piezoceramic layers,

$$\begin{Bmatrix} d_x \\ d_y \\ d_{xy} \end{Bmatrix} = \begin{Bmatrix} d_{31} \\ d_{31} \\ 0 \end{Bmatrix} \tag{B14}$$

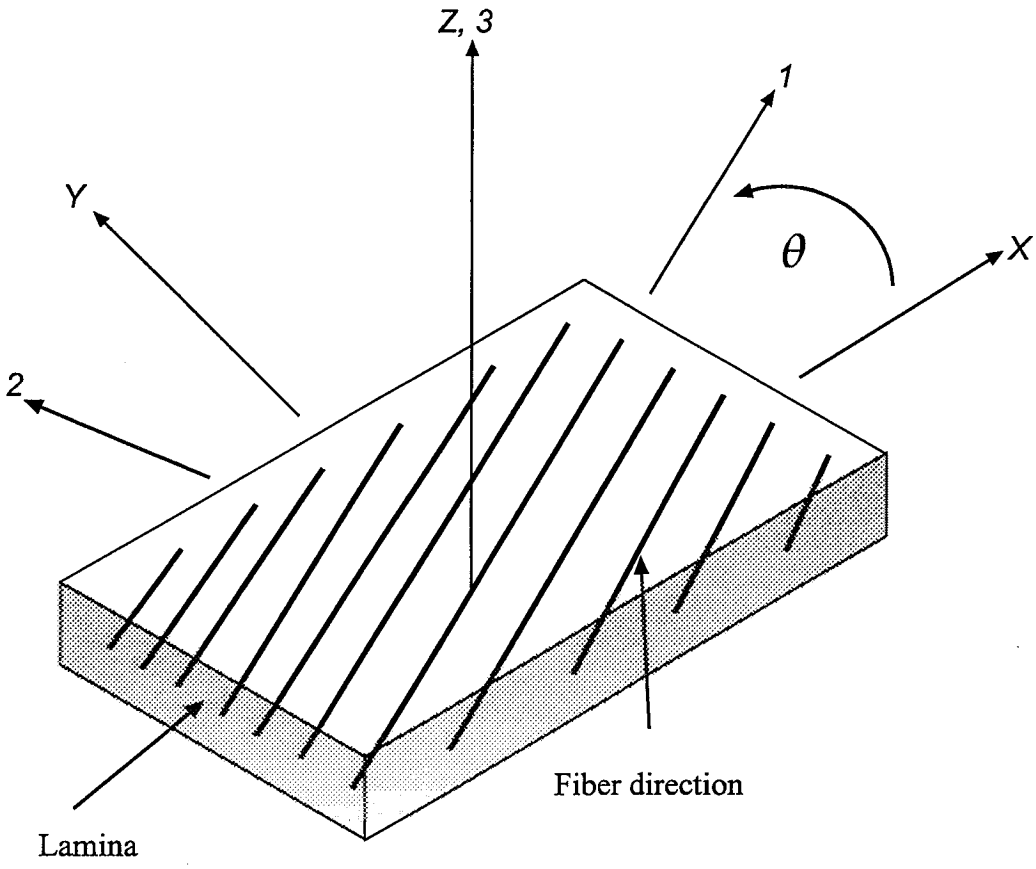

Fig. B.1 Principle material coordinates

APPENDIX C

ELECTROSTATICS

C.1 Introduction

Electric charge establishes an electromagnetic field. The strength of the electromagnetic field is a function of the magnitude, location, velocity, and acceleration of the charges present. An electrostatic field results from stationary charges, hence is a function of position only. In the special case of electrostatics, note that the terminology is modified by dropping *magnetic* from the root electromagnetic. This infers that magnetic results from dynamic charge behavior. In essence, electric charges in motion (i.e. electric current) produce a magnetic field.

C.2 Electrostatic Fields

Coulomb's Law established experimentally, that a force exist between two charged bodies, which tend to repel or attract each other. The direction of the force depends on whether both bodies have similar or dissimilar charges. If two small spherical bodies, each of charge q_1 and q_2 respectively, are present in an infinite homogeneous insulating medium separated by distance r, then Coulomb's force is expressed as

$$F = \frac{q_1 q_2}{4\pi\epsilon r^2} \tag{C1}$$

The direction of the force is along the line between the two charges, where ϵ is called the permittivity or dielectric constant of the medium. In free space or a vacuum, ϵ is defined as ϵ_0=8.854x10^{-12} Farad/meter, where the subscript o indicates free space. The permittivity of other materials are referenced to the permittivity of free space through their relative permittivity, that is $\epsilon=\epsilon_0\epsilon_r$. In the MKS system, the unit of charge was previously defined as the coulomb (one ampere of current flowing for one second transports one coulomb of charge). Thus in order to leave Maxwell's field equations

independent of the constant 4π, the units of Coulomb's force law were rationalized by a constant of 4π.

In the above example imagine that the q_2 charge is fixed and consider q_1 as being available to move about, i.e. a test probe charge. As the test probe charge is located at various positions near the fixed charge it experiences a force. The magnitude and direction of the force depends on the location relative to the fixed charge. Hence surrounding the fixed charge there exists an electric force field. This electric force field is described to have a strength **E,** which has units of force per unit charge. The magnitude of the force is given by Eq. (C1) and the magnitude of the electric field strength is

$$E = \frac{q}{4\pi\epsilon r^2} \tag{C2}$$

Note that the magnitude of the force is directly proportional to the magnitude of the test probe charge, however the electric field strength is defined as a force per unit charge thus independent of the magnitude of the test probe charge. Hence if the magnitude of the test charge approaches zero, the force diminishes; however the normalized force remains constant. Thus the electric field resulting from a charge exists, regardless of the presence of a test probe charge. In effect the test charge can be utilized to verify the existence of an electric field, and abstractly, if any charge q exists, then an electric field exists. The electric field around a point charge is a vector quantity and can be written as

$$\mathbf{E} = \frac{q}{4\pi\epsilon r^2}\hat{\mathbf{r}} \tag{C3}$$

where $\hat{\mathbf{r}}$ is a unit radial outward vector from charge q.

C.3 Electric Displacement

Equation (C3) indicates that the electric field is a function of the magnitude and position of the charge and the permittivity material. It is desirable to introduce the *electric displacement* or *electric flux,* that is independent of the material permittivity. The electric flux is best described by the results of Faraday's famous experiment with concentric spheres [16]. Faraday placed a metallic sphere with charge Q inside of another metallic sphere. Great care was taken to keep the spheres separated at all times. Then the outer sphere was grounded to earth for a very short time and then again with great diligence using insulating tools the inner sphere was removed. Once the outer sphere was reassembled, the charge on it was measured. The charge on the outer sphere was found to be equal and opposite in sign to the charge placed on the inner sphere. This experiment was repeated for several sphere sizes and with several dielectric materials and the results were always the same. Hence there is an electric flux or displacement through the dielectric. The displacement being a function of the magnitude of charge and independent of permittivity

$$\Psi = Q \tag{C4}$$

Consider an isolated point charge far from any other particle. The *electric displacement density* or electric displacement per unit area on any point of a sphere surrounding the point charge is

$$D = \frac{\psi}{4\pi r^2} = \frac{q}{4\pi r^2} \tag{C5}$$

The displacement density is a vector quantity with its direction outward normal to the sphere

$$\mathbf{D} = \frac{\psi}{4\pi r^2}\hat{\mathbf{r}} \tag{C6}$$

Upon examination of Eq. (A.3) and Eq. (A.6), **D** and **E** are related and can be written as the electromagnetic constitutive relation

$$\mathbf{D} = \epsilon \mathbf{E} \tag{C7}$$

where the permittivity is a tensor for the most general anisotropic materials

$$\epsilon = \begin{bmatrix} \epsilon_{11} & \epsilon_{12} & \epsilon_{13} \\ \epsilon_{12} & \epsilon_{22} & \epsilon_{23} \\ \epsilon_{13} & \epsilon_{23} & \epsilon_{33} \end{bmatrix} \tag{C8}$$

C.4 Potential Function

The electric field is a conservative force field. Hence there is no dissipation mechanism and all energy must be stored in either potential or kinetic form. The work done, on the system above, in moving the test probe charge around the fixed charge, i.e. against the force F, can be calculated as

$$\text{work} = -\int_{\infty}^{R} F dr \tag{C9}$$

As with any conservative force field an arbitrary reference may be chosen. As shown above, infinity is commonly selected as the reference. Thus the work done on the test probe charge is

$$\text{work} = -\int_{\infty}^{R} \frac{q_1 q_2}{4\pi\epsilon r^2} dr$$

$$= \frac{q_1 q_2}{4\pi\epsilon R} \tag{C10}$$

The normalized work done on the test probe charge is defined as the electric potential at a point due to the presence of charge q_1, hence

$$V \equiv \frac{\text{work}}{\text{unit charge}} = \frac{q_1}{4\pi\epsilon R} \tag{C11}$$

Note that potential is a scalar quantity. The potential has a unit of joule per coulomb which is the MKS units for a volt. For electrostatics, the terms potential, potential difference and voltage are synonymous. Another useful relationship is the differential work or differential voltage required in moving a positive unit charge an infinitesimal distance. For example, the differential work is

$$dW = dV = -\mathbf{E} \cdot ds \tag{C12}$$

where dV can be expressed as $\nabla V \cdot ds$, thus $\mathbf{E} = -\nabla V$ and the electric field strength at any point is simply the negative of the potential gradient at the point. If Eq. (C12) is integrated the potential difference will become much clearer. For example, consider the potential difference between two points a and b as

$$\int_a^b dV = -\int_a^b \mathbf{E} \cdot ds \tag{C13}$$

Thus the potential difference between point a and b is

$$V_a - V_b = \int_a^b \mathbf{E} \cdot ds \tag{C14}$$

C.5 Capacitance

The capacitance between two conductors is defined as the ratio of charge on the conductors, to the voltage or potential difference between each of the conductors

$$C = \frac{Q}{V} \tag{C15}$$

Note that the capacitance is defined irrespective of the size and shape or distance between the conductors. Gauss's law can be used to verify that the total charge on one of the conductors is indeed proportional to the potential difference, and the proportionality is capacitance.

C.6 Electrostatic Energy

When a capacitor is charged, a voltage or potential difference exists between the conductors. As previously discussed, the voltage will establish a conservative electric force field between the two conductors. Thus energy storage is present in a charged capacitor, since no dissipation mechanism exists within a conservative force field. The amount of energy stored, is simply the work required to charge the capacitor. Recall that potential was defined as work done per unit charge in Eq.(C11), thus the differential work is

$$dW = Vdq \tag{C16}$$

and the total work is computed as

$$W = \int_0^Q \frac{q}{C} dq = \frac{Q^2}{2C} \tag{C17}$$

The stored energy of a charge capacitor can also be written as

$$U = \frac{1}{2} V^2 C \tag{C18}$$

Another approach to visualize the energy stored or work done in charging a capacitor is to consider the necessary energy required in establishing a charge distribution in space. If a free space is considered, and N discrete charges are brought into a given volume, then the work done or energy expended in locating the charges will be

$$W = \frac{1}{8\pi\epsilon} \sum_{i=1}^{N} \sum_{j=1}^{N} \frac{q_i q_j}{R_{ij}} \qquad i \neq j \tag{C19}$$

If a continuous charge distribution is considered instead of discrete charges, Eq. (C19) can be written in integral form as

$$W = \frac{1}{8\pi\epsilon} \int_{V_1} \int_{V_2} \frac{\rho_c(\mathbf{r}_1)\rho_c(\mathbf{r}_2)}{R} dV_1 dV_2 \tag{C20}$$

where q_i and q_j were replaced with volume charge densities $\rho_c(\mathbf{r}_1)d\mathcal{V}_1$ and $\rho_c(\mathbf{r}_2)d\mathcal{V}_2$ respectively, and $R = |\mathbf{r}_1 - \mathbf{r}_2|$. Recall that potential is defined as work per unit charge in Eq. (C11), so work done on the charge distribution can be written as the potential by

$$V(\mathbf{r}) = \frac{W}{\rho_c(\mathbf{r}_1)} = \frac{1}{4\pi\epsilon}\int_{\mathcal{V}_2}\frac{\rho_c(\mathbf{r}_2)}{R}d\mathcal{V}_2 \tag{C21}$$

Substituting Eq. (C21) into Eq. (C20) expresses the work necessary to create a continuous charge distribution

$$W = \frac{1}{2}\int\rho(\mathbf{r})V(\mathbf{r})d\mathcal{V} \tag{C22}$$

If the vector identity $\nabla\cdot(V\mathbf{D}) = V\nabla\cdot\mathbf{D} + \mathbf{D}\cdot\nabla V$ is applied to Eq. (C22) it may be re-written as

$$W = \frac{1}{2}\int_{\mathcal{V}}\rho V d\mathcal{V}$$

$$= \frac{1}{2}V\nabla\cdot\mathbf{D}d\mathcal{V}$$

$$= \frac{1}{2}\int_{\mathcal{V}}[\nabla\cdot(V\mathbf{D}) - \mathbf{D}\cdot\nabla V]d\mathcal{V}$$

$$= \frac{1}{2}\int_{S}V\mathbf{D}\cdot d\mathbf{a} + \frac{1}{2}\int_{\mathcal{V}}\mathbf{D}\cdot\mathbf{E}d\mathcal{V} \tag{C23}$$

For a piezoelectric generator, the externally applied voltage is zero and a mechanical deformation or strain results in a Maxwell's self induced electric field. The electrical energy density thus becomes

$$W = \frac{1}{2}\int_{\mathcal{V}}\mathbf{D}\cdot\mathbf{E}d\mathcal{V} \tag{C24}$$

This work formulation assumes that there is no free or space charge present within the piezoceramic.

APPENDIX D

PIEZOCERAMIC ADHESIVE

The adhesive used to bond the piezoceramic patch to the panel was Micro-Measurements GA-2 strain gage adhesive system [23]. The GA-2 system is an epoxy adhesive that is combined with the hardener 10-A. The adhesive is specified to have 10% to 15% elongation capabilities after 40 hours of curing time at 21^{o} C. It is recommended that a clamping force of 5-20 psi be applied to the patch during the curing process to assure a complete bond. Once the epoxy is mixed with the hardener the pot life is approximately 15 minutes at 21^{o} C. The adhesive is a dielectric which prohibits electrical conduction between the piezoceramic and the plate.

APPENDIX E

CHARGE AMPLIFIER DATA

The charge amplifier used, model number 422M77, was provided by PCB Piezotronics, Inc. [27]. The gain is fixed at 0.2537 mV/pC with a bias voltage of 11.09 V, a feedback capacitance of 4000 pF and a feedback resistance of $3x10^8$ ohms.

REPORT DOCUMENTATION PAGE

Form Approved OMB No. 0704-0188

1. AGENCY USE ONLY (*Leave blank*)	2. REPORT DATE	3. REPORT TYPE AND DATES COVERED
	April 1998	Contractor Report

4. TITLE AND SUBTITLE
Analysis and Testing of Plates With Piezoelectric Sensors and Actuators

5. FUNDING NUMBERS
WU 538-03-14-01

NAG1-1684

6. AUTHOR(S)
Jeffrey S. Bevan

7. PERFORMING ORGANIZATION NAME(S) AND ADDRESS(ES)
Dept. of Aerospace Engineering
College of Engineering & Technology
Old Dominion University
Norfolk, VA 23529-0247

8. PERFORMING ORGANIZATION REPORT NUMBER

9. SPONSORING/MONITORING AGENCY NAME(S) AND ADDRESS(ES)
National Aeronautics and Space Administration
Langley Research Center
Hampton, VA 23681-2199

10. SPONSORING/MONITORING AGENCY REPORT NUMBER
NASA/CR-1998-207667

11. SUPPLEMENTARY NOTES
Master's Thesis. Principal Investigator: Professor Chuh Mei
Langley Technical Monitor: Travis L. Turner

12a. DISTRIBUTION/AVAILABILITY STATEMENT
Unclassified-Unlimited
Subject Category 71 Distribution: Standard
Availability: NASA CASI (301) 621-0390

12b. DISTRIBUTION CODE

13. ABSTRACT *(Maximum 200 words)*

Piezoelectric material inherently possesses coupling between electrostatics and structural dynamics. Utilizing linear piezoelectric theory results in an intrinsically coupled pair of piezoelectric constitutive equations. One equation describes the direct piezoelectric effect where strains produce an electric field and the other describes the converse effect where an applied electrical field produces strain. The purpose of this study is to compare finite element analysis and experiments of a thin plate with bonded piezoelectric material. Since an isotropic plate in combination with a thin piezoelectric layer constitutes a special case of a laminated composite, the classical laminated plate theory is used in the formulation to accommodated generic laminated composite panels with multiple bonded and embedded piezoelectric layers. Additionally, the von Karman large deflection plate theory is incorporated. The formulation results in laminate constitutive equations that are amiable to the inclusion of the piezoelectric constitutive equations yielding in a fully electromechanically coupled composite laminate. Using the finite element formulation, the governing differential equations of motion of a composite laminate with embedded piezoelectric layers are derived. The finite element model not only considers structural degrees of freedom (d.o.f.) but an additional electrical d.o.f. for each piezoelectric layer. Comparison between experiment and numerical prediction is performed by first treating the piezoelectric as a sensor and then again treating it as an actuator. To assess the piezoelectric layer as a sensor, various uniformly distributed pressure loads were simulated in the analysis and the corresponding generated voltages were calculated using both linear and nonlinear finite element analyses. Experiments were carried out by applying the same uniformly distributed loads and measuring the resulting generated voltages and corresponding maximum plate deflections. It is found that a highly nonlinear relationship exists between maximum deflection and voltage versus pressure loading. In order to assess comparisons of predicted and measured piezoelectric actuation, sinusoidal excitation voltages are simulated/applied and maximum deflections are calculated/measured. The maximum deflection as a function of time was determined using the linear finite elements analysis. Good correlation between prediction and measurement was achieved in all cases.

14. SUBJECT TERMS	15. NUMBER OF PAGES
Piezoelectric Materials; Finite Element Method; Large Deflections; Composite Plates; Vibrations; Sensors; Actuators	132
	16. PRICE CODE: A07

17. SECURITY CLASSIFICATION OF REPORT	18. SECURITY CLASSIFICATION OF THIS PAGE	19. SECURITY CLASSIFICATION OF ABSTRACT	20. LIMITATION OF ABSTRACT
Unclassified	Unclassified	Unclassified	

NSN 7540-01-280-5500

Standard Form 298 (Rev. 2-89)
Prescribed by ANSI Std. Z-39-18
298-102